Tittle: Speed control of BLDC Motor by using PWM current controller technique for electric vehicle propulsion

Million Gerado Geda

Thesis Submitted to

The department of Electrical Power and Control Engineering
School of Electrical Engineering and Computing

Presented in Partial Fulfillment of the Requirement for the Degree of Master's in Electrical Power and Control Engineering (Power Electronics)

Office of Graduate Studies
Adama Science and Technology University

Adama, Ethiopia
September-2018

Tittle: Speed control of BLDC Motor by using PWM current controller technique for electric vehicle propulsion

Million Gerado Geda

Advisor:
Prof. Venkata L.N.K

Thesis Submitted to

The department of Electrical Power and Control Engineering
School of Electrical Engineering and Computing

Presented in Partial Fulfillment of the Requirement for the Degree of Master's in Electrical Power and Control Engineering (Power Electronics)

Office of Graduate Studies
Adama Science and Technology University

Adama, Ethiopia
September-2018

Approval of Board of Examiners

We, the undersigned, members of the Board of Examiners of the final open defense by Million Gerado Geda have read and evaluated his thesis entitled "Speed Control of BLDC Motor by Using PWM Current Controller Technique for Electric Vehicle Propulsion'' and examined the candidate. This is, therefore, to certify that the thesis has been accepted in partial fulfillment of the requirement of the Degree of Master's in Power Electronics.

____________________	____________________	____________________
Advisor	Signature	Date
____________________	____________________	____________________
Chairperson	Signature	Date
____________________	____________________	____________________
Internal Examiner	Signature	Date
Mengesha Mamo (PhD) __	____________________	__October 9/2018_
External Examiner	Signature	Date

Declaration

I hereby declare that this M.Sc. thesis entitled Speed control of BLDC motor by using PWM current controller technique for electric vehicle propulsion has been compiled by me under the supervision of prof. Venkata L.N.K at Faculty of Electrical Engineering ASTU, Adama, Ethiopia. This thesis contains no material which has been accepted for the award of any other degree or diploma, except where due reference is made. To the best of my knowledge, this thesis contains no material previously published or written by another person except where due reference is made in the text of the thesis.

Name: Million Gerado Geda

Signature: ____

This MSc. thesis have been submitted for examination with my approval as thesis advisor

Name: ____

Signature: ____

Date of submission: ____

Advisor approval sheet

To: Electrical Power and Control Engineering department

Subject: Thesis Submission

This is to certify that the thesis entitled "Speed control of BLDC motor by using PWM current controller technique for electric vehicle propulsion, submitted in partial fulfillment of the requirements for the degree of Master's in Electrical Power and Control Engineering department (specialization in Power Electronics), the Graduate program of the department of Electrical power and control engineering, and has been carried out by Million Gerado Geda, Id. No GSR/0048/09, under my supervision. Therefore, I recommend that the student has fulfilled the requirements and hence hereby he can submit the thesis to the department.

______________________	______________________	______________
Name of Advisor	Signature	Date

ACKNOWLEDGEMENT

First and foremost my deepest gratitude goes to my advisor Prof. Venkata L.N.K for accepting me as a M.Sc. student. I would like to thank for his guidance and support through my research thesis work.

I would like to express my deepest gratitude to prof. Y.J. Kim for his unlimited support, teaching, material support and advice during my research study.

This work would have not been completed without the contribution of various institutions, organizations and individuals; among which BISHOFTU Buss Factory particularly Ms. Genet, Center of transportation and Vehicle engineering specifically Dr. Tefese Asrat (Ph.D) for his encouragement, Electrical Engineering department specially Mr. Kena Likassa (Msc.) for his encouragement and support.

Lastly, I would like to thank my family to whom I dedicate this thesis. Words cannot express how grateful I am to my mother, father, my sisters and brothers for their love, encouragement and all of the sacrifices that they have made on my behalf.

Table of Contents

DECLARATION I

ACKNOWLEDGEMENT III

LIST OF TABLES VII

LIST OF FIGURES AND ILLUSTRATIONS VIII

LIST OF ACRONYMS AND ABBREVIATIONS XI

ABSTRACT XIII

CHAPTER 1 1

1. INTRODUCTION 1
   - 1.1. Background 1
   - 1.2. Statement of the problem 3
   - 1.3. Objective of the study 3
   - 1.4. Significance of study 4
   - 1.5. Motivation 4
   - 1.6. Scope 4
   - 1.7. Limitation 4
   - 1.8. Areas of application 5
   - 1.9. Definition of terms 5
   - 1.10. Thesis Outline 5

CHAPTER 2 6

2. LITERATURE REVIEW 6
   - 2.1. Electric motor varieties 6
   - 2.2. The Drive Train of Electric Vehicles 7
     - 2.2.1. DC Brushed Motor 9
     - 2.2.2. Induction (Asynchronous) Motor 9
     - 2.2.3. Switched Reluctance (SR) Motors 9
     - 2.2.4. Permanent magnet synchronous A.C motor (PMSM) 10
     - 2.2.5. BLDC Motor 10
     - 2.2.6. Performance comparison of BLDC motor with DC brushed motor and induction motor 11
   - 2.3. Electric vehicle batteries 13
     - 2.3.1. Advantages of lithium-ion batteries for vehicle 13

2.4. Brushless DC motor drives 14
2.4.1. Depending on inverter controlling technique... 16
2.4.1.1. Six step inverter feed VVS based speed control of BLDC motor drive 16
2.4.1.2. Hysteresis current controller based BLDC motor drive 16
2.5. Closely related works on BLDC motor speed control 17
CHAPTER 3 19
3. METHODOLOGY 19
3.1. Introduction.. 19
3.2. Materials... 19
3.3. Methods.. 19
3.4. Analysis of an Electric vehicle dynamics 21
3.4.1. Motive force, Motive power and Motive torque of the Vehicle 21
3.4.1.1. Rolling resistance force 22
3.4.1.2. Gradient resistance 23
3.4.1.3. Aerodynamic drag 23
3.4.1.4. Acceleration forces 24
3.4.2. Vehicle specification.. 27
3.4.3. Reducer 320Nm &Drive shaft 28
3.4.4. Traction motor.. 28
3.4.4.1. Selection of Traction Motor 28
3.4.4.2. Traction motor specification.. 30
3.4.5. Battery specifications.. 32
3.4.5.1. Matching Power Battery Parameters 32
3.4.5.2. Lithium ion battery pack.. 32
3.5. Modeling of Brushless DC motor Drive for Electric Vehicle Propulsion 34
3.5.1. Mathematical Modeling of the BLDC Motor 34
3.5.1.1. Modelling of Trapezoidal Back Electromotive Force 35
3.5.1.2. Mechanical Equation of Motion.. 37
3.5.1.3. Modeling of Hall Effect sensor 38
3.5.1.4. Transfer function of BLDCM and the load 38
3.5.2. Transfer function of inverter.. 40
3.5.3. Current feedback and Speed feedback 40
3.5.4. Design of Current and Speed Controller... 40

3.5.4.1. Current controller 41
3.5.4.2. Speed controller 44
3.6. BLDC motor drive proposed system setup 55
3.6.1. Battery source 55
3.6.2. Speed controller 56
3.6.3. Hall Sensor Decoder 56
3.6.4. Reference current generation 58
3.6.5. Three phase inverter drive 59
3.6.5.1. Hysteresis current controller based inverter drive 59
3.6.5.2. PWM current controller based inverter drive 61
3.7. Summary 63
CHAPTER 4 64
4. RESULTS AND DISCUSSIONS 64
4.1. Results 64
4.1.1. PWM current controller based BLDC motor driving output results 64
4.1.2. Hysteresis current controller based BLDC motor driving output results 68
4.2. Discussion of the results 70
4.2.1. Speed dynamic performance of the BLDC motor drive 70
4.2.2. Current harmonic distortion 72
4.2.3. BLDC motor torque ripple 73
CHAPTER 5 76
5. CONCLUSIONS AND RECOMMENDATIONS 76
5.1. Conclusions 76
5.2. Recommendations 77
REFERENCES 78
REFERENCE LINKS: L 83
APPENDIXES 84
APPENDIX A: APPENDIXES RELATED TO ANALYSIS OF DATA'S AND SYSTEM MODELING 84
APPENDIX B: APPENDIXES RELATED TO RESULT AND DISCUSSION 104
APPENDIX C: APPENDIXES RELATED TO DATA COLLECTION 118

List of Tables

Table 2. 1: Electric vehicles available in the world market 8
Table 2. 2: Comparison study of BLDC motor and DC Motor... 11
Table 2. 3: Comparison study of BLDC motor and Induction motor.................................. 12
Table 2. 4: Dynamic performance analysis of BLDC motor under variable load............... 18

Table 3. 1: The coefficient of friction for different types of surface 24
Table 3. 2: Tractive motor & vehicle specifications 27
Table 3.3: Reducer & Drive shaft specifications... 28
Table 3. 4: Parameters specification of BLDCM used in this thesis.................................. 32
Table 3. 5: Battery specifications used 33
Table 3. 6: Hall Effect sensors with rotor position.. 38
Table 3. 7: The truth table of hall sensor decoder 56

List of Figures and Illustrations

Figure 2. 1: Motors classification 6
Figure 2. 2: Brushed DC motor 9
Figure 2. 3: Switched reluctance motor geometries 10
Figure 2. 4: PMSM motor and induction motor 10
Figure 2. 5: BLDC motor 11
Figure 2. 6: Comparison of electric motors out of 75 points. 12
Figure 2. 7: Batteries in terms of power density and Energy density 13
Figure 2. 8: Schematic diagram of a two pole BLDC motor and its drive system 14
Figure 2. 9: The internal view of a BLDC motor 15
Figure 2. 10: Ideal current, back-EMF and commutation signals of BLDC motor drive ... 15
Figure 2. 11: Hysteresis current controller based BLDC motor drive for each phases 16

Figure 3. 1: Block diagram of the research methodology 20
Figure 3. 2: Block diagram of the proposed control system 20
Figure 3. 3: Pure Electric Vehicle Power System Structure 21
Figure 3. 4: Exerted forces on moving electric vehicle 22
Figure 3. 5: The approaching angle and departure angle of the car 22
Figure 3. 6: Aerodynamic dragging force versus speed of the car in Km/hr. 23
Figure 3. 7: Motive force versus approaching angle of the vehicle 24
Figure 3. 8: Motive force versus speed of the vehicle in Km/hr. 25
Figure 3. 9: The motive power conception with respect to an approaching angle 26
Figure 3. 10: Consumed power versus speed of the vehicle in (km/hr.) 26
Figure 3. 11: Power and torque characteristics of BLDC motor 27
Figure 3. 12: Reducer and Shaft [L3] 28
Figure 3. 13: Stator currents, EMF and output power ratio of BLDC motor to PMSM 29
Figure 3. 14: Torque density and power output of BLDCM and PMSM 30
Figure 3. 15: Rated and maximum values of BLDCM parameters used for EV 31
Figure 3. 16: Phase resistance versus temperature 32
Figure 3. 17: SOC in percentage versus mileage in kilometer 34
Figure 3. 18: Stator connected three phase BLDC motor winding 35
Figure 3. 19: Three phase trapezoidal rotor position waveforms 37
Figure 3. 20: Trapezoidal induced EMF in stator winding 37

Figure 3. 21: Block diagram of the BLDC motor drive S-function model 41
Figure 3. 22: S-function model of current control loop... 42
Figure 3. 23: The Command current versus stator current by using PI controller 43
Figure 3. 24: PI and PID-ZN tuning based current controller 44
Figure 3. 25: Representation of the outer speed loop in the BLDC motor drive................. 44
Figure 3. 26: PI based BLDCM motor speed versus reference speed 47
Figure 3. 27: Block diagram of PID controller parameters 48
Figure 3. 28: PID controller in proportional action 48
Figure 3. 29: Determination of sustained oscillation Pcr 48
Figure 3. 30: Simulink internal structure of PID controller 49
Figure 3. 31: Speed controlled BLDC motor by using PI and PID-ZN tuning method 50
Figure 3. 32: The flow chart for implementation of GA based PID optimization 51
Figure 3. 33: The selected PID parameters after 400 generation 54
Figure 3. 34: Speed control of BLDC motor by using ZN-PID versus GA-PID 55
Figure 3. 35: MATLAB/Simulink model of Lithium-ion battery 56
Figure 3. 36: Hall sensor decoder Simulink block diagram 57
Figure 3. 37: Hall sensor with its decoded signals 57
Figure 3. 38: Simulink model of reference current generation... 58
Figure 3. 39: Reference current and decoded hall sensors (dotted line)............................. 58
Figure 3. 40: Three phase BLDC motor inverter drive 59
Figure 3. 41: Simulink model of current controller.. 61
Figure 3. 42: Reference current and Stator current based hysteresis control 61
Figure 3. 43: General PWM inverter driving signal generation for each phases 62
Figure 3. 44: Triangular carrier generation 62
Figure 3. 45: Simulink inverter switching control logic circuit 63

Figure 4. 1: Command speed (RPM), motor speed (RPM) and SOC % 64
Figure 4. 2: The trapezoidal back EMF of BLDCM with its zoomed out part 65
Figure 4. 3: The per unit value of the command speed ($Wr*$) & motor speed (Wr), command torque ($Ten*$) & motor output torque (Ten) and rotor position in radian......... 66
Figure 4. 4: Reference current, the output stator current and output power of BLDCM 67
Figure 4. 5: The induced EMF and the rotor position of BLDCM..................................... 68
Figure 4. 6: Three phase inverter output voltage of BLDCM 68

Figure 4. 7: Hysteresis controller based controlled reference speed, output rotor speed and reference torque vs output torque of BLDCM 69
Figure 4. 8: Hysteresis current controller three phase output current of BLDCM 69
Figure 4. 9: Speed dynamic performance comparison of BLDC motor drive based on speed regulators at no load 70
Figure 4. 10: Comparison of BLDCM speed control based on inverter commutation techniques 71
Figure 4. 11: Speed dynamic performance comparison of BLDCM drive based on inverter driving techniques 72
Figure 4. 12: Zoomed part of a reference current versus a phase stator current of PWM current controlled inverter 72
Figure 4. 13: Three phases hysteresis current controller based BLDCM speed control 73
Figure 4. 14: PWM current controller based controlled electrical torque output developed by BLDCM and reference torque 73
Figure 4. 15: Hysteresis current controller based controlled electrical torque output of the BLDCM 74
Figure 4. 16: Six step inverter feed variable VS controlled electrical torque output value of BLDCM 74
Figure 4. 17: Inverter driving techniques in terms of their torque ripple output values...... 75

List of Acronyms and Abbreviations

A_f	Frontal area of the car
B	Friction coefficient (Nms/rad)
BLDC......	Brushless Direct Current
BLDCM .	Brushless DC Motor
C_{rr}	The coefficient of rolling resistance
DSP	Digital Signal Processor
EMF	Electromotive Force
$E_{a,b,c}$	Induced EMF in phase a, b &c
EV	Electric vehicle
$f_{a,b,c}(\theta_e)$.	Rotor position function
g	Gravitational acceleration (m/s^2)
GA	Genetic Algorithm
$I_{a,b,c}$	The phases current
I_{ps}	Peak value of PMSM stator currents
I_p	Peak value of BLDM stator currents
I_{sy}	Rms value of PMSM stator currents
I_d..........	Value of BLDM stator currents
J	The rotor moment of inertia (Kgm^2)
K_r	value of the line to line inverter gain
K_ω	Speed feedback gain
M	Mass in (Kg)
NI-MH ...	Nickel-Metal Hydride
P	Power
P	The number of poles
PI	Proportional Integral
PID........	Proportional Integral Differential
PID-GA ..	Genetic algorithm based PID controller
PID-ZN ..	Ziegler Nicolas based PID controller
P_m	Input power of the motor controller
PMAC ...	Permanent magnet AC motor
PWM	Pulse Width Modulation

Rk4 …….	……………………………...	Runga-kutta fourth order method
SPWM…	……………………………...	Sinusoidal Pulse Width Modulation
S ……….	……………………………...	Endurance mileage
SR ……..	……………………………...	Series Reluctance
SVPWM .	……………………………...	Space Vector Pulse Width Modulation
$T_e\ (a, b, c)$	……………………………...	Electric torque in phase a, b & c
THD …...	……………………………...	Total Harmonic Distortion
T_l ………	……………………………...	Load torque (N-m),
T_m ……..	……………………………...	Mechanical time constant
T_r ………	……………………………...	Delay time of the inverter switches
T_ω ……...	……………………………...	Speed feedback delay
V_{cm} …….	……………………………...	The maximum control voltage
V_{in} ……..	……………………………...	Inverter output voltage
VSI …….	……………………………...	Voltage Source Inverter
VS ……..	……………………………...	Voltage Source
VVS …...	……………………………...	Variable Voltage Source
W_{road} ….	……………………………...	Energy needed for mileage S
ZN ……..	……………………………...	Zeigler Nicolas method
θ_r ………	……………………………...	Electrical rotor position (rad)
ω_m ……..	……………………………...	Mechanical speed of the rotor (rad/sec)
ω_r ……...	……………………………...	Electrical rotor speed (rad/sec.)
φ_m ……..	……………………………...	Maximum flux linkage of each winding
λ_p ……...	……………………………...	Flux linkage
η_m ……..	……………………………...	The motor and controller assembly efficiency

Abstract

Due to their high efficiency and zero greenhouse gas emissions the electric vehicles are the best solution for green transportation. Several types of electric motors have been used as the propulsion system of electric vehicles. Brushless DC (BLDC) motor is selected because of its advantages compared with other electric motors. The only drawback of BLDC motor is its larger torque ripple. Electric vehicle propulsion needs good speed dynamic performance, low current ripple and low torque ripple which needs an accurate model of BLDC motor drive. In this research study PWM current controller is used to control the speed of BLDC motor for electric vehicle propulsion. The BLDC motor specification is analyzed by using MATLAB (version.15)/code. Then mathematical modeling of the proposed system is performed. Proportional integral controller (PI), Zeigler Nicolas based proportional integral differential (PID-ZN) controller and genetic algorithm based proportional integral differential speed (PID-GA) controller are compared based on their dynamic speed control performance. PID-GA controller gives settling time of 0.01 second per 3600 RPM of rotor speed with zero percent overshoot. But, PID speed controller results the settling time of 0.05 seconds with 2.777% overshoot at the same conditions. As the result of comparison PID-GA controller is found to be focused because of its better control response. Then the proposed system is simulated by using MATLAB software (version.15). The result shows that BLDC motor has efficiently controllable speed torque characteristic, reduced torque ripple, fast dynamic performance (low rise time, low peak time, low settling time and low percent overshoot). The proposed inverter drive technique is compared with another inverter control techniques like hysteresis current control modulation technique and six step inverter feed variable voltage source based BLDC motor drive for the same motor specifications and speed regulator parameters. The result shows PWM current controller gives better control mechanism by having the torque ripple less than 8%. But, the torque ripple becomes 18.18% in the case when hysteresis current controller is used with PID-GA speed controller. In general PWM current controller and PID-GA speed regulator based BLDC motor control is recommended for electric vehicle propulsion.

Key words: *Electric vehicle, BLDC motor, PWM current controller and PID-GA based speed controller*

CHAPTER 1

1. INTRODUCTION

1.1. Background

The idea of using electricity instead of fossil fuels for propulsion system of the vehicles is not new. Scientists and manufacturers have attempted to design and improve electric vehicles (EV) from long time ago. As the result Rodert Anderson built the first electric carriage in 1839. In 1870 David Salomon developed an electric car with a light electric motor. The batteries were heavy at the time, therefore performance was poor [1]. But, nowadays with an improvement of battery technology EV have better performance. Engine based vehicle is one of the environmental pollutant machine. Besides, the fossil fuel is going to be finish after a few decades. The only solution to continue the transportation is to replace the engine based vehicle by electric based vehicle. EV is essential and simple to use for the country like Ethiopia which are expecting very big MW power generation.

Motor is the propelling part of EV. In this study BLDC motor is selected for EV propulsion. BLDC motor is a permanent magnet synchronous motor with a trapezoidal Back EMF waveform shape [2]. The first BLDC motor was developed in 1962 by T.G. Wilson and P.H. Trickey [3]. BLDC motor is the most suitable motor for high performance electric vehicles compared with other electric motors [4]. BLDC motor has better performance than brushed DC motors [4]. The ratio of torque delivered to the size of this motor is higher, making it useful in applications where space and weight are critical factors. However, the production cost of this motor is larger compared with another electric motors due to the permanent magnet material used on the rotor part of this motor. In addition the maintenance of this motor is more than the maintenance cost of induction motor.

BLDC motor control depends on the position of the permanent magnet rotor. The inverter switching electronic commutation and instability of the system due complicated design of the speed regulator increases the complexity of the BLDC motor drive. Precise model and simulation of BLDC motor is required to study the behaviour of the motor for different control algorithms. The mathematical model and the principle of three phases, star connected BLDC motor drive with ideal trapezoidal back-EMF waveforms is discussed. BLDC motor has some torque ripple compared with other motors. Torque ripple reduces the life span of the vehicle and makes the sit uncomfortable to the passenger. Torque ripple is due to stator current distortion as electrical torque of the motor is proportional to the stator current of the motor. The stator current depends on its corresponding reference current. The generated reference current is proportional to the speed regulator output value. Therefore BLDC motor needs the speed controller with better dynamic performance. Several techniques and algorithms are proposed by researchers for BLDC motor speed regulators. Among them PI controller, PID controllers have been widely used for speed and position control of BLDC motor. Besides, different inverter switching drives techniques are used for the purpose of the BLDC motor drive. The first one is six steps inverter feed variable voltage source drive is the one. This control scheme is the simplest but used in the case of variable voltage source power supply. The second one is Hysteresis current controller based inverter drive. The inverter switch depends on the difference of the stator current and reference current. The smaller hysteresis band width the smaller torque ripple and the larger hysteresis band width the larger torque ripple. But if the hysteresis band width is smaller the inverter switching loss is larger. Because of this reason PWM current controller is used in this work to fulfill the proposed objectives.

In 2017 the center of transportation and vehicle engineering members proposed EV production in Ethiopia. Some data specification of the traction motor is obtained from this proposal. Besides, some data specification of the vehicle of similar to that proposed by this members but engine based is collected from Bishoftu Buss Factory. Modeling and analysis of the BLDC motor drive specified data is performed for the purpose of getting the missing data's, to design controllers and to understand the working principle of the system. MATLAB software version 15.0 is used for the purpose of analysis and discussion of data's thought this study.

In this work comparison of PI, Zeigler Nicolas based PID and genetic algorithm based PID speed controller is performed. The result shows genetic algorithm based PID optimization gives better speed dynamic performance. Besides, PWM current controller based BLDC motor inverter drive is compared with Hysteresis current controller based BLDC motor inverter drive. As the result, PWM current controlled BLDC motor gives lower torque ripple. In summary PWM current controller based inverter drive and PID-GA based speed regulator gives better BLDC motor working performance and hence suitable for EV propulsion application.

1.2. Statement of the problem

Due to the emission of carbon dioxide the environmental pollution is increasing around the world. Besides, the cost of the fossil fuel is increasing. Even though the above mentioned problems are the reality, there is no local production of electric vehicles. In order to avoid the above mentioned problems fossil fuel based vehicle must be replaced by electric vehicle. The motor is the main part of EV which needs the efficient and appropriate control techniques. BLDC motor has better performance characteristics in many aspects. But, it has higher torque ripple compared with other electric motors especially PMSM. The source of torque ripple is current distortion. Torque ripple is reduced by reducing the stator current distortion. It is the first step to model the BLDC motor drive system appropriately in order design the motor speed controllers. The speed dynamic performance characteristics of the motor is essential in the case of EV. Therefore the speed controller of BLDC needs to be designed and modeled by using an appropriate algorithm. This work is also intended to answer the following basic questions:

- ✓ How to analyze the tractive power and other specifications of a motor for EV propulsion?
- ✓ How to reduce torque ripple of BLDC motor drive?
- ✓ How to drive a BLDC motor with better speed dynamic performance, i.e. (reduced settling time, reduced percent overshoot, and reduced rise time of speed)?
- ✓ How to model BLDC motor drive by using MATLAB/code?

1.3. Objective of the study

The goal this research thesis is to model BLDC motor drive and speed control of BLDC motor by using pulse width modulation current controller for the purpose of electric vehicle propulsion. Specifically, the objectives of this research thesis is:

- To model three phase BLDC motor drive for Electric Vehicle.
- To model speed controller for BLDC motor drive.
- To control the speed of the BLDC motor.
- To reduce the current distortion of BLDC motor.
- To reduce the torque ripple of BLDC motor.
- To simulate the system by using MATLAB software.

1.4. Significance of study

The worldwide are shifting the energy source usage from non-renewable source that will not available after a few decades to renewable energy source that can exist forever. In a similar ways center of transportation and vehicle engineering members are trying to develop EV in Ethiopia. Since the above mentioned objectives are certainly full filled, this research study can support the trend started by center of transportation and vehicle engineering members.

1.5. Motivation

Due to the futurity of electric vehicles technology it is very interesting to do the research around this area. The one who is professional EV drive is undoubtedly beneficial because huge market is coming. The battery technology is updating from time to time which gives hope to use EV easily. BLDC motor is getting popularity rapidly. BLDC motor has been increasingly used in Automotive, Aerospace, Consumer, Medical, Industrial Automation Equipment and Instrumentation, due to its better torque speed characteristics, compact size, higher efficiency, wide speed range and longer operational life. The ratio of torque delivered to the size of the BLDC motor is higher, making it very interesting in the applications where space and weight are critical factors like in electric vehicle application.

1.6. Scope

The research study includes the modeling and simulation of speed control of BLDC motor by using MATLAB software. The performance of BLDC motor drive techniques in case of both speed controllers and inverter driving techniques are compared and analyzed. DSP hardware implementation is not included. This work is only focused on the BLDC motor drive and simulation by using MATLAB software. The traction specification of the motor specified by the center of transportation and vehicle engineering is used. But, some missing data is obtained by using graphical analysis of existing data and calculation. The study doesn't include the detail about battery source and other parts of the EV.

1.7. Limitation

The comparison of the motors for Electric vehicle propulsion is taken from literature because it is very difficult to get PMSM motor, SR motor and BLDC motor around. If they would have available the comparison was done in laboratory. The trend was to implement the speed control of BLDC motor using PWM current controller by using DSP. However due to specification rating current mismatch of the BLDC motor and DSP kit manual that we had the device is burnt out before having the required result outputs. It is difficult to get the device again, therefore the hardware implementation of the research work could be excluded.

1.8. Areas of application

The result of this research thesis could be applicable to:

- Electric vehicle drive
- Electric train drive, in industry and etc.

Specifically, the aim of the research study is to support the idea of producing Electric Vehicle named ECADO-4EV which is undergoing in ASTU by the center of transportation and vehicle engineering since 2017. ECADO-4EV is named by prof. Yong. Joo Kim who had been the director of the center of transportation and Vehicle engineering. According to him ECADO-4EV means that ''Ethiopia can do four wheel Electric vehicle''.

1.9. Definition of terms

- ☞ **Approach angle**: is the maximum angle of a ramp onto which a vehicle can climb from a horizontal plane without interference.
- ☞ **Departure angle**: is the maximum ramp angle from which the car can descend without damage. Approach and departure angles are also referred to as ramp angles.
- ☞ **Optimization:** Making the best or most effective use that is done by determining the appropriate values of PID parameters.
- ☞ **Propulsion**: The force that drives a load forward.
- ☞ **Current harmonic distortion:** Is the distortion of phase current from its corresponding reference current values

1.10. Thesis Outline

This thesis is organized into five chapters.

Chapter 1: The first chapter presents the introduction of BLDC motor drive, statement of the problem, objectives of the study, Significance of study, motivation, scope and limitation, area of application, methodology and definition of terms.

Chapter 2: In chapter two reviewed papers on the background and structural overview, advantage of brushless DC motor compared with the other electric motors, its today's word wide application and existing control mechanism of BLDC motor are discussed.

Chapter 3: covers the analysis of data's, BLDC motor drive modeling and the proposed system development are covered.

Chapter 4: The proposed system results are discussed in chapter four.

Chapter 5: Finally conclusion and recommendation is made in chapter five.

CHAPTER 2

2. LITERATURE REVIEW

In this chapter the background and varieties of electric motors, advantage of brushless DC motor compared with the other electric motors and its todays word wide application, the existing controlling mechanism and other related applications of BLDC motor are reviewed and discussed.

2.1. Electric motor varieties

Nowadays, several types of electric motors are used for electric vehicle propulsion. But because of their drawbacks all types of motors are not used equally. The classification feature of electric motors can be organized as the following figure (2.1) [4].

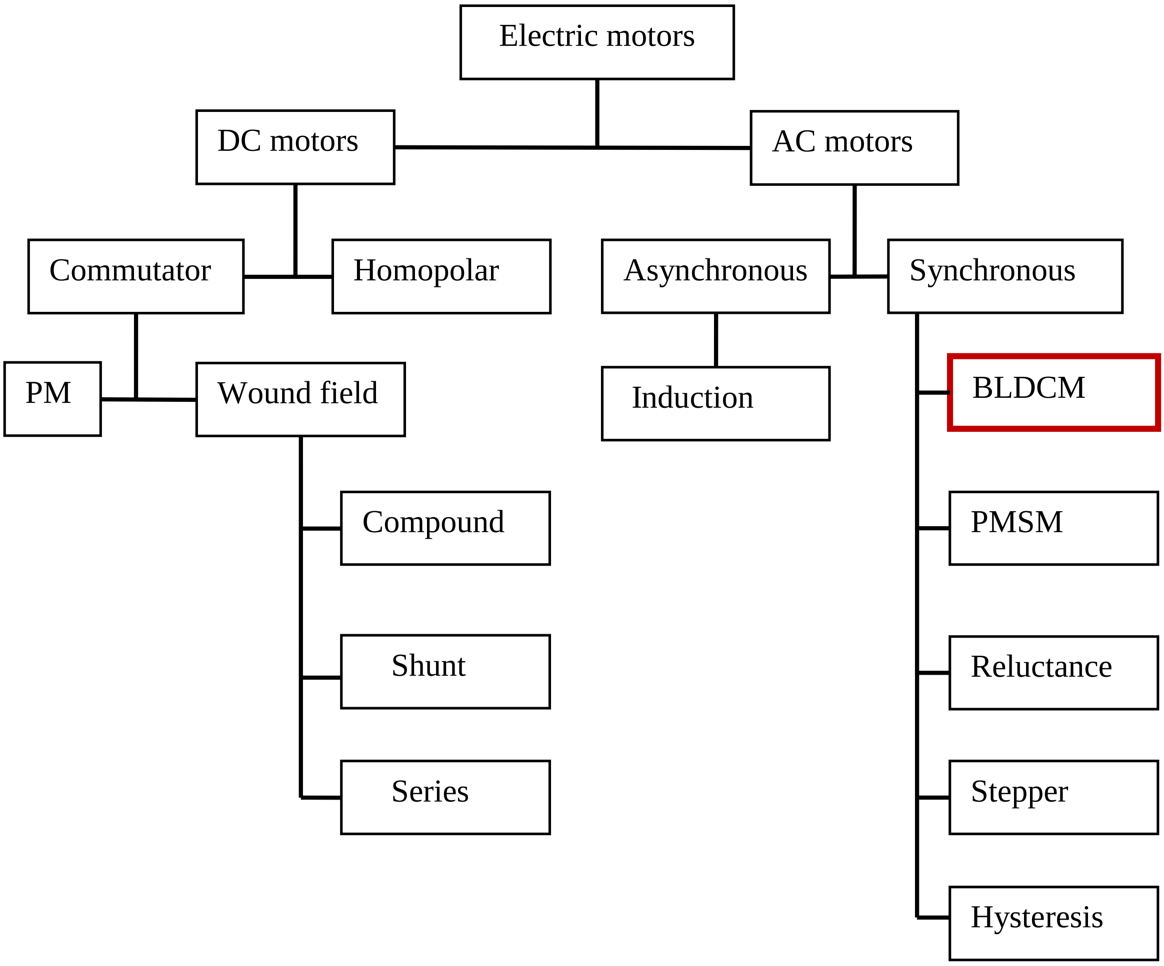

Figure 2. 1: Motors classification

Out of the motor varieties shown in the figure (2.1), BLDC motor, Induction motor, SR motor and DC motor are widely used for electric vehicles propulsion.

2.2. The Drive Train of Electric Vehicles

The electric vehicle drive train specifications available in the world market are given in table (2.1) [5]. From this table it can be seen that BLDC motor and induction motors are most popular from the manufacture's point of view. In order to select an appropriate motor which can mostly fulfil the EV motor technology requirements, an overall comparison of electric motors is needed based on EV requirements. The most important requirements of the EV motors are [6]:

- High efficiency;
- High dynamic response (fast torque and speed response);
- High torque at low speeds;
- High torque/power to size ratio;
- Constant power in wide speed range;
- Accurate electronic controllability;
- Robustness and reliability of the motor and its drive;
- Maintenance cost (life expectancy) ;
- The production cost of the motor

A single electric motor cannot fulfill all of the above mentioned electric vehicle qualification requirements. For example BLDC motor has lower constant power in wide speed range than induction motor and SR motor but, higher than that of DC motor. Even though BLDC motor has lower maintenance cost than brushed DC motor, it has higher maintenance cost than induction motor and SR motor. The production cost of the BLDC motor is also larger due to the cost of the permanent magnet used on the rotor part of this motor. It is the overall summation of EV requirements which determine the appropriate electric vehicle propelling motor we have to select as shown in figure (2.6).

Table 2. 1: Electric vehicles available in the world market [7] [8] [9][L1]

No	EV name	Manufacturer Company	Passenger Capacity	Electric Motor	Power (KW)	Top speed (Km/h)	Country/ Release year
1	Smart	Smart Automobile	2	BLDC	30	120	Germany/2009
2	BYD E6	BYD Auto	5	BLDC	160	140	China/2010
3	Mitsubishi i-MiEV	Mitsubishi	4	BLDC	47	130	Japan/ 2009
4	Morgan Plus E	Morgan motors	2	BLDC	70	185	UK
5	MyCar	EuAuto Technology	2	BLDC	---	64	Hong Kong/2003
6	Nissan Leaf	Nissan	5	BLDC	80	150	Japan/2010
7	BMW MiniE	BMW	2	Induction	150	153	Germany/2013
8	ZeCar	Stevens Vehicles	5	Induction	52.2	90	UK/2008
9	C1 ev'ie	Citroen	4	Induction	30	97	France/200
10	Electron	Ross Blade	4	Induction	55	110	Australia/2010
11	Think City	Think Global	2	Induction	34	120	Norway/2008
12	REVAi REVA	Electric	2	Induction	13	80	India/2001
13	Tesla	Tesla Motors	5	Induction/BLDC	310	200	USA/2012
14	QBEAK	ECOmove	2	2in-wheel PMAC	35.4	120	Denmark/2012
15	Lightning GT	Lightning car	2	2in-wheel PMAC	300	200	UK/2013 GT Car
16	Buddy	Buddy Electric	3	Brushed DC motor	13	80	Norway/2010

In addition electric motors used in electric vehicle should have important attributes like simple design, high specific power, low maintenance cost, and good control [6][10]. Even though their performance quality of Brushed DC motors, BLDC motor, Induction motor, Synchronous motor and Switched Reluctance motor is not the same, they are widely used for EV propulsion.

2.2.1. DC Brushed Motor

The main drawback of this motor is damage to the brush, which causes the expenditure of money for its usual maintenance. The friction between brushes and commutators, limits the maximum motor speed. In addition to this brushed DC motor has poor power density compared to PMSM or BLDC motor for use in electric vehicles [6]. But, DC brushed motors have the ability to achieve high torque at low speeds, which makes them suitable for traction system [6].

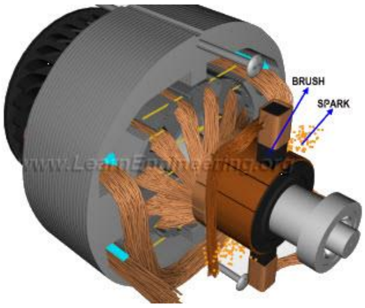

Figure 2. 2: Brushed DC motor

2.2.2. Induction (Asynchronous) Motor

Three phase induction motors are widely used in electric vehicles because of their high efficiency, good speed regulation and absence of commutators. The interaction between revolving magnetic field that is due to induced EMF in the stator winding and field due to induced currents in the rotor gives rise to unidirectional torque [6]. Induction motor has larger rotor inertia compared to that of BLDC motor of the same power output and hence lower speed dynamic response [11].

2.2.3. Switched Reluctance (SR) Motors

Switched reluctance motors are also known as variable reluctance motors. The structure of the SR motors is similar to the structure of BLDC motors. But, SR motors, motor has a ferromagnetic rotor instead of a permanent magnet rotor therefore cheaper than BLDC motor. Due to its mechanical control complexity, noise and vibration problem, lower level of efficiency and lower power density SR motor is quite late accepted in the application of electric motor drive. The switched reluctance geometry is shown in the figure (2.3) [12].

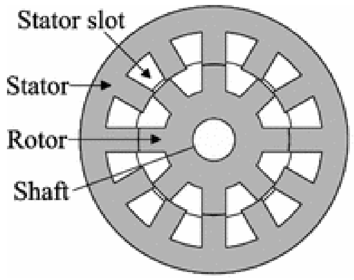

Figure 2. 3: Switched reluctance motor geometries

Even though it has the above mentioned drawbacks, this type of drive is supposed to have a tremendous potential in the field of electric vehicle propulsion system due to some of its useful features like, simple construction, very low manufacturing cost and outstanding torque speed characteristics for use in use in the EV propulsion system [10] [12].

2.2.4. Permanent magnet synchronous A.C motor (PMSM)

Synchronous motor with sinusoidal back EMF is called permanent magnet synchronous motor. Along with most of the drive this motor gives direct competition with an induction motor [10]. But differ from induction motor, the magnetic field excited by using high energy permanent magnet leads an overall reduction in the weight and volume of this motor for a given output power [12]. Besides, PMSM motor has no rotor copper loss and heat rises in the stator can be evenly distributed. The efficiency and reliability of PMSM motor is quite higher. But the drawback of this motor is its higher production and controller cost [13].

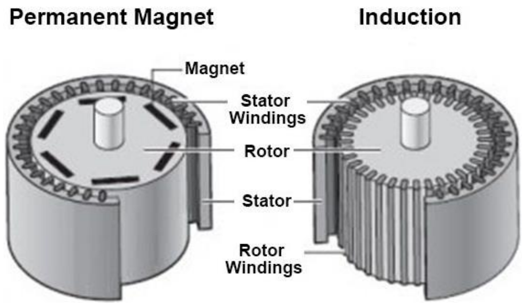

Figure 2. 4: PMSM motor and induction motor

2.2.5. BLDC Motor

Synchronous motor with trapezoidal wave back EMF is known as BLDC motor or permanent magnet brushless DC motor. A BLDC motor with the trapezoidal back-EMF produces larger torque compared to a PMSM with the sinusoidal back-EMF. Due to its elimination of brushes, greatest efficiency, higher power density, larger torque output, high speed ranges and high dynamic response (low inertia of the rotor) the permanent magnet brushless D.C motor is an ideal choice for being used in the electric vehicle propulsion system [7].

The trapezoidal EMF is generated by using MATLAB code as shown in appendix B.

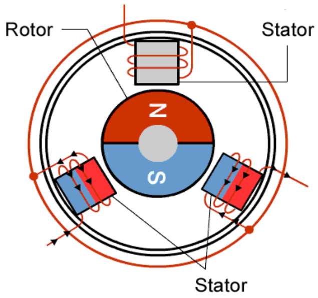

Figure 2. 5: BLDC motor

2.2.6. Performance comparison of BLDC motor with DC brushed motor and induction motor

BLDC motors have many advantages over brushed DC motors and induction motors in many applications because of its higher efficiency, reliability, lower acoustic noise, smaller and lighter, greater dynamic response, better speed versus torque characteristics, higher speed range and longer life than the others [14]. In general the performance comparison of BLDC motor with DC motor and Induction motor for electric vehicle application purpose is explained as in table (2.2) and table (2.3) respectively [15] [7].

Table 2. 2: Comparison study of BLDC motor and DC Motor

No.	Futures	BLDC motor	DC motor
1	Commutation	Electronic commutation.	Brushed commutation
2	Power and torque [6]	Higher	Poor power
3	Speed torque characteristics	Flat in nature as the result it can operate at all speeds with rated load.	Moderately flat, at higher speeds brush friction increases reduction of useful torque.
5	Life span	Longer	Shorter
6	Rotor inertia	Lower and hence better dynamic response time.	Higher and hence limited dynamic response time.
7	Speed range	Higher	Lower
8	Electric noise	Lower	Larger
9	Cost and efficiency	Expensive but, higher efficiency	Cheaper but, lower efficiency

Table 2. 3: Comparison study of BLDC motor and Induction motor

No.	Futures	BLDC motor	Induction motor
1	Speed torque characteristics	Flat in nature	Nonlinear in nature. It enables lower torque at lower speeds
2	Output power/frame size	Higher	Moderate
3	Rotor inertia	Lower i.e. better dynamic characteristics	Higher. i.e. Poor dynamic characteristics
4	Starting current	Equal to rated current Special starter circuit is not required.	It will be approximately up to 7 times of rated current
5	Cost	Expensive but higher efficiency	Cheaper but lower efficiency

In general the comparison performance of BLDC motor for EV propulsion can be summarized as shown in figure based on fifteen motor performance characteristics of each maximum of five points (2.6) [16] [7].

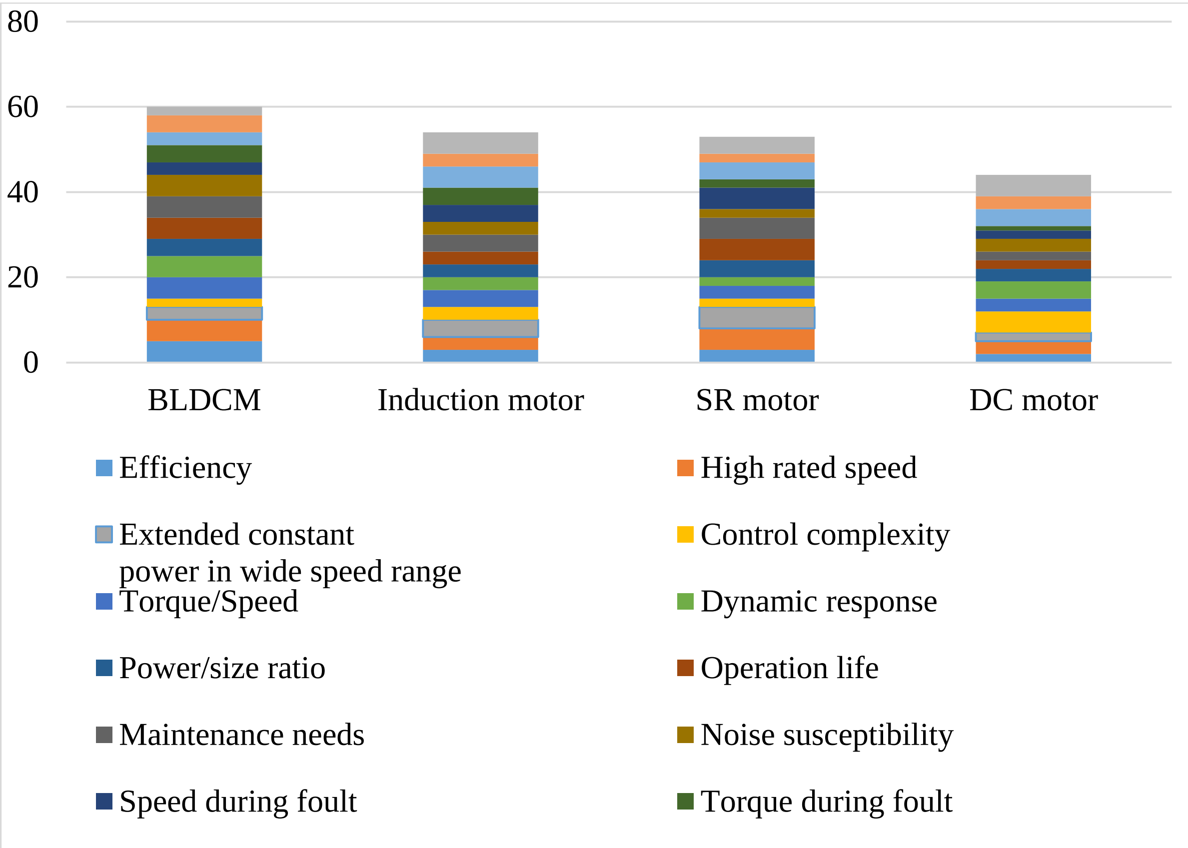

Figure 2. 6: Comparison of electric motors out of 75 points.

The reviewed result study shows BLDC motor is the most suitable choice as drive train of the high performance electric vehicles. As the drawback BLDC motor is expensive due to the cost of the permanent magnet on its rotor part.

2.3. Electric vehicle batteries

Lithium-ion batteries are most popularly used battery for hybrid electric vehicle and full-pure electric vehicles. The other types of batteries, such as lead-acid and nickel-metal hydride are continuing to retain considerable market share in the world. Lithium-ion going to dominate the world market.

2.3.1. Advantages of lithium-ion batteries for vehicle

Lithium-ion batteries are the most suitable existing technology for electric vehicles. Compared with other relevant battery types, lithium-ion batteries have the highest power density [17]. This makes the lithium-ion density to be lighter and smaller than other rechargeable batteries of the same power and energy capacity. This is the reason why the lithium-ion batteries are already widely used for consumer electronics such as cell phones, laptop computers and another electric power consuming devices. Therefore, it is important that the battery manufacturing takes place near auto manufacturing [17]. The above statement can be summarized as shown in figure (2.7).

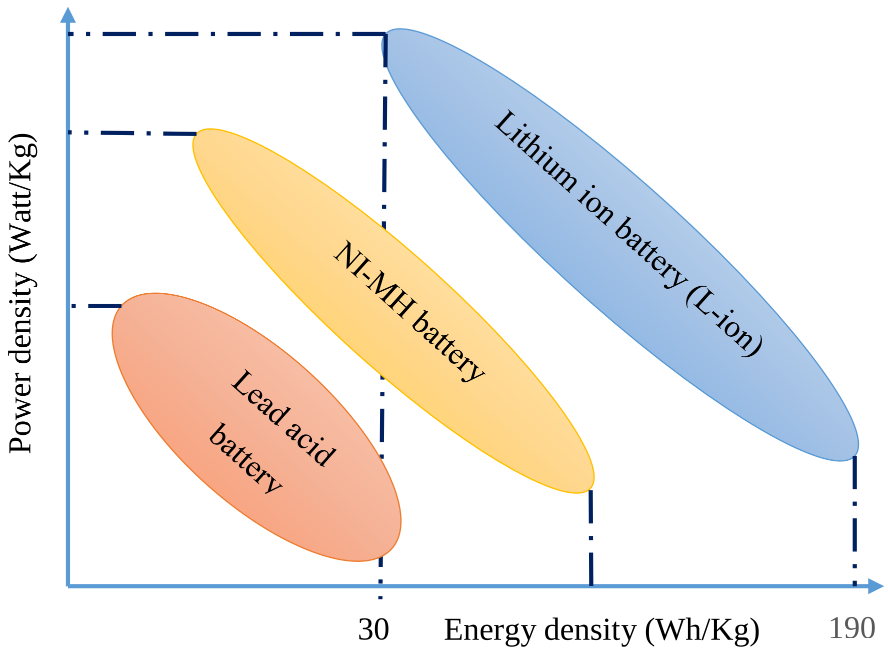

Figure 2. 7: Batteries in terms of power density and Energy density [17]

2.4. Brushless DC motor drives

The main components of brushless DC motor drives are: power source, inverter with its control part, speed regulator and Hall sensor. The common schematic diagram of two pole BLDC motor and its drive is shown as the in the figure (2.8). BLDC motor consists of concentric wound stator, permanent magnet rotor and hall sensor mounted on stationery part of the motor. The permanent magnet rotor of the BLDC motor can vary from two pole pairs to eight pole pairs [4]. The magnetic material is chosen with respect to the required magnetic field density in the rotor. Since ferrite magnets have the disadvantages of low flux density, alloy materials such as Neodymium, Samarium Cobalt, Ferrite and Boron, of higher flux density are used instead to produce more torque. They improve power to size ratio of the BLDC motor [18]. BLDC motor needs a complex control algorithm due to the electronic commutation that is done according to the exact position of the permanent magnet rotor. There are two methods for rotor position detection.

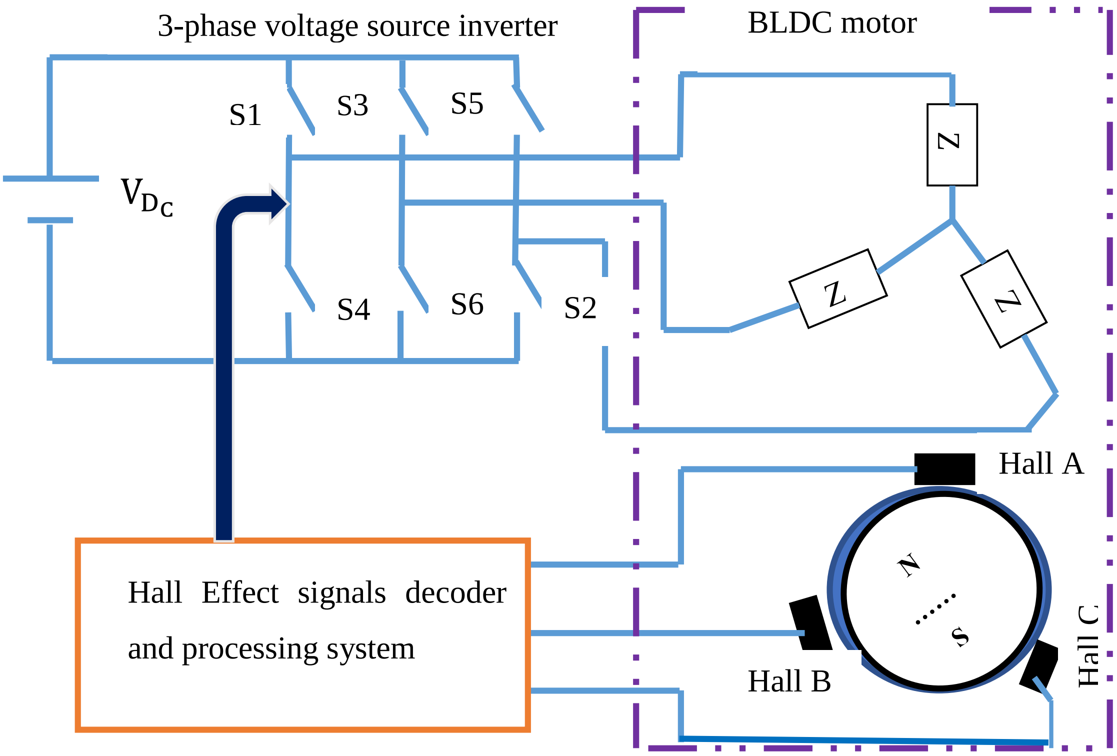

Figure 2. 8: Schematic diagram of a two pole BLDC motor and its drive system [19]

The first one is by using sensors (Hall Effect sensors) and the second one is sensor less detection [20]. In this work hall sensor is used to detect the rotor position, because the cost of the sensor is negligible compared with the overall cost of the vehicle and complexity of using sensor less algorithm. Hall Effect sensors are normally mounted on the non-rotating end inside the BLDC motor with 120 degree phase difference at the constant position to detect rotor angle. The internal view of a BLDC motor with hall sensor is shown below.

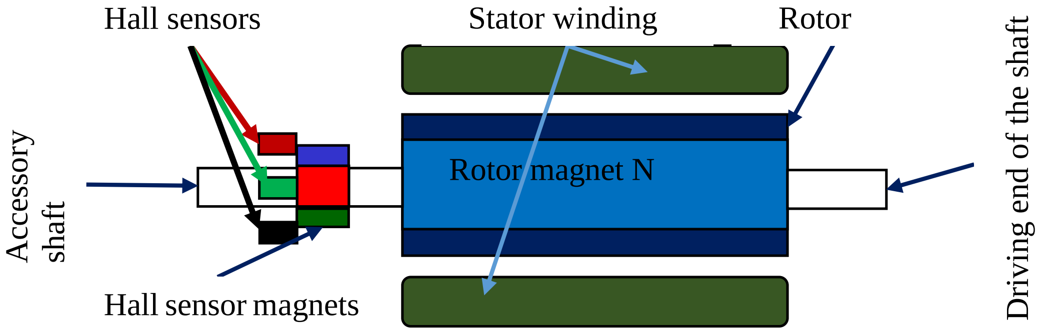

Figure 2. 9: The internal view of a BLDC motor

The detected signals are decoded to choose the electrical EMF angular position at which the inverter switch need to be ON or OFF. An ideal back-EMF voltage, stator current and Hall sensor signals are shown in as in figure (2.10).

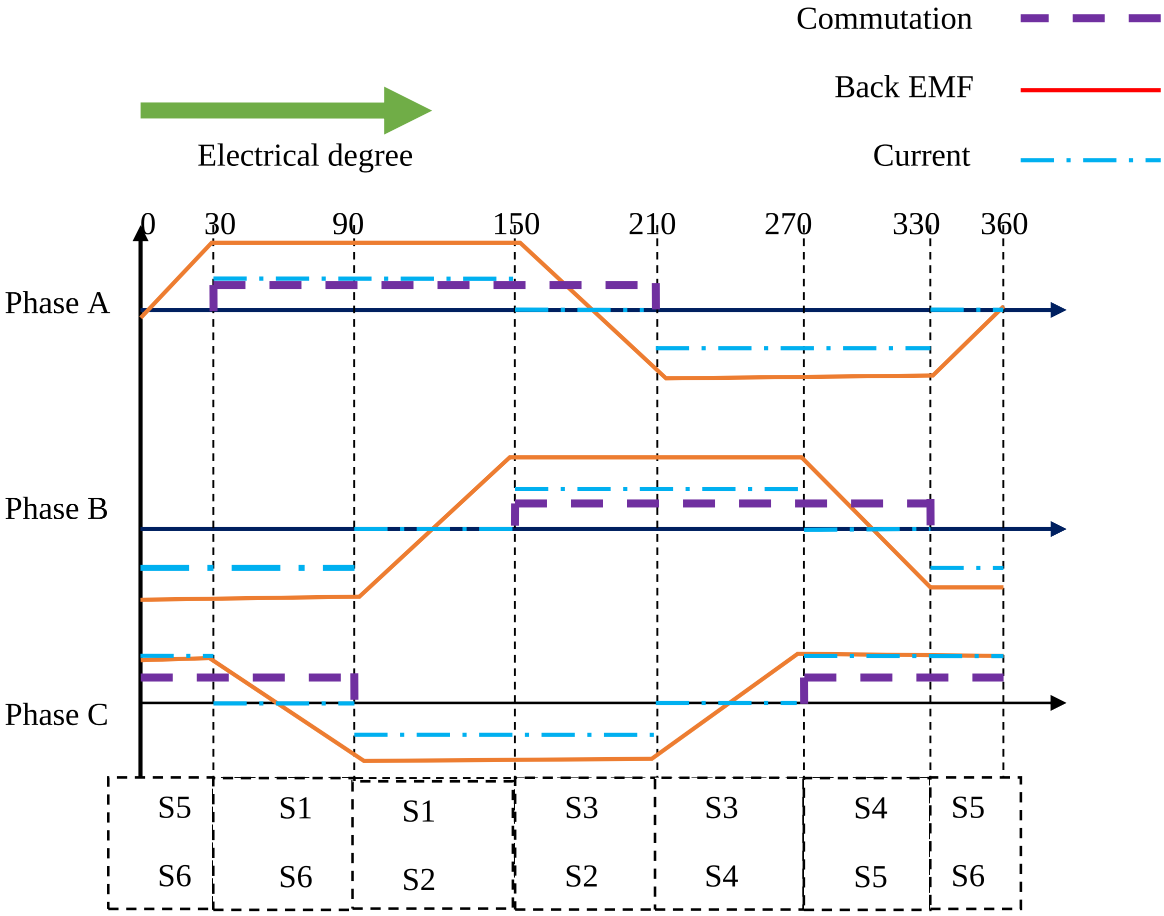

Figure 2. 10: Ideal current, back-EMF and commutation signals of BLDC motor drive

The BLDC motor winding is energized in a sequence based on the rotor position. When the permanent magnet BLDCM is near the hall sensor-A then the winding of phase A will be positively energized. Since permanent magnet on the rotor of BLDM and the positively energized stator winding of phase-A have the same magnetic polarity repel each other. Then the winding of phase-B will be negatively energized so that the permanent magnet rotor will be attracted toward stator winding of phase B. The same process is followed for the stator winding of phase C. As the result the rotation of the BLDCM rotor will be continued based on the required command speed by the user.

There are a number of ways to drive the inverter for BLDC motor drive. Some of them are explained below.

2.4.1. Depending on inverter controlling technique

2.4.1.1.Six step inverter feed VVS based speed control of BLDC motor drive

This technique is applicable in the case of, if variable voltage source is used. The duty cycle of the speed controller output determines the input voltage to the inverter. The inverter switches will be controlled depending on rotor position. The hall sensor rotor position signal is decoded to the exact required duty cycle and` generate zero and one via logical gates to drive the inverter switches.

2.4.1.2. Hysteresis current controller based BLDC motor drive

Hysteresis current controller can be used for trapezoidal BLDC motor drive. Differ from a six step inverter feed VVS based BLDC motor drive, the output of speed regulator will not directly control input voltage but through the inverter switches control. The output of the speed regulator produces reference torque. The peck value of the reference current is produced by multiplying torque and torque constant. Then the reference current of each phases are produced multiplying the peak reference current and decoded hall sensor signal. Then it is the difference of reference current and phase current that determines the ON- OFF states of the inverter switches by using comparator and logical circuits.

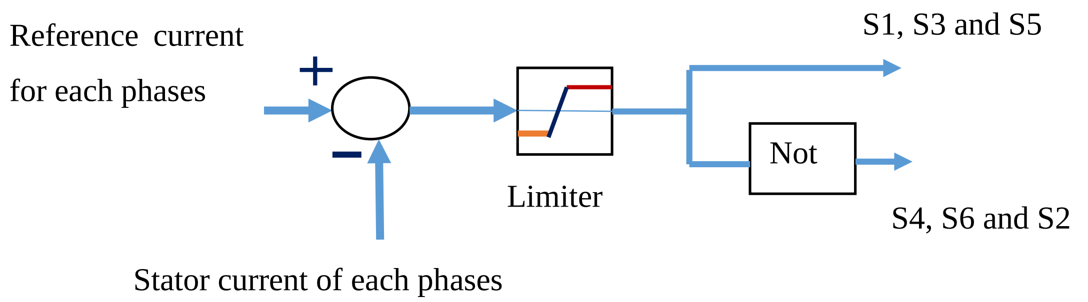

Figure 2. 11: Hysteresis current controller based BLDC motor drive for each phases

2.5. Closely related works on BLDC motor speed control

Researchers reported several papers on BLDC motor speed control by using several methods and algorithms. Even though the same common schematic diagram explained in figure (2.7) is used by researcher's different inverter switching drive techniques, different speed regulator and current controller algorithms are used. As the result, they got different outputs results. The closely related work to the proposed research thesis with their corresponding output results, merits and demerits are discussed in the case of both switching drive technique and speed regulation techniques they used as the following:

An electric vehicle parameters matching based on vehicle performance with 15.29kW electric power consumption per 100Km is designed for the Chinese typical urban cycle [21]. The investigation of the motor capacity and simulation for an Electric Vehicle studies are in literature [22]. The comparative study of the commutation methods for the three-phase permanent magnet brushless DC motor shows that trapezoidal commutation generates torque ripples at low speeds and is relatively efficient in the high speed range but, the sinusoidal commutation provides smooth operation at low speeds, but it is inefficient in the high speed range [23].

The analysis of BLDC motor speed control based hysteresis current controller modulation technique with the PI speed controller is performed in literature [24]. The result of the study is concluded as the hysteresis current modulation technique works better when compared with six switched controlled inverter feed variable voltage source method. However, from the result, it can be seen that the rise time is about 0.4Sec per 1000rpm. Therefore the dynamic response time of the speed specifically rise time needs improvement. In a similar ways the modeling and simulation of torque hysteresis controller for BLDC motor drives is performed, and it is concluded as the hysteresis controller can offer inherent current protection/limitation and robustness in controlling the motor torque. But the result shows that, torque ripple is about 33% and speed dynamic performance specific rise time of the speed is 0.3 per 30rpm [25]. In similar algorithm the closed loop speed control of a laboratory fabricated brush-less DC motor drive prototype using position sensor is performed [26]. Their result shows that torque ripple is about 15% and 20% from designed end and control end respectively.

BLDC motor speed control by using PI based fuzzy logic is performed in the literature by using a hysteresis current controller based modulation. Their result shows that the speed dynamics performances of the motor has the rise time 0.05, overshoot 10% and settling time

0.09Sec. Comparing with PI controller, PI based fuzzy logic gives us better control performance. But the drawback of their work is larger torque ripple i.e. about (35%) and also they did not show what the result will be under variable speed and load [27] [28]. Instead of the PI controller if PID controller is used for speed control of Brushless DC Motor by using a hysteresis current controller the dynamic characteristics are highly desirable in industrial drive and automotive applications [29]. The performance analysis of a BLDC drive under varying load by using variable voltage source control method with PI controller is performed [30]. The result shows that the dynamic performance of the speed is quite good and can be further improved if PID controller is used instead of PI. The result of their study can be summarized as shown in table (2.4).

Table 2. 4: Dynamic performance analysis of BLDC motor under variable load

	Cases of study				
No	Dynamic performance of the motor	No load	Sudden application of load	Sudden removal of the load	Gradual application of the load
1	Overshoot (%)	2.83	5.23	5.23	2.83
2	Rise time (sec)	0.026	-	-	0.026
3	Settling time(sec)	0.085	0.065	0.088	0.085
4	Peak time(sec)	0.035	-	-	0.035

In general the performances of BLDC motor with PI and PID controller are discussed. Accordingly PID based speed regulator gives better performance characteristics than PI based speed regulator [31] [32]. Even though the performance of PID controller is better than that of the PI controller still the dynamic performance of PID controller can be increased by selecting appropriate values of PID parameters. If the output signal of PID controller is smooth. The smoothness of PWM modulating signal depends on the smoothness of the PID output signal. If the modulating signal is not smooth enough (tuned) the larger current distortion will be generated. This research thesis focused on analyses of speed control characteristics of the BLDC motor by PWM current controller modulation instead of hysteresis current controller modulation by using PID based (tuning) optimization method.

CHAPTER 3

3. METHODOLOGY

3.1. Introduction

This chapter includes data analysis, design of speed controller, mathematical modeling of the BLDC motor drive, comparisons of speed regulators and BLDC motor drive system setup in MATLAB software. The analysis of the identified motor specification and vehicle dynamics is performed. BLDC motor comparisons with an induction motor, Brushed DC motor, SR motor are explained in the literature. In a similar ways, in order to show BLDC motor is the best selection for EV the comparisons is further made with its highly competitive counter motor PMSM in terms of power output and torque output of the motors. Then modeling of the overall BLDC motor drive is performed. Finally the system is simulated by using MATLAB software.

3.2. Materials

MATLAB software of version 15.0 is used throughout this research study. MATLAB is the general purpose computing software which consists of a vast range of specialized toolboxes. This toolbox performs symbolic algebraic/mathematical manipulative operations with a lot of built-in interactivity [33]. It is a high-level mathematical package designed for doing numerical computations and graphics. MATLAB also has powerful symbolic math ability [34]. MATLAB is undoubtedly popular among computer and multi-disciplinary scientists, engineers and particularly with experts in the area of computational mathematics and Engineering.

3.3. Methods

The following method is used to study the specific objectives of the proposed thesis. First the closely related works are reviewed. Then the necessary data's used throughout this work is collected manually. Some of the specifications value of the tractive motor, inverter and reducer have taken from the center of transportation and vehicle engineering (ASTU). The specification of similar size with the proposed vehicle by the center of transportation and vehicle engineering but, engine based one is obtained from Bishoftu Bass Factory. Then the collected data is analyzed for the purpose of understanding and developing the system modeling. The modeling BLDC motor drive with its speed controller is developed. Then the system is simulated by using MATLAB/Simulink /Code. The result of the simulation is compared for different control algorithms in the case of inverter driving techniques and speed controller schemes. In general the method followed throughout the research study can be summarized as the following flow chart.

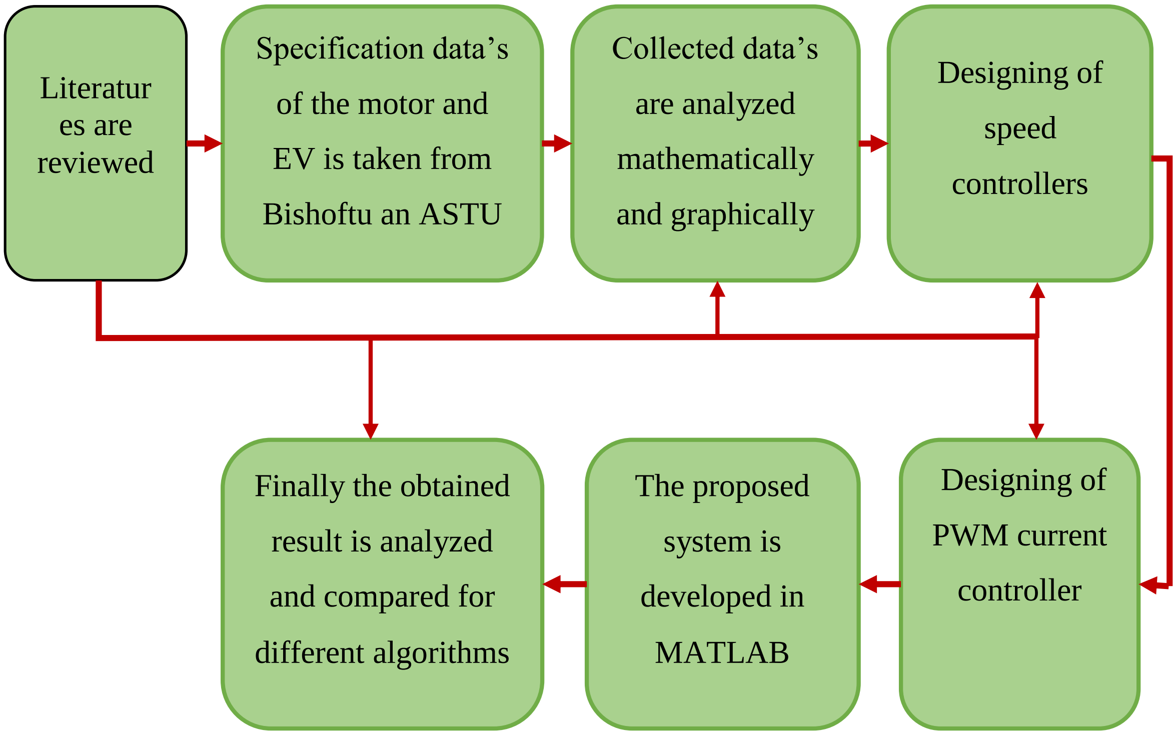

Figure 3. 1: Block diagram of the research methodology

The block diagram of the proposed system is shown below:

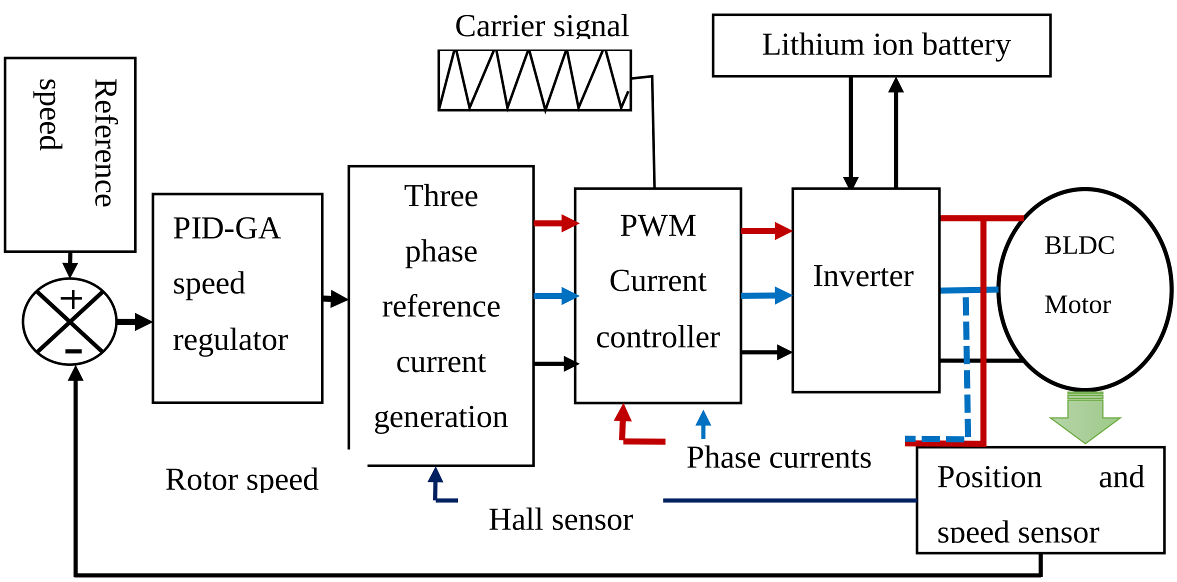

Figure 3. 2: Block diagram of the proposed control system

The working principle of this block diagram is shown as the following. The difference of the reference speed and rotor speed is controlled by using speed regulator. GA-PID speed controller is proposed. Then the output of speed regulator gives the torque command. The peak reference current is generated by dividing the torque command by torque constant. Reference current is generated by multiplying the peak reference current and decoded hall sensors. Two phases of the stator current is taken as the stator current feedback because, once the two current phases are known the third phase is negative summation of the two phases. The difference of phase current and the corresponding reference current is controlled by using PWM current controller. PWM current controller consists of current regulator, comparator and logical circuit which is used to generate inverter driving signals.

3.4. Analysis of an Electric vehicle dynamics

Before modeling and simulation of BLDC motor speed controller it is necessary to analysis the collected data's of proposed vehicle to find the missing data's and to understand the performance analysis as well as the relationship between parameters of the vehicle. The five main components of EV are shown in figure (3.3). Those are: battery, BLDC motor controller, BLDC motor, reducer and the load. The parameters of these components are essential to analyze the performance of the EV. It is the first step to analyze the motive force of the vehicle under different condition to determine the values of the motor parameters. The size of the tractive motor (power rating) depend on the load going to be derived.

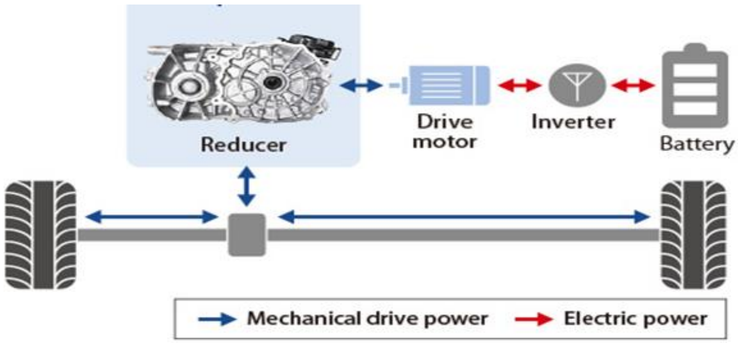

Figure 3. 3: Pure Electric Vehicle Power System Structure [L2]

3.4.1. Motive force, Motive power and Motive torque of the Vehicle

The force propelling the electric vehicle has to overcome the rolling resistance force (F_R), gradient resistance force (F_G), aerodynamic drag forces (F_A) and forces required for acceleration (F_{ac}). In this thesis the car of gross weight 1500kg is considered as per collected data from center of transportation and vehicle engineering in order to select the required motor power rating and another specification of data's of tractive motor. The total force required for driving a vehicle is calculated as in equation (3.1) [35] [36] [37].

$$F_{total} = F_R + F_G + F_A + Fac \quad (3.1)$$

The total force is the tractive force that the motor must overcome, in order to drive the vehicle.

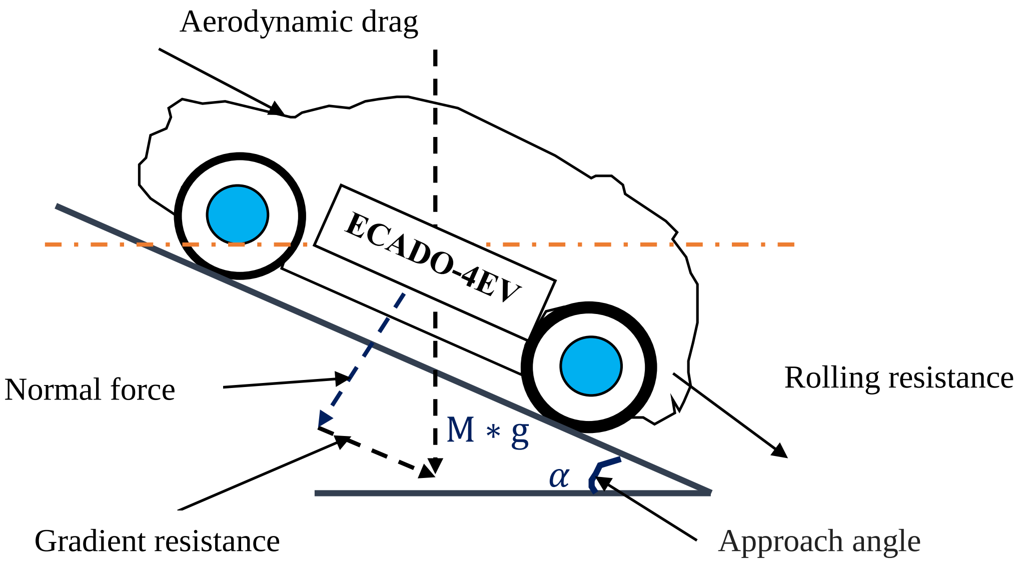

Figure 3. 4: Exerted forces on moving electric vehicle

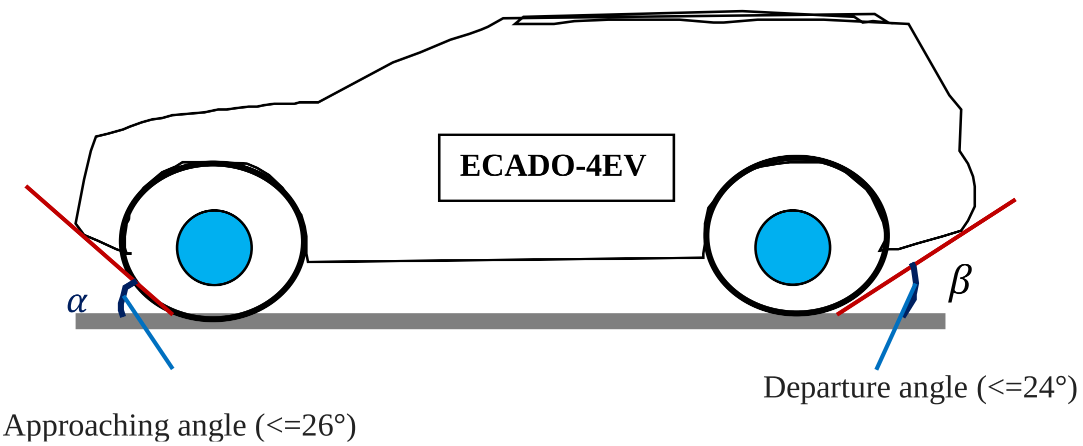

Figure 3. 5: The approaching angle and departure angle of the car

The main forces need to be overcome by the EV are shown as the following points:

3.4.1.1. Rolling resistance force

Rolling resistance force is the resistance occurred on the vehicle due to the contact of the tires with road and it is calculated as in equation (3.2) where, C_{rr} is the coefficient of rolling resistance (table 3.1), g is acceleration due to gravity and M is the gross mass of the vehicle in kg [21] [36] [37].

$$F_R = C_{rr} * M * g * \cos(\Theta) \quad (3.2)$$

$$F_R = C_{rr} * M * g * \cos(\Theta) = 0.01 * 1500 * 9.81 * \cos(26°) = 132.12272N$$

The power required to overcome the rolling resistance of the 132.12272N is:

$$P_R = F_{rolling} * velocity\left(\frac{m}{sec}\right) = 132.12272 * \frac{100}{3600} = 3.673KW$$

3.4.1.2. Gradient resistance

Gradient resistance of the vehicle is the resistance offered to the vehicle while climbing a hill or flyover or while travelling in downward slope. The angle between the ground and slope of the path is represented as α as shown in figure (3.4).

$$F_G = M * g * \sin(\Theta) = 1500 * 9.81 * \sin(26°) = 6450.631425N$$

$$P_{gradient} = F_{gradient} * velocity\left(\frac{m}{sec}\right) = 6450.631425 * \frac{51.444}{3600} = 92.1795KW$$

3.4.1.3. Aerodynamic drag

Aerodynamic drag is the resistive force offered due to viscous force acting on the vehicle. It is largely determined by the shape of the vehicle. The formula for calculating the aerodynamic drag is given by the equation. [21] [36] [37]

$$F_A = 0.5 * C_A * A_f * \rho * (V + V_0)^2 \qquad (3.3)$$

Equation (3.3) shows that, the aerodynamic force of the car is directly proportional to the square of the sum of the speed of the vehicle and the speed of the air. Substituting the values of constants in equation (3.3), the aerodynamic force as the speed of the vehicle varies from 0 to 110 km/hr can be plotted as shown in figure (3.6) by taking the assumption that the speed of the air is zero.

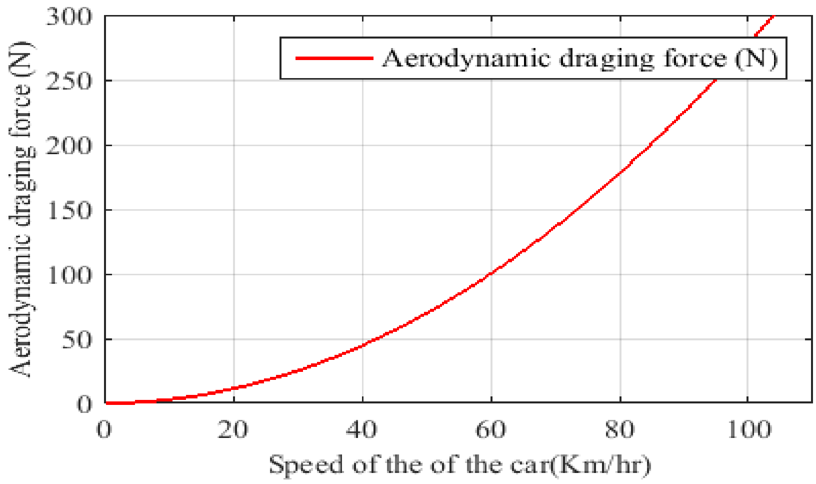

Figure 3. 6: Aerodynamic dragging force versus speed of the car in Km/hr.

3.4.1.4. Acceleration forces

There are the three main forces which act on the vehicle when it travels at constant speed. But, while the vehicle is accelerating or decelerating the effect of force due to inertia also acts up on the vehicle. Gradient force increases as the approaching angle of the road increases and aerodynamic force is constant if the speed of the vehicle is assumed to be constant. The total motive force with each component of force acting on the vehicle is shown in figure (3.7). In this figure the vehicle is assumed to move up a hill with constant speed of 51.444Km/hr and the velocity of the air is also assumed to be zero.

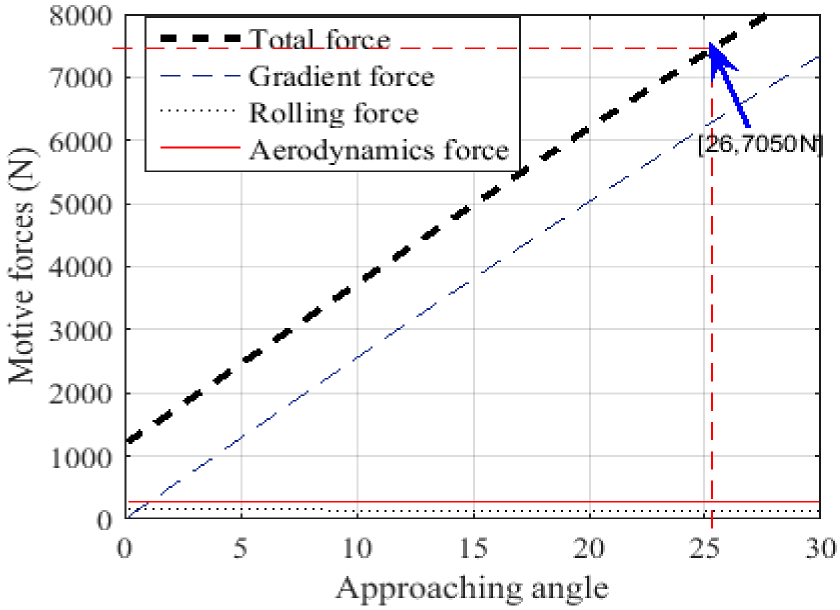

Figure 3. 7: Motive force versus approaching angle of the vehicle

The coefficient of friction of different types of surface used in the analysis of data is taken from literatures.

Table 3. 1: The coefficient of friction for different types of surface [37] [36]

Contact surface	Coefficient of friction
Concrete surface (good/fair/poor)	0.010/0.015/0.02
Asphalt (good/fair/poor)	0.012/0.017/0.022
Macadam (good/fair/poor)	0.015/0.022/0.037
Snow/dirt	0.025/0.037
Mud (firm/medium/smooth)	0.037/0.09/0.15
Grass (firm/soft)	0.055/0.037
Sand (firm/soft/dune)	0.060/0.15/0.3

In a similar ways when the vehicle is moving on straight rod, the gradient force acting on the vehicle will be zero. The total motive force with each components of force acting on the vehicle is shown in figure (3.8). In this figure the vehicle is assumed to be moving within the range of an average speed from (0 to 130Km//hr) with $0.5\text{m}/\text{sec}^2$ acceleration on straight line. The kinetic friction and static friction of the road is assumed to be 0.01 and 0.1 respectively.

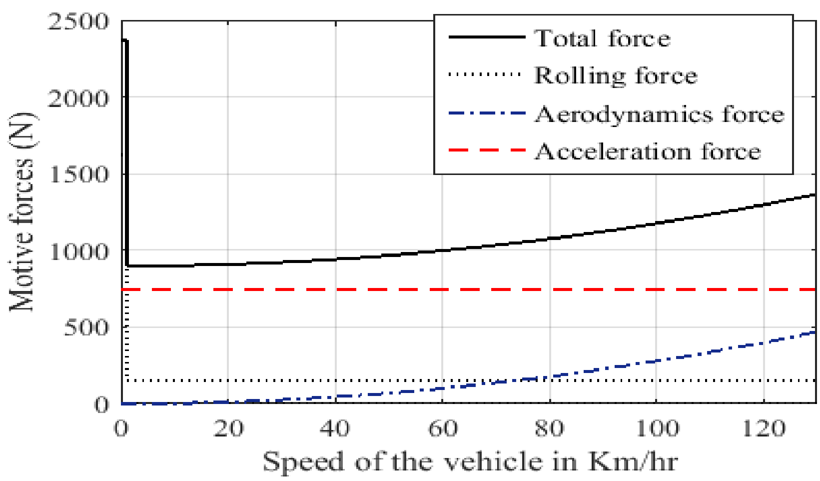

Figure 3. 8: Motive force versus speed of the vehicle in Km/hr.

From figure (3.7) and (3.8) we can determine the required maximum power need to be generated by BLDC motor in order to propel the vehicle in all conditions of motion. Therefore, the maximum tractive power required to propel the vehicle will be:

$$P_{total(max)} = 3.673\text{KW} + 92.1795\text{KW} + 1.5\text{KW} = 97.3525\text{KW}$$

But, electric motor with output power rating of 97.3525KW should not be selected. The losses due transmission of power to the wheel must be included. Therefore, the mechanical power output (Motor tractive) required to drive the vehicle is given by equation below:

$$M_{tractive(peak)} = \frac{P_{out\ total(max)}}{\eta_{\ of\ transmission\ gear\ system}} = \frac{97.3525\text{KW}}{0.95} \approx 100\text{KW}$$

The maximum tractive power is supplied when the vehicle is clamping the hill of maximum approaching angle which is 26 degree with its full load at the speed of 51.444Km/hr. The reason why the speed of the vehicle is reduced while clamping the hill is to increase torque with limited power supply of battery and limited power output of the motor. If we need to use larger battery size and motor of larger power rating the penalty is cost and weight increment. Figure (3.9) shows the power need to be supplied by the motor to drive the vehicle at constant speed of 51.444Km/hr. with various approaching angle.

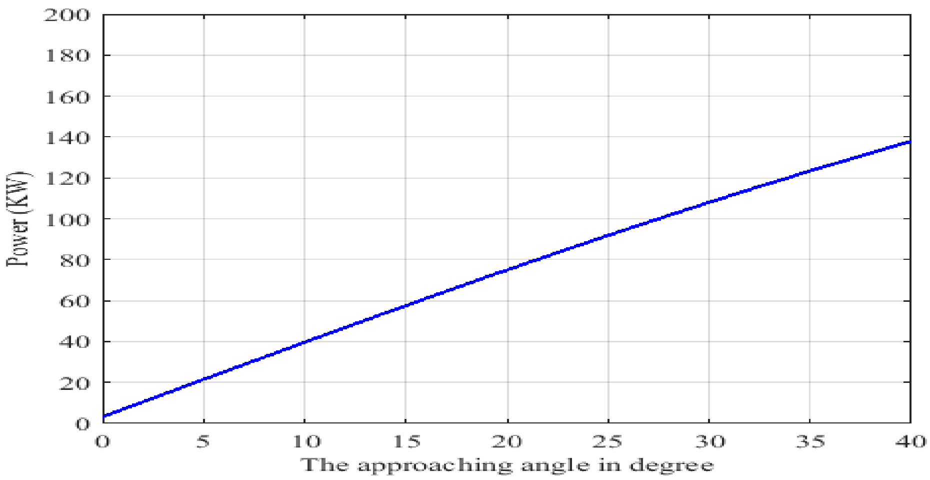

Figure 3. 9: The motive power conception with respect to an approaching angle

In this figure it is assumed that the car is moving with constant speed of 51.444Kmph and suddenly come to face an inclined road of a defined approaching angle. From this figure we can see that 100KW power is enough to propel the car over maximum approaching angle of 26 degree, but with reduced speed of 51.444Km/hr. As the speed of a vehicle increasing its power consumption will also increase. Therefore, it's necessary to identify the maximum power and rated power of a defined vehicle propelling motor, so that the speed as well as torque requirements will be fulfilled. A vehicle with its full load with an initial speed of zero meter per second starts to move with an acceleration of $1m/s^2$ on the straight line road is considered. The speed versus consumed power of the vehicle can be as shown in figure (3.10).

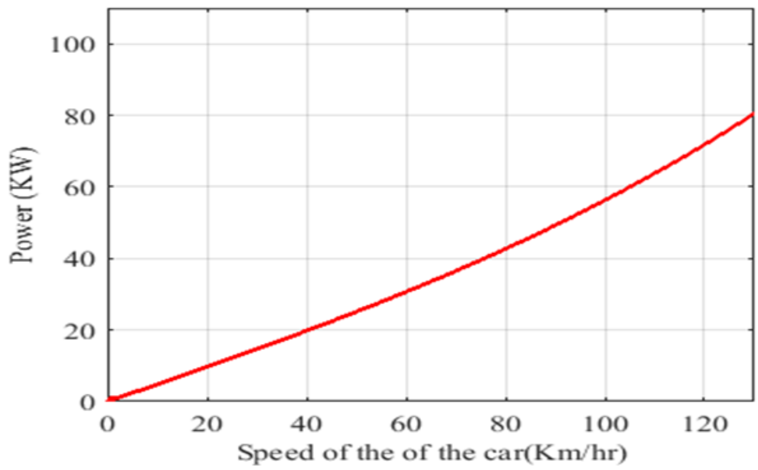

Figure 3. 10: Consumed power versus speed of the vehicle in (km/hr.)

From the above figure we can say that, the vehicle can move with the speed of 130 km/her with power consumption of 80KW that is below the identified maximum power. It is also necessary to identify the rated torque and maximum torque of the motor requirement in order to model the system. Once the power output of the motor required to propel the vehicle is known the torque and the speed of the vehicle can be corrected by the gear system. The rated torque can be found from figure (3.11) at the rated speed of 3600rpm which is 159.23Nm. It is also shown that if we need to increase the speed beyond the base speed torque need to be reduced since a vehicle is working with a limited power supply and for the purpose of heating reduction.

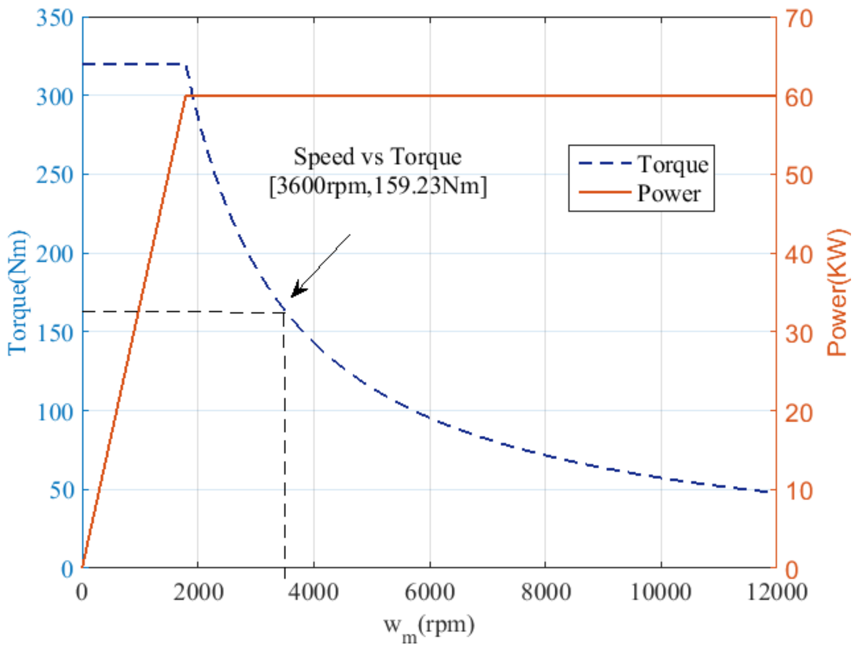

Figure 3. 11: Power and torque characteristics of BLDC motor

3.4.2. Vehicle specification

Table 3. 2: Tractive motor & vehicle specifications

Parameters	Values
Maximum power (KW)	100
Gross weight (Kg)	1500
Rated power(KW/rpm)	60/3600
Maximum torque (Nm/rpm)	320/1978
Rated torque (Nm/rpm)	159.23/3600
Maximum speed (Km/hr.)	130
Rated speed (Km/hr.)	100
Approaching angle/departure angle (°)	26/24
Seating capacity (persons)	4

3.4.3. Reducer 320Nm &Drive shaft

The reducer is the bridge between the motor and the driving shaft that. Drive shaft transfer the power, torque and rotational speed from the motor to the front wheel. Reducer specification is shown in the following table [ECADO-4EV].

Figure 3. 12: Reducer and Shaft [L3]

Table 3.3: Reducer & Drive shaft specifications

Performance	
Torque (max)	320Nm
Input speed (max)	12000rpm
Gear ratio	9.96

Dimension	
Length	521.3mm
Height	388.6mm
Stator diameter	253.24mm
Weight	28Kg

3.4.4. Traction motor

3.4.4.1. Selection of Traction Motor

In literature, it is shown that BLDC motor is the best selection for EV compared to induction motor, RS motor and DC motors. But PMSM motor is highly competent with BLDC motor especially in the case of weight, efficiency, having less torque ripple and so on. Even though these two motors are highly competent to each other BLDC motor has better futures in case of having a higher power output, higher torque density, cost and simplicity. The power output ratio of these two motors is derived as the following, based on equal cupper losses principle of their stators. Let I_{ps} and I_p be the peak value of PMSM stator currents and the Peak value of BLDM stator currents respectively. The rms values of these currents are:

$$I_{pmsm} = \frac{Ips}{\sqrt{2}} \text{ and } I_{BLDCM} = I_p * \sqrt{\frac{2}{3}} \quad (3.4)$$

Equating the cupper losses of the two motors and substituting for the currents in terms of their peak currents as

$$3I_{pmsm}^2 R_a = 3\, I_{BLDCM}^2 R_a \qquad (3.5)$$

Substituting the rms currents in equation (3.5) and solving for the peak current of BLDC motor in terms of the peak current of PMSM motor:

$$I_p = \frac{\sqrt{3} x I_{ps}}{2} \qquad (3.6)$$

The peak values of the induced EMF in PMSM and BLDCM are equal and denoted by E_p. As we can see from the basic excitation wave form of BLDC motor shown in figure (3.13), it is shown that only two phases conduct at the same time and output power is contributed by only two phases. On the contrary, the PMSM has the currents in all its phases and hence power output is contributed by all the three phases. The output power of the two motor is given as:

$$P_{out}BLDCM = 2E_p x I_p \qquad (3.7)$$

$$p_{out}PMSM = \frac{3E_p x I_{ps}}{2} \qquad (3.8)$$

$$\text{Output Power ratio} = \frac{\text{PM dc brushless power}}{\text{PM synchronous power}} = 1.1547 \qquad (3.9)$$

Assuming the P.F of PMSM is unity and using equation (3.6) into equation (3.7) the power output ratio of BLDC motor to PMSM will be as in equation (3.9): Equation (3.9) shows that BLDC motor has 15% more output power density than the PMSM.

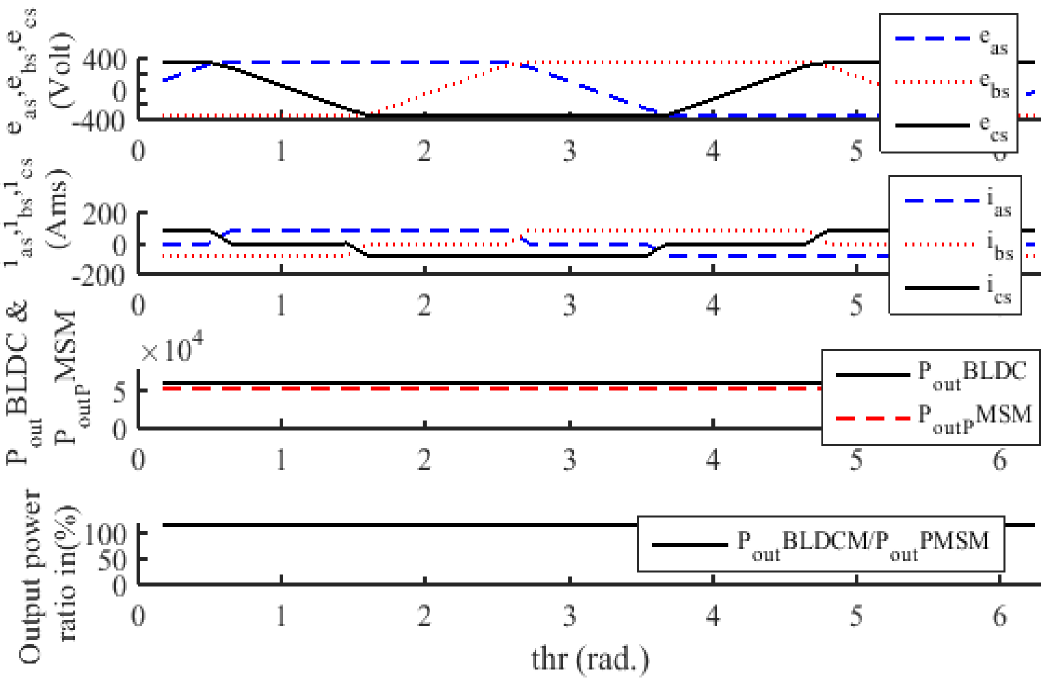

Figure 3. 13: Stator currents, EMF and output power ratio of BLDC motor to PMSM

By using equations from (3.4) to (3.9) in MATLAB the induced three phase stator voltage, three phase stator current and power output of BLDCM as well as the power density ratio of BLDCM to PMSM is shown as in figure (3.13).

If the similar condition missioned above is considered the torque output density of BLDC motor is larger than the torque output density of PMSM. If the base speed of 180 rad/sec and the rated power of 60KW as well as maximum torque of the 320Nm of BLDC motor of the same cupper loss compared with its counter PMSM motor is considered, the output torque and output power of the two motors can be summarized as in figure (3.14). From this figure it can be seen that the power output and torque density of BLDCM is larger than that of PMSM by 15.47% and hence suitable for the applications which require larger torque values like EV, train and industries. Therefore BLDCM is recommended for EV propulsion.

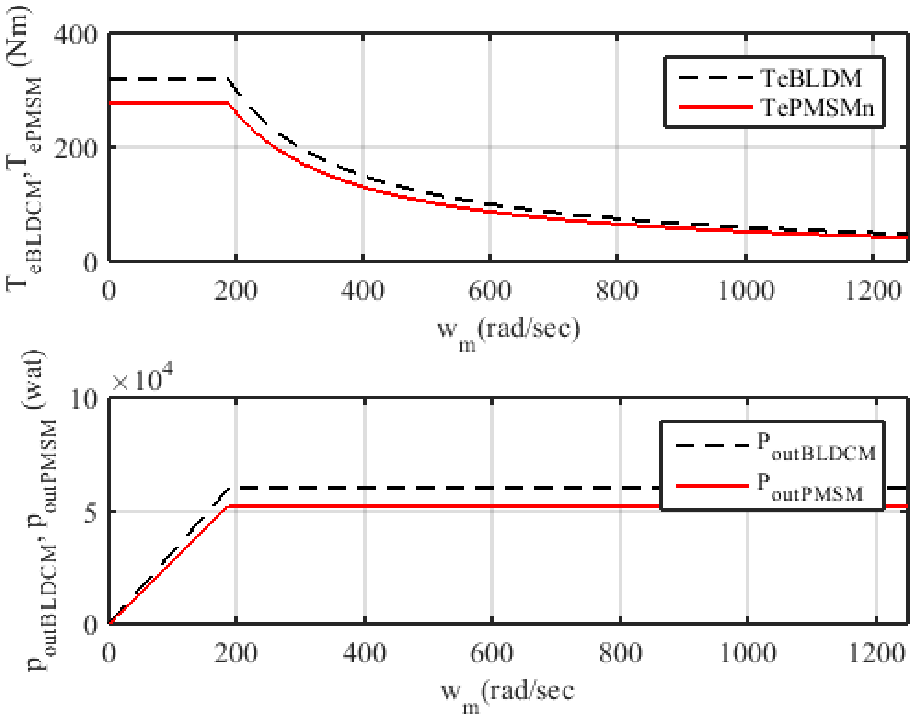

Figure 3. 14: Torque density and power output of BLDCM and PMSM

Even though, BLDC motor has larger output power and torque density than PMSM it is inferior to PMSM in high speed range and field weakening operational application. Furthermore, BLDC motor has higher torque ripple than PMSM.

3.4.4.2.Traction motor specification

Figure (3.15) shows the BLDCM parameters as the stator current is increasing from 0 Amps to 320 Amps. The objective of this figure is to find the rated value of the phase current. The maximum power and power rating of the motor is the summation of power loss and the mechanical power required to propel the vehicle. The current rating of the motor is the current at the rated power which is found to be 172amps. Besides, the power loss, output power and efficiency of the motor with respect to stator current is also shown. The efficiency of the motor is maximum at the stator current 45 amps to 85 amps.

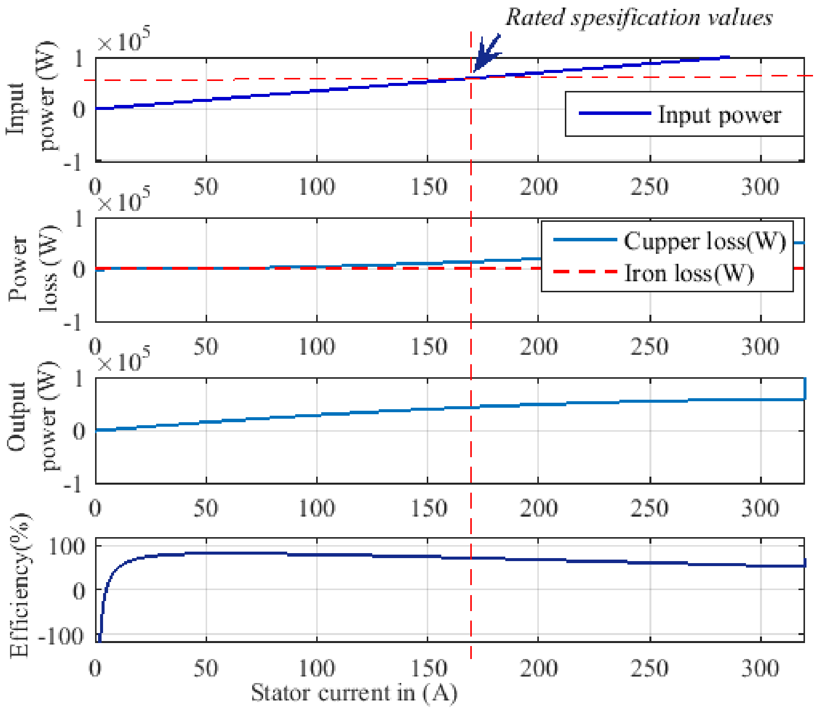

Figure 3. 15: Rated and maximum values of BLDCM parameters used for EV

$$\text{power(max)} = 2 * \text{Em} * I_m$$

$$\text{Em} = \frac{\text{power(rated)}}{2 * I_m} = \frac{60\text{KW}}{2 * 172} = 174.186\text{V}$$

$$\text{EMF constant } (K_b) = \frac{E_m}{\omega_{\text{rated}}} = \frac{174.186\text{V}}{3600\left(\frac{2\pi}{60}\right)} = 0.46204\left(\frac{\text{V}}{\frac{\text{rad}}{\text{sec}}}\right)$$

If two phase operating system of BLDCM is considered $K_b = 2 * 0.46204 = 0.924$.

$$\text{Torque(rated)} = k_t I_{m\ \text{rated}} = \frac{2 * E_{m\ \text{rated}} * I_{m\ \text{rated}}}{\omega_{\text{rated}}} = \frac{2 * 174.186 * 172}{376.99118\text{rad/sec}}$$

$$\text{Torque constant } (K_t) = 0.924$$

$$\text{Rated torque} = K_t * I_{m\ \text{rated}} = 0.924 * 172 = 159\text{Nm}$$

The resistance of the phase winding increases with the increment of temperature. This result in power loss and damage to the motor if it exceeded a certain limit. Therefore appropriate cooling must be used. The phase resistance of the BLDC motor used in this thesis is taken at from figure (3.16) at 80 degree Celsius which if found to be **1.2** ohm.

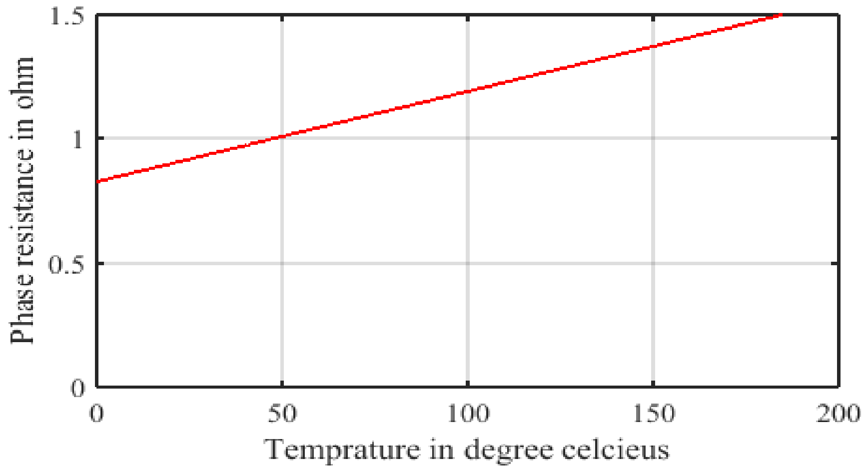

Figure 3. 16: Phase resistance versus temperature

In general the BLDC motor specifications used in this thesis is given as in table (3.4).

Table 3. 4: Parameters specification of BLDCM used in this thesis

Parameters	Values
Poles	4
Efficiency	90.4% @ rated value
Phase winding resistance	1.2 Ohm @80℃
Phase inductance	2.95×10−3
Power factor	0.85
Viscous damping	0.001 (N.m.s)
Moment of inertia	8.495×10^-3 (kg-m^2)
Torque constant	0.924
EMF constant	0.46204

3.4.5. Battery specifications

3.4.5.1. Matching Power Battery Parameters

The power source of the pure electric vehicles is battery. The selection of battery parameters must meet the demand of endurance mileage requirements and maximum power of vehicle driving. Lithium ion battery is selected as the power source for electric vehicles due to its long life and mass energy density.

3.4.5.2. Lithium ion battery pack

The lithium battery pack can able to store the DC power for EV. The lithium battery packs consists of standard lithium battery module in serial. The standard lithium battery module is connected in serial. Each battery module have 4KWh storage. The serially linked more than eight battery modules i.e. more than 32KWh total battery pack power with rated DC voltage of 350V is required for proposed EV. By using the battery specification listed in table (3.5) the SOC of the battery can be explained as shown in figure (3.17).

Table 3. 5: Battery specifications used [ECADO-4EV]

Parameters	**Values**
Cell type	Lithium polymer
Total battery power pack	32KWh
Rated DC power supply	350V
Capacity (mAh)	90Ah
Dimension (W*D*H)	52*225*231cm
Mass	4.3kg
Nominal voltage	4.2V
Energy density	154Wh/kg
Operating temperature	-10 to 50℃
Energy	666Wh

$$P = P_{max}x0.15 + 0.85xP@_{zero\ grad\ and\ constant\ speed} \quad (3.10)$$

$$P_m = \frac{P}{\eta_m} \quad (3.11)$$

$$W_{road} = P_m t = \frac{P_m S}{V} \quad (3.12)$$

$$SOC\ \% = \frac{(W_{rated} - W_{road})x100\%}{W_{rated}} \quad (3.13)$$

Where P is the power required for the automobile at constant speed, S is endurance mileage, W_{road} is the energy needed for mileage S, P_m is the input power of the motor controller and η_m is the motor and motor controller assembly efficiency.

By considering the EV with the 32KWh pack energy and 25KW input power to the traction motor of the vehicle moving at constant speed of 100K/hr, the SOC versus mileage in kilometer can be analyzed as shown in figure below.

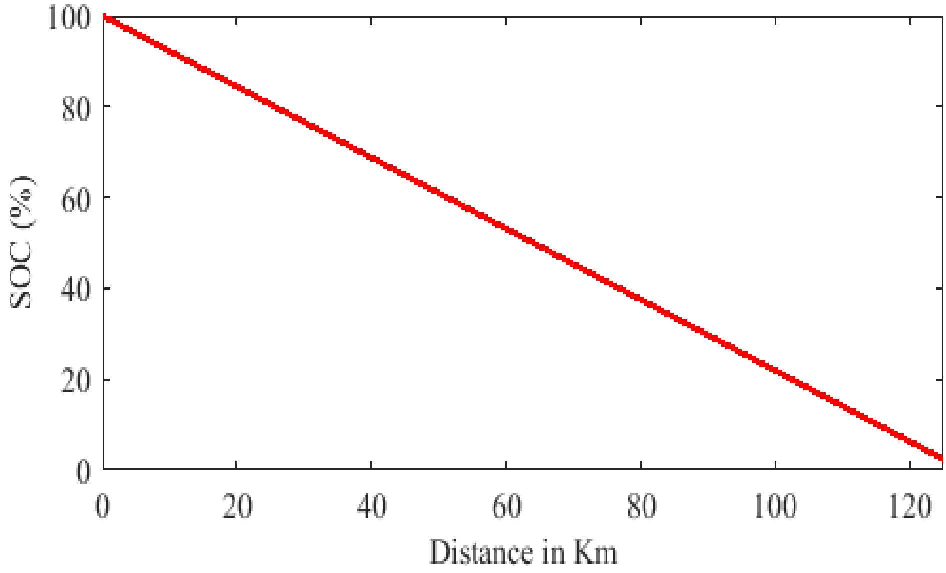

Figure 3. 17: SOC in percentage versus mileage in kilometer

From this figure it is seen that, the vehicle can move more than 110 Km per charging time at a constant sped of 100Km/hr with total battery pack energy of 32KWhr, which achieves the performance index of the mileage for at least 80km per charging time [21].

3.5. Modeling of Brushless DC motor Drive for Electric Vehicle Propulsion

An accurate and precise model of the BLDC motor drive is required to study the control algorithms of the motor drive. In this thesis three phase star connected BLDC motor with hall sensor control technique is considered because of the reason mentioned in the previous chapter. An accurate model of the BLDC motor which gives, the precise values of torque, speed, current and back-EMF is required to study the various control schemes of the motor drive. The modelling of BLDC motor, BLDC motor controllers and overall BLDC motor drives are discussed and simulated in this section.

3.5.1. Mathematical Modeling of the BLDC Motor

The modeling of BLDC motor helps us to understand the nature and characteristics and the working principle of the motor. Three phase, 4-pole and star connected concentric full-pitch winding with salient permanent magnet rotor of BLDC motor is considered. Since the flux distribution of brushless DC motor is trapezoidal, the d-q rotor reference frame model developed for PMSM and induction motor is not applicable [38].

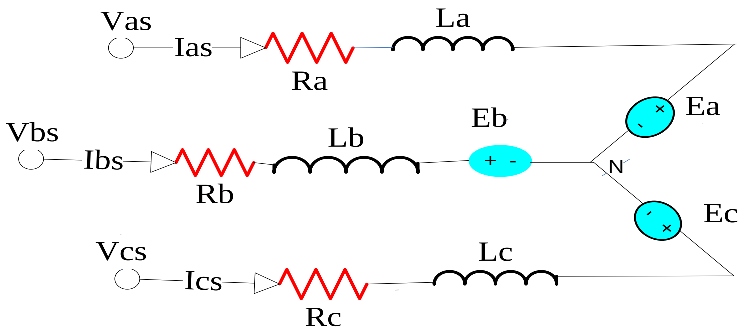

Figure 3. 18: Stator connected three phase BLDC motor winding

Following assumptions are made to simplify the mathematical equations and the overall BLDC motor model.

- Magnetic circuit saturation is ignored;
- The corresponding stator resistance, self-inductance and mutual inductances of each phases are equal;
- Hysteresis and eddy current losses are eliminated;
- Inverter semiconductor switches are ideal

The derivation of this model is based on the assumptions that the induced currents in the rotor due to stator harmonic fields, iron loss and stray losses are neglected. For the balanced three phase stator phase winding motor the self-inductance of each phase are equal to each other. In a similar ways the mutual inductance between each phase of the winding are equal and the sum of phase or line current of the stator becomes zero. Then the phase voltage of and induced EMF of BLDCM can be given by equation (3.14 & 3.15) respectively where x represents the A, B and C phases of the stator.

$$\begin{bmatrix} V_A \\ V_B \\ V_C \end{bmatrix} = \begin{bmatrix} R & -R & 0 \\ 0 & R & -R \\ -R & 0 & R \end{bmatrix} \begin{bmatrix} i_a \\ i_b \\ i_c \end{bmatrix} + \begin{bmatrix} L-M & 0 & 0 \\ 0 & L-M & 0 \\ 0 & 0 & L-M \end{bmatrix} \frac{d}{dt} \begin{bmatrix} i_A \\ i_B \\ i_C \end{bmatrix} + \begin{bmatrix} E_a \\ E_b \\ E_c \end{bmatrix} \qquad (3.14)$$

$$E_x = \frac{d\lambda_x}{dt} \qquad (3.15)$$

The flux and line to line voltage of the stator is shown in appendix A.1 and A.2 respectively.

3.5.1.1. Modelling of Trapezoidal Back Electromotive Force

The back EMF signals have a phase shift of 120 electrical degrees with respect to each other due to symmetrical distribution of the phase winding in the stator. The EMF of each phase can be expressed as in equation (3.16);

$$E_a = \omega_m \left(\frac{K_b}{2}\right) f_A(\theta_r)$$

$$E_b = \omega_m \left(\frac{K_b}{2}\right) f_A\left(\theta_r + \frac{2\pi}{3}\right) \tag{3.16}$$

$$E_c = \omega_m \left(\frac{K_b}{2}\right) f_A\left(\theta_r - \frac{2\pi}{3}\right)$$

Provided, that K_b is the EMF voltage constant of the motor, ω_m is the mechanical speed ω_r is the electrical speed of the motor (rad/Sec). For the given values of the maximum permanent magnet flux linkage of each winding (λ_p) and the number of poles (P), the electrical speed of the motor and voltage constant of EMF can be given as shown in equation (3.17 & 3.18).

$$\omega_r = \left(\frac{P}{2}\right)\omega_m \tag{3.17}$$

$$K_b = P\lambda_p \tag{3.18}$$

The rotor position function, $f_{A,B,C}(\theta_r)$, is generated by writing MATLAB program with respect to the electrical angle of the permanent magnet rotor position as shown in (appendix B) depends on the following equations:

$$f_A(\theta_r) = \begin{cases} \left(\frac{6}{\pi}\right)\theta_r & 0 < \theta_r \le \frac{\pi}{6} \\ 1 & \frac{\pi}{6} < \theta_r \le \frac{5\pi}{6} \\ \left(-\frac{6}{\pi}\right)\theta_r + 6 & \frac{5\pi}{6} < \theta_r \le \frac{7\pi}{6} \\ -1 & \frac{7\pi}{6} < \theta_r \le \frac{11\pi}{6} \\ \left(-\frac{6}{\pi}\right)\theta_r - 1 & \frac{11\pi}{6} < \theta_r \le 2\pi \end{cases} \tag{3.20}$$

$$f_B(\theta_r) = f_A\left(\theta_r + \frac{2\pi}{3}\right)$$
$$f_c(\theta_r) = f_A\left(\theta_r - \frac{2\pi}{3}\right) \tag{3.21}$$

The trapezoidal rotor position function are limited between +1 and -1 and these functions are modeled as the following diagram.

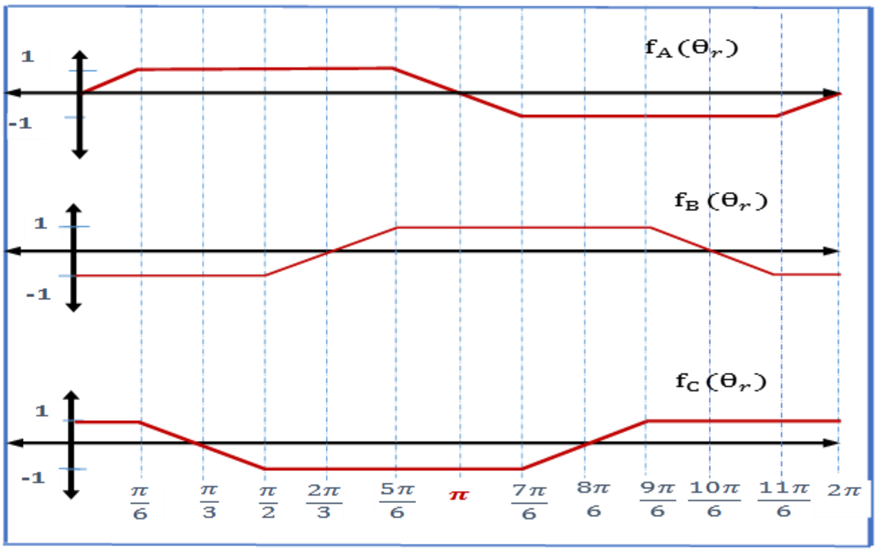

Figure 3. 19: Three phase trapezoidal rotor position waveforms

An ideal reference back-EMF waveforms of the BLDC motor model with respect to the rotor electrical degree is shown in Figure (3.20). This figure shows that EMF voltage is the constant multiplication of generated trapezoidal rotor position function.

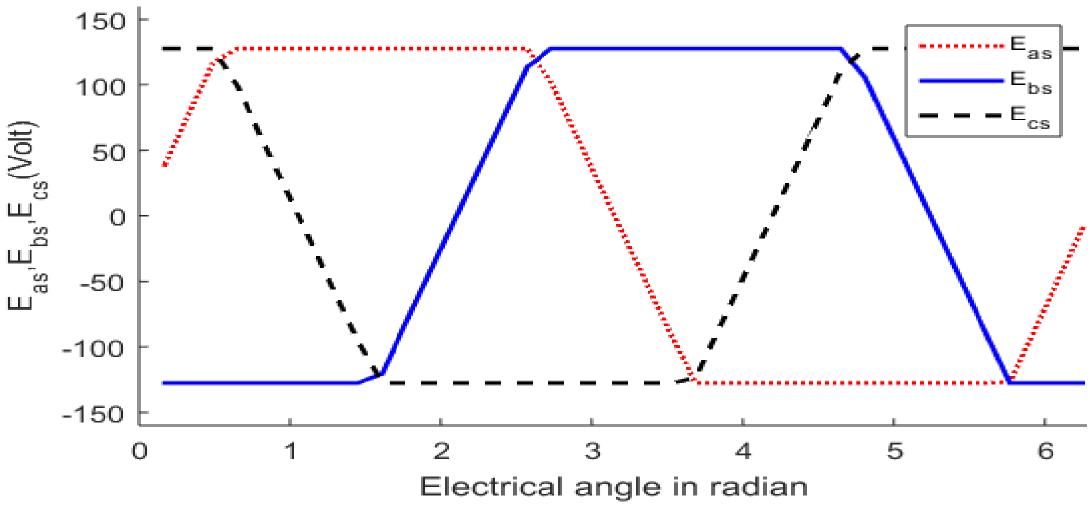

Figure 3. 20: Trapezoidal induced EMF in stator winding

The trapezoidal EMF is due to the stator phase current lagging of the motor.

3.5.1.2. Mechanical Equation of Motion

The mechanical part of the equation of motion is given as the following equations.

$$T_e = T_a + T_b + T_c = \frac{E_a I_a + E_b I_b + E_c I_c}{\omega_m} \quad (3.22)$$

$$T_e = J\frac{d\,\omega_m}{dt} + B\omega_m - T_L \quad (3.23)$$

$$\omega_r = \frac{d\,\theta_r}{dt} \quad (3.24)$$

3.5.1.3. Modeling of Hall Effect sensor

Three hall-effect sensors (H_a, H_b and H_c) are displaced by an angle of 120° phase shift on stationary part of BLDC motor to detect the position of the rotor. Hall-effect sensor is modeled based on the electrical degree of angle as shown in table (3.6) [39].

Table 3. 6: Hall Effect sensors with rotor position

Sequence number	Electrical angles in degree	Hall Effect sensors		
		Ha	Hb	Hc
0.	0-60	1	0	0
1.	60-120	1	1	0
2.	120-180	0	1	0
3.	180-240	0	1	1
4.	240-300	0	0	1
5.	300-60	1	0	1

In general the Simulink model of the three phase BLDC motor is modeled as shown in (appendix A.1).

3.5.1.4.Transfer function of BLDCM and the load

BLDC motor is very similar to the DC motor. But the similarity holds only when two phases are conducted during the interval where the rotor flux linkages are constant as seen from these phases and all the phases are electrically symmetric and balanced [40]. During two-phase conduction, the inverter output voltage, V_{is} is applied to the two phases having an impedance which is given by equation (3.24).

$$Z = 2\{R_s + s(L - M)\} = R_a + sL_a \quad (3.24)$$

The inverter output voltage is the same as the stator voltage and is given as:

$$V_{is} = (R_a + sl_a)I_{as} + E_{as} - E_{cs} \quad (3.25)$$

The induced emf in phase A and C are equal and opposite during the regular operation of the drive scheme and given as:

$$E_{as} = -E_{as} = \lambda_p \omega_m \tag{3.26}$$

$$V_{is} = (R_a + sl_a)I_{as} + 2\lambda_p\omega_m = (R_a + sl_a)I_{as} + K_b\omega_m$$

Where the emf constant for both the phases is combined into one constant as

$$K_b = 2\lambda_p \frac{V}{rad/sec} \tag{3.27}$$

The electromagnetic torque for two phases combined is given by

$$T_e = 2\lambda_p I_{as} = K_b I_{as} \tag{3.28}$$

The load is assumed to be proportional to speed. If it is not proportional to the speed the load torque is truly a disturbance. In that case it is incorporated in the block diagram suitably but, ignored in the controller design for most of the applications.

$$T_l = B_l \omega_m \tag{3.29}$$

The simplified transfer function of the BLDC motor can be given as shown in equation 3.20.

$$\frac{I_{as}(s)}{V_{is}(s)} = K_1 \frac{1 + sT_m}{(1 + sT_1)(1 + sT_2)} \tag{3.30}$$

The simplification procedure to these transfer function is shown in appendix (A.3).

$$-\frac{1}{T_1}, -\frac{1}{T_2} = -\frac{1}{2}\left[\frac{B_t}{J} + \frac{R_a}{l_a}\right] \pm \sqrt{\frac{1}{4}\left(\frac{B_t}{J} + \frac{R_a}{L_a}\right)^2 - \left(\frac{{K_b}^2 + R_a B_t}{JL_a}\right)} \tag{3.31}$$

Substituting for the values of identified BLDC motor in the above equations the transfer function of the motor is performed as the following:

$$T_m = \frac{J}{B_t} = \frac{0.008495}{0.001} = 8.495\text{sec}$$

$$B_t = B_1 + B_l = 0.001\text{N.m.s}$$

$$T_1 = 0.0084324 \text{ and } T_2 = 0.00346854$$

$$K_1 = \frac{B_t}{{K_b}^2 + R_a B_t} = \frac{0.001}{0.925^2 * 0.001} = 0.0011671$$

$$\frac{\omega_m(s)}{I_{as}(s)} = \frac{925}{1 + 8.495s}$$

$$\frac{I_{as}(s)}{V_{is}(s)} = 0.0011671 \frac{1 + 8.495s}{(1 + 0.0084324s)(1 + 0.00346854s)}$$

3.5.2. Transfer function of inverter

The transfer function of inverter is represented as a first-order lag with a gain given by equation (3.32).

$$G_r(s) = \frac{V_{is}(s)}{V_c(s)} = \frac{K_r}{1 + sT_r} \tag{3.32}$$

Where K_r value of gain is evaluated for line to line output voltage and T_r delay time of the inverter switches which is calculated as:

$$K_r = 0.65\frac{V_{dc}}{V_{cm}} = 0.65 * \frac{350}{10} = 22.75$$

$$T_r = \frac{1}{2f_c} = \frac{1}{2 * 8000} = 6.25 * 10^{-5}$$

Provided that, V_{dc} is the dc link voltage input to the inverter, V_{cm} is the maximum control voltage and f_c is the switching (carrier) frequency of the inverter.

$$G_r(s) = \frac{22.75}{1 + 6.25 * 10^{-5}s}$$

3.5.3. Current feedback and Speed feedback

A low pass filter with the time constant of less than a millisecond which is in the order of a few PWM sampling times may be included in the analysis of current controller design. But in this thesis no filtering is used for current feedback analysis. But, the speed feedback with a low-pass filter shown as in equation (3.33) is used. Where K_ω is the gain and T_ω is the time constant of the filter respectively.

$$G_\omega(s) = \frac{K_\omega}{1 + sT_\omega} \tag{3.33}$$

3.5.4. Design of Current and Speed Controller

The overall closed loop BLDC motor drive system contains two main closed loops. Those are the current closed loop and speed closed loop. The design of control loops proceed from the inner to outer loop, because of several reasons. The first one is, to reduce complexity i.e. to calculate the gain and time constant of the controller at a time instead of solving the gain and time constants of all controller simultaneously. The second one is every motor drive not need to be speed-controlled but may be torque controlled. In that case, the current loop is essential and exists whether the speed loop is going to be closed or not. Besides the performance of the outer loop is dependent on the inner loop and therefore the tuning of the inner loop has to precede the design and tuning of the outer loop. The overall block diagram of BLDC motor drive model is as shown in figure below:

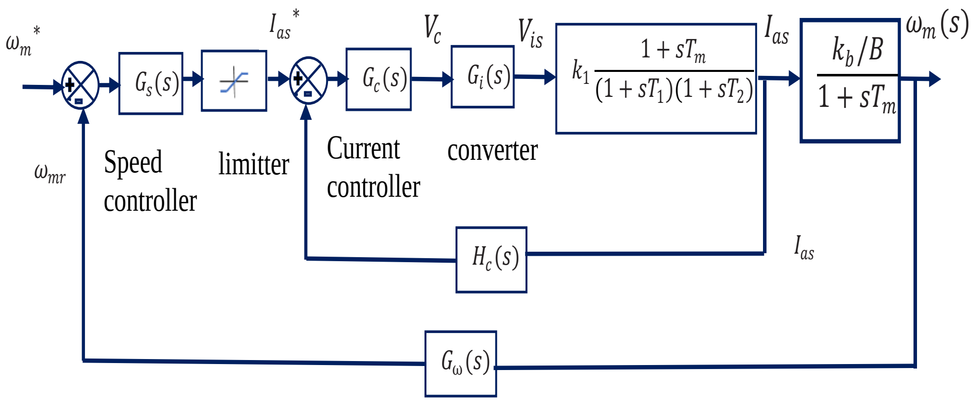

Figure 3. 21: Block diagram of the BLDC motor drive S-function model

3.5.4.1. Current controller

The PI, PID and PID-ZN controllers are compared and the one with best control capacity is selected as a controller.

3.5.4.1.1. PI current controller

The current control loop with PI current controller gain loop function shown in figure (3.21) is given as:

$$\mathrm{GH_i(s)} = \left\{\frac{\mathrm{K_1K_cK_rH_C}}{\mathrm{T_c}}\right\} * \frac{(1+\mathrm{sT_m})(1+\mathrm{sT_c})}{\mathrm{s}(1+\mathrm{sT_1})(1+\mathrm{sT_2})(1+\mathrm{sT_r})} \tag{3.34}$$

The mechanical time delay, $\mathrm{T_m}$ is in the order of a second and in the vicinity of the gain crossover frequency. Therefore the following approximation is valid.

$$1 + sT_m \cong sT_m \tag{3.35}$$

The time constants in the denominator are seen to have the relationship $\mathrm{T_r} < \mathrm{T_2} < \mathrm{T_1}$ and selecting PI current controller time constant $\mathrm{T_c} = \mathrm{T_2}$ the equation (3.34) will be reduced to second order gain function in order to facilitate a simpler controller synthesis.

$$\mathrm{GH_i(s)} = \frac{\mathrm{K}}{(1+\mathrm{sT_1})(1+\mathrm{sT_r})} \tag{3.36}$$

$$\mathrm{K} = \frac{\mathrm{K_1K_cK_rH_CT_m}}{\mathrm{T_c}} \tag{3.37}$$

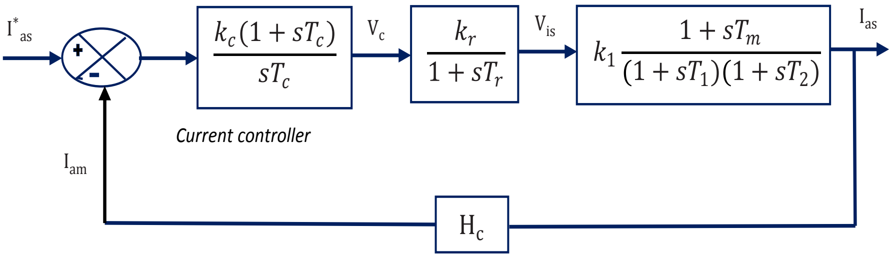

Figure 3. 22: S-function model of current control loop

From the characteristic equation between command current and stator current shown in equation (3.34), the natural frequency (ω) and damping ratio (ε) can be written as:

$$(1 + sT_1)(1 + sT_r) + K = T_rT_1\left\{s^2 + s(\frac{T_r + T_1}{T_rT_1}) + \frac{K + 1}{T_rT_1}\right\}$$

$$\omega_n^2 = \frac{k + 1}{T_rT_1} \tag{3.38}$$

$$\varepsilon = \frac{\left\{\frac{T_r+T_1}{T_rT_1}\right\}}{2\sqrt{\frac{k+1}{T_rT_1}}}$$

It is an accepted practice to have a damping ratio of 0.707 for good dynamic performance [41] and hence equating the damping ratio to 0.707,

$$K + 1 = \frac{\left(\frac{T_r+T_1}{T_rT_1}\right)^2}{\frac{2}{T_rT_1}} \tag{3.39}$$

Realizing that, K>>1 and $T_1 \gg T_r$ the value of K can be approximated as:

$$K \cong \frac{T_1^2}{2T_rT_1} \cong \frac{T_1}{2T_r} \tag{3.40}$$

Equating equation (3.37) and (3.40)

$$K_c = \frac{1}{2}.\frac{T_cT_1}{T_r}\left(\frac{1}{K_1K_rH_CT_m}\right) = 1.03737324 \tag{3.41}$$

The speed loop is designed by replacing the second order current loop with an approximate first-order model in order to reduce the order of overall speed gain function. This approximation is done by adding the time delay (T_r) in the converter block to (T_1) of the motor. Due to the cancellation of one motor pole with a zero of the current controller, the transfer function of the current and its commanded value is given by:

$$\frac{I_{as}(s)}{I_{as}^{*}(s)} = \frac{\frac{K_1 K_r K_C T_m}{T_c} x \frac{1}{(1+sT_3)}}{1 + \frac{K_1 K_c K_r H_C T_m}{T_c} x \frac{1}{(1+sT_3)}} = \frac{K_i}{1 + sT_i} \tag{3.42}$$

Provided that,

$$T_3 = T_1 + T_r = 0.0084324 + 6.25x10^{-5} = 0.0084949$$

$$K_{fi} = \frac{K_1 K_c K_r H_C T_m}{T_c} = \frac{0.0011671 * 1.03737324 * 22.75 * 1 * 8.495}{0.00346854} = 67.4592$$

$$T_i = \frac{T_3}{1 + K_{fi}} = \frac{0.0084949}{1 + 67.4592} = 1.24087x10^{-4}$$

$$K_i = \frac{K_{fi}}{H_c} x \frac{1}{1 + K_{fi}} = \frac{67.4592}{1} x \frac{1}{1 + 67.459267.4592} = 0.98539$$

Finally the simplified transfer function of the current controller is given as the following.

$$\frac{I_{as}(s)}{I_{as}^{*}(s)} = \frac{K_i}{1 + sT_i} = \frac{0.98539}{1 + 1.24087x10^{-4}s}$$

The current feedback gain (H_c) is 1

The resulting model of the current loop is a first-order system, suitable for use in the design of speed loop. The stator current and reference current response of the above transfer function shows that, the stator current has about 18.75%.

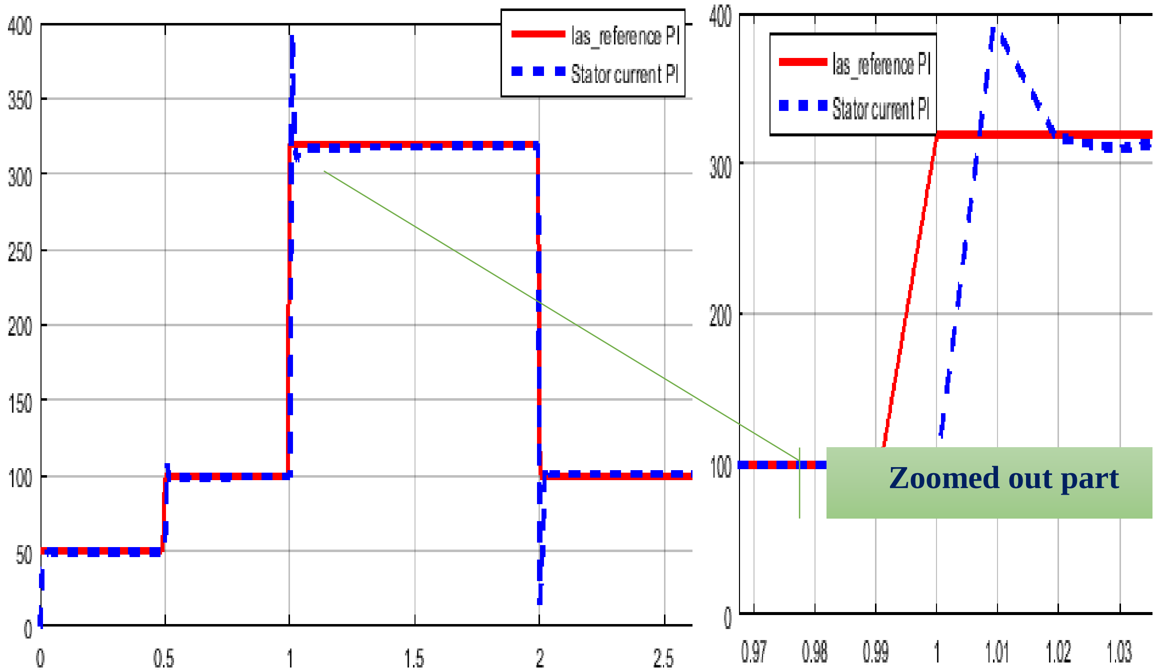

Figure 3. 23: The Command current versus stator current by using PI controller

3.5.4.1.2. ZN-PID current controller

The comparison of ZN-PID current controller PI current controller is performed. As we can see from figure (3.24) ZN-PID current controller has better performance than PI current controller.

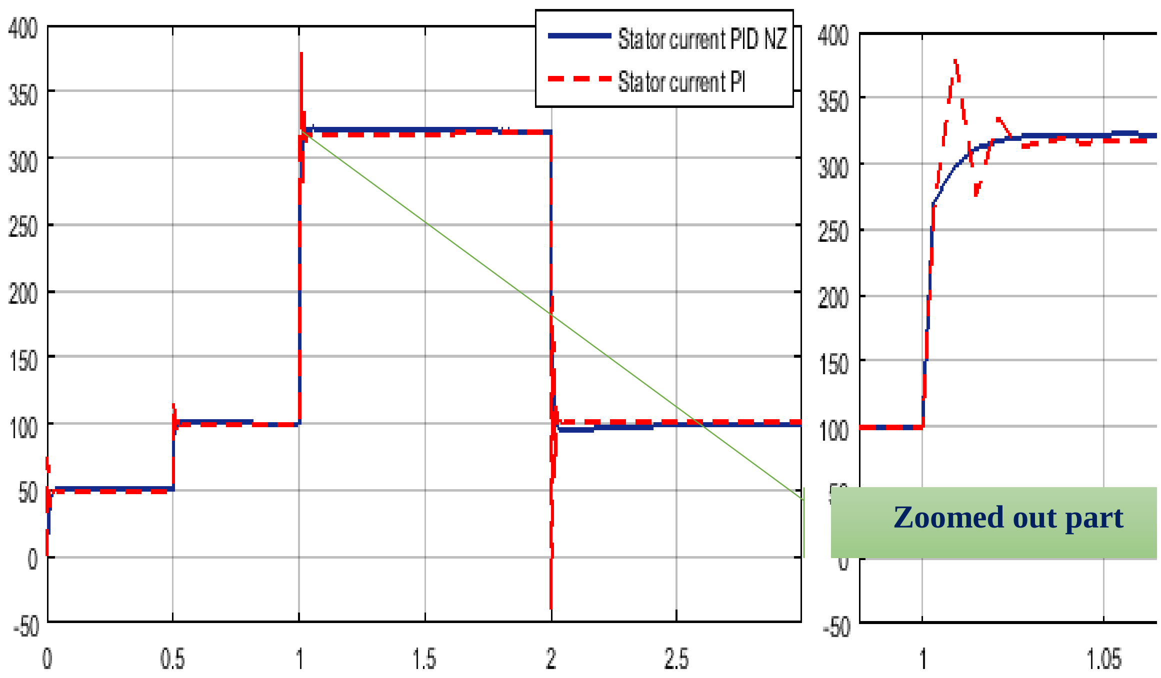

Figure 3. 24: PI and PID-ZN tuning based current controller

3.5.4.2. Speed controller

3.5.4.2.1. Design of PI speed controller by using symmetric optimal approximation method

The speed controller design can be based on any linear control system technique. Out of them the symmetric optimum technique is considered here.

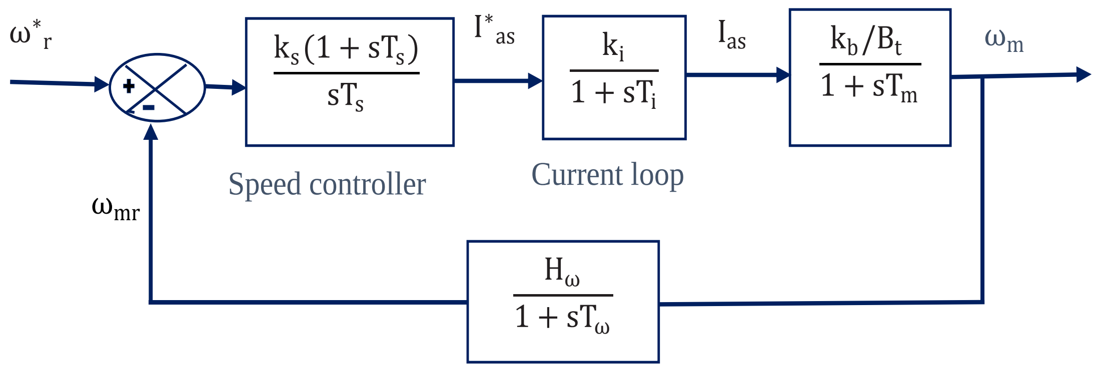

Figure 3. 25: Representation of the outer speed loop in the BLDC motor drive

The loop gain function is given as

$$GH_s(s) = \left\{\frac{K_s K_i K_b H_\omega}{B_t T_s}\right\} \frac{(1 + sT_s)}{s(1 + sT_i)(1 + sT_m)(1 + sT_\omega)} \quad (3.43)$$

In order to reduce the order of the system for the design of speed controller approximation is used. The first approximation is based on the vicinity of the gain crossover frequency. The second approximation is building the equivalent time delay of the speed feedback filter and current loop. Their sum is very much less than the integrator time constant (T_s) and hence the equivalent time delay (T_4) can be considered as the sum of the two delays, (T_i) and ($T\omega$).

$$\begin{gathered} 1 + sT_m \cong sT_m \\ T_4 = T_i + T_\omega \end{gathered} \quad (3.44)$$

The approximate loop gain function of the speed loop shown in figure (3.25) given as in equation (3.45).

$$GH_s(s) \cong \frac{K_s K_2}{T_s} \frac{(1 + sT_s)}{s^2(1 + sT_4)} \quad (3.45)$$

Provided that, $K_2 = \frac{K_i K_b H_\omega}{B_t T_m}$

The closed loop transfer function of speed to its command is given as:

$$\frac{\omega_m(s)}{\omega_m^*(s)} = \begin{cases} \dfrac{1}{H_\omega}\left[\dfrac{\frac{K_2 K_s}{T_s}(1 + sT_s)}{s^3 T_4 + s^2 + sK_2 K_s + \frac{K_2 K_s}{T_s}}\right] \\ \textbf{\textit{or}} \\ \dfrac{1}{H_\omega}\left[\dfrac{(\alpha_o + \alpha_1 s)}{\alpha_0 + \alpha_1 s + \alpha_2 s^2 + \alpha_3 s^3}\right] \end{cases} \quad (3.46)$$

Provided that,

$$\begin{gathered} \alpha_0 = \frac{K_2 K_s}{T_s} \\ \alpha_1 = K_2 K_s \\ \alpha_2 = 1 \\ \alpha_3 = T_4 \end{gathered} \quad (3.47)$$

This transfer function is optimized to have a wider bandwidth and a magnitude of one over a wide frequency range by looking at its frequency response. Its magnitude is given by:

$$\left|\frac{\omega_m(j\omega)}{\omega_r^*(j\omega)}\right| = \frac{1}{H_\omega}\sqrt{\frac{\alpha_0^2 + \omega^2\alpha_1}{\{\alpha_0^2 + \omega^2(\alpha_1^2 - 2\alpha_0\alpha_2) + \omega^4(\alpha_2^2 - 2\alpha_1\alpha_3) + \omega^6\alpha_3^2\}}} \tag{3.48}$$

This is optimized by making the coefficients of ω^2 and ω^4 equal to zero and which yields the following conditions:

$$\begin{aligned} \alpha_1^2 &= 2\alpha_0\alpha_2 \\ \alpha_2^2 &= 2\alpha_1\alpha_3 \end{aligned} \tag{3.49}$$

Substituting these conditions in terms of the motor and controller parameters given in equations (3.49):

$$\begin{aligned} T_s K_s &= \frac{2}{K_2} \\ K_s &= \frac{1}{2T_4K_2} \\ T_s &= 4T_4 \end{aligned} \tag{3.50}$$

Then, substituting for the values of each variables in equations (3.50) then the values of speed controller parameters, PI gain and time constant can be obtained as:

$$T_4 = T_i + T_\omega = 1.24087\text{x}10^{-4}\text{sec} + 0.005\text{sec} = 5.12481\text{x}10^{-3}\text{sec}$$

$$T_s = 4 * 5.12481\text{x}10^{-3}\text{sec} = 0.020499\text{sec}$$

$$K_2 = 107.1894366$$

$$K_s = 1.09865$$

Substituting for K_s and T_s into Equation (3.46) the closed loop transfer function of the speed to its command is simplified as the following.

$$\frac{\omega_m(s)}{\omega_r^*(s)} == \frac{1}{0.999}\text{x}\frac{1 + 0.020499s}{1.07677\text{x}10^{-6}s^3 + 2.101094\text{x}10^{-4}s^2 + 0.020499s + 1}$$

By using the above transfer function in MATLAB the speed profile of the symmetric optimal approximation method (simplified) PI based speed controller versus un simplified PI based speed controller is shown in the figure below. This figure shows that symmetric optimal approximation method (simplified) PI based speed controller has better speed performance than un-simplified one.

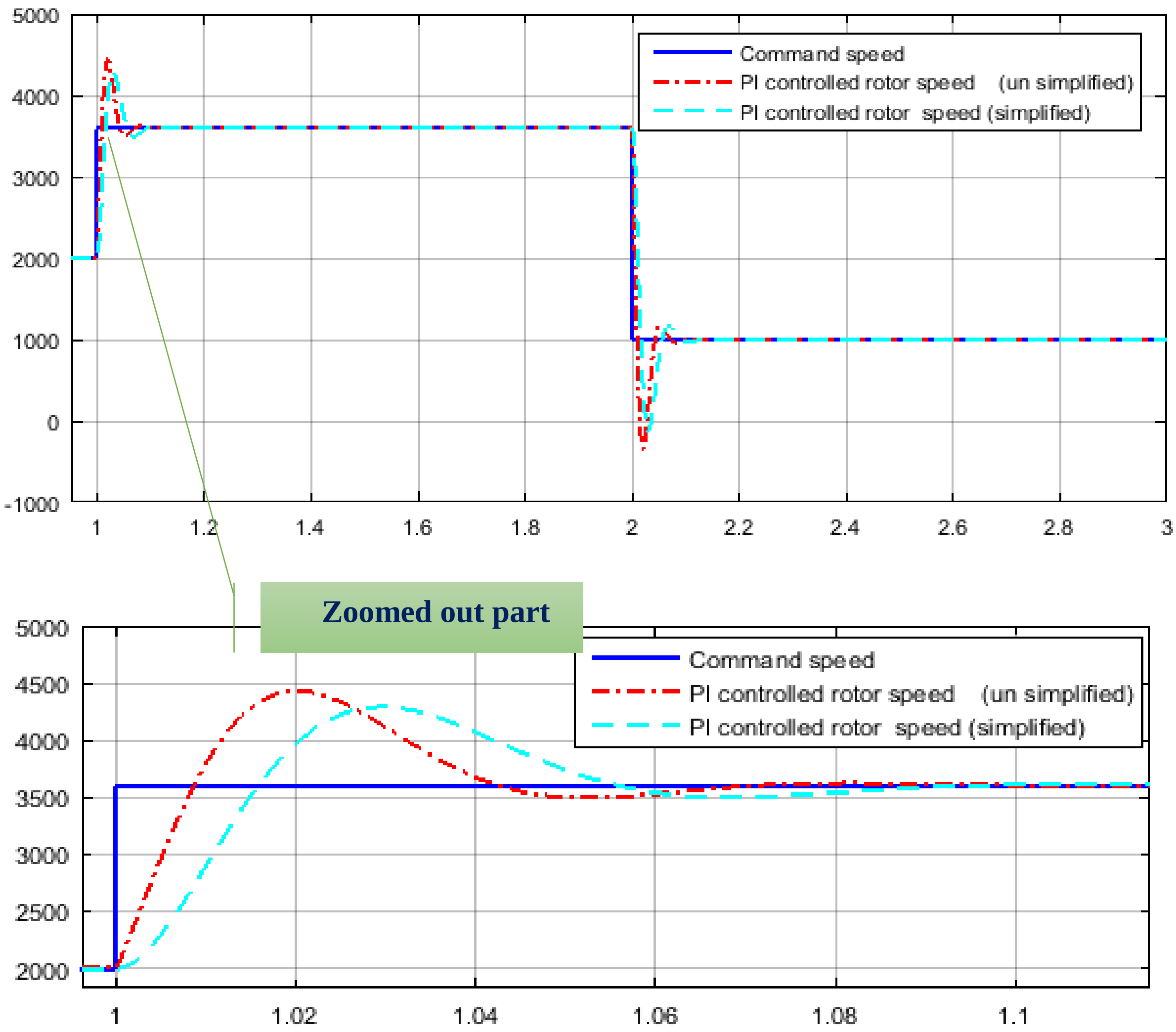

Figure 3. 26: PI based BLDCM motor speed versus reference speed

3.5.4.2.2. ZN-PID based speed controller

Most of commercial controllers provide full PID (also called three term) control action. The process of selecting the controller parameters to meet a given performance specifications is called PID tuning [42]. The PID controller has three term control signal [43].

$$\begin{aligned} U(S) &= K_p\left[1+\frac{K_i}{sK_p}+\frac{sK_d}{K_p}\right]E(s) \\ T_f(s) &= \frac{U(s)}{E(s)} = \frac{K_p(T_iT_ds^2+T_is+1)}{sT_i} \\ T_i &= \frac{K_p}{K_i} \\ T_d &= \frac{K_d}{K_p} \end{aligned} \quad (3.51)$$

Definition: Td is called the derivative action time and is formally defined as, the time interval in which the part of the control signal due to proportional action increases by amount equal to the part of control signal due to derivative action when the error is changing at constant rate [43]. In order to select the proper controller parameters, Ziegler-Nichols PID Tuning specifically Ziegler second Method is described below. In the Ziegler 2nd method, the parameters are assumed in such a way that, $T_i = \infty, T_d = 0$ and proportional controller action K_p is increased from zero to a critical value K_{cr} at which the output first exhibits sustained oscillations. Even if the inertia of the rotor due to the load is larger there is a certain point of K_p at which the response exhibit an oscillation or the system becomes unstable.

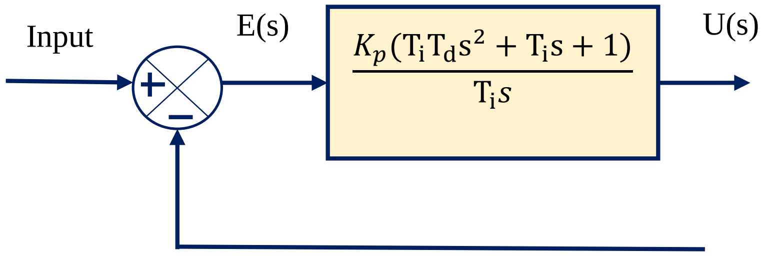

Figure 3. 27: Block diagram of PID controller parameters

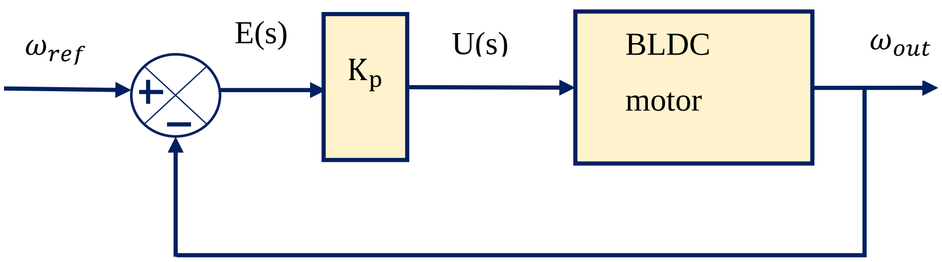

Figure 3. 28: PID controller in proportional action

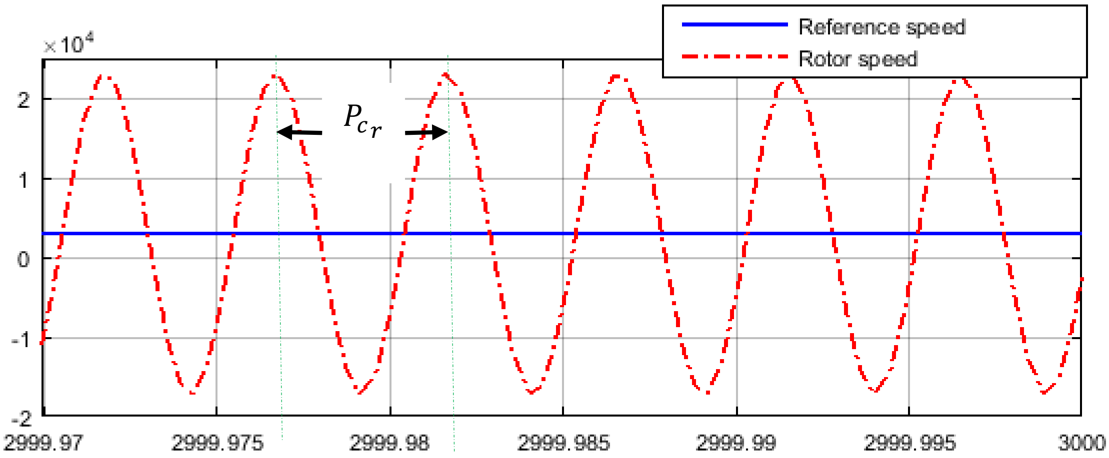

Figure 3. 29: Determination of sustained oscillation P_{cr}

According to Ziegler and Nichols, once the values of critical gain K_{cr} and the critical period (P_{cr}) is determined the values of the parameters K_p, T_i and T_d should set according to the following formula: [42].

$$K_p = 0.6K_{cr}, T_i = 0.5P_{cr}, \text{and } T_d = 0.125P_{cr}$$

The critical gain (K_{cr}) for which the plant output gives a sustained oscillation and the corresponding period (P_{cr}) is found to be 77.10408 and 0.005 respectively. Substituting this values in the above set equation;

$$K_p = 45.3553$$

$$T_i = 0.0025$$

$$T_d = 0.000625$$

There is the risk if K_{cr} is increased by accident to slightly above the marginal stability value, full instability can occur, resulting in damage to the system. Therefore we need to limit K_{cr} using actuator saturation. One of the practical problems of implementing the PID control is that actuator saturation and integral wind-up. Since the range of the increment has the limits, once it is saturated, increasing the magnitude of the control signal has no effect. However if there is the difference between desired and measured values, the resulting error will cause a continuing increase in the integral term, referred to as integral wind-up [42]. When the error term changes its sign, the integral term, started to wind-up and this can cause long time delays and possible instability. Therefore the solution is to limit the maximum value that the integral term can have by using saturation block. The MATLAB/Simulink block diagram of PID controller and saturation block is shown in the following figure:

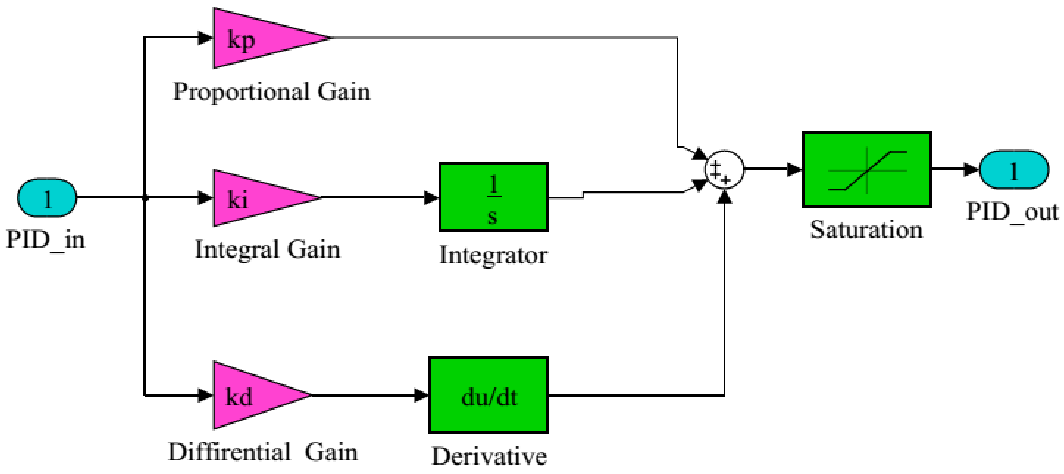

Figure 3. 30: Simulink internal structure of PID controller

The speed dynamic performance comparison of the speed control of BLDC motor by using PI and PID optimization by using Ziegler method explained in figure (3.31) shows that PID-ZN based speed controlled BLDC motor has better speed dynamic performance.

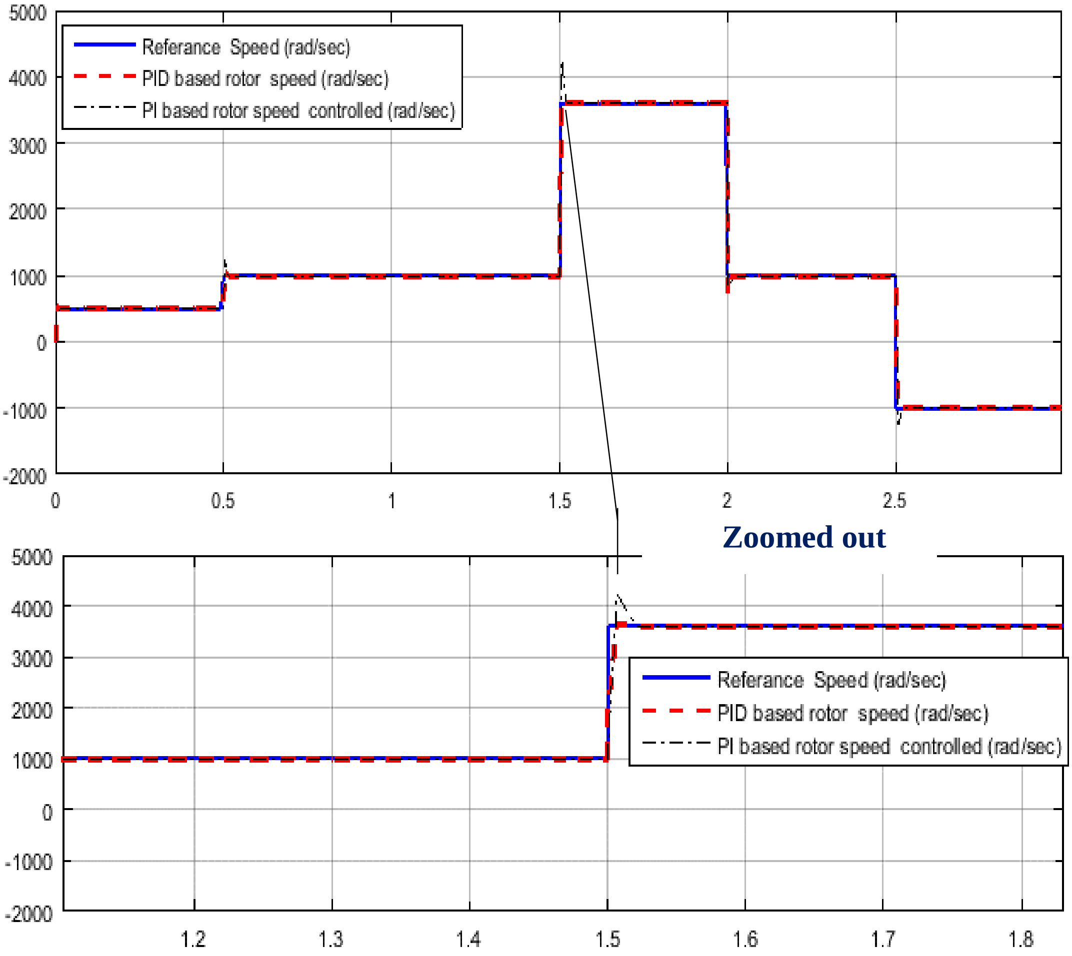

Figure 3. 31: Speed controlled BLDC motor by using PI and PID-ZN tuning method

3.5.4.2.3. GA-PID based speed controller design

Genetic algorithm is a robust technique for optimization based on natural selection that is used to optimize a function called fitness function [44]. GA starts with an initial population containing a number of chromosomes where each individual chromosome represents a solution of the problem and its performance is evaluated by a fitness function. Genetic algorithm consists of three main stages: Selection (reproduction), Crossover and Mutation. Selection retains a fit set of chromosome in the given population. Crossover and mutation involves swapping between two parent strings and flipping a random bit in the set of chromosome respectively [44]. The application of these three basic operations allows the creation of new individuals which may be better than their parents. This algorithm is repeated for many generations and finally stops when reaching individuals that represent the optimum solution to the problem. The GA performance procedure is shown in figure (3.32) [45] [46].

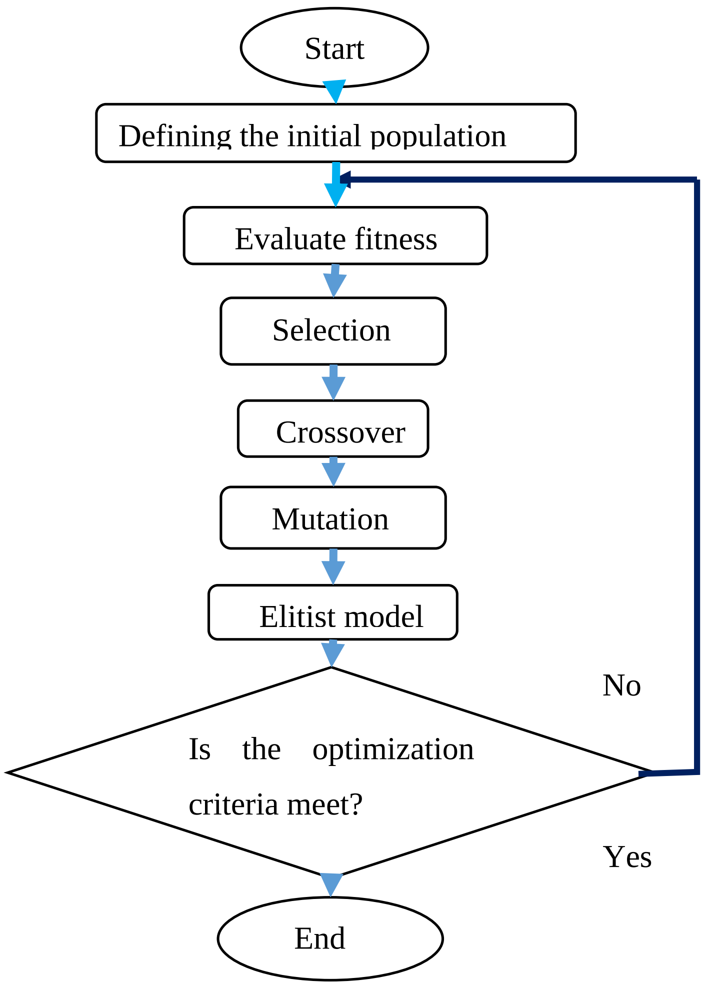

Figure 3. 32: The flow chart for implementation of GA based PID optimization

A. Initializing the Population of the Genetic Algorithm

Initialization is the first step in the implementation of GA based optimization. The initialization of the population size, variable bounds and the evaluation function are required. These are the initial input that are required start the process GA. The initializing MATLAB code for GA is shown below.

```
Initialising the genetic algorithm
populationSize=80;
variableBounds=[0 1000;0 1000;0 1000];
evalFN='PID_ga_objfun_ITAEm';
evalOps=[];
options=[1e-6 1];
initPop=initializega(populationSize,variableBounds,evalF, evalOps,options);
```

PopulationSize: This command defines the population size of the GA. The bigger the population size the better is the final approximation.

VariableBounds: This command defines the three strings of PID (P, I and D) assigned to each member of the population. The number of rows in the ‘’variablebounds’’ matrix represents the number of terms in each member of the population. The above MATLAB code illustrates a population of eighty members being initialized with values randomly selected between 0 and 1000.

EvalFN: The evaluation function is used to declare the objective function. It will fetch the file name of the objective function and execute the codes and return the values back to the main codes.

Options: Binary strings have two main drawbacks;

- ✓ It takes longer time to evaluate due to the fact they have to be converted to real number from binary number.
- ✓ Binary strings will lose its precision during the conversion process.

Therefore real (floating point) numbers is used to encode the population. In the option command used in above MATLAB code, ‘1e-6’ term is the floating point precision and‘1’ term indicates that real numbers are being used as 0 indicates binary encoding is being used. **Initialisega:** This command will combines all the previously described terms and creates an initial population of 80 real valued members between 0 and 1000 with 6 decimal place precision.

B. Setting the GA Parameters

The MATLAB code and the detail explanation of setting GA parameters is explained below.

```
Setting the parameters for the genetic algorithm
bounds= [0 1000; 0 1000; 0 1000];
evalFN='PID_ga_objfun_ITAEm';
evalOps=[];
startPop=initPop;
opts=[1e-6 1 0];
termFN='maxGenTerm';
termOps=400;
selectFN='normGeomSelect';
selectOps=0.08;
xOverFNs='arithXover';
xOverOps=4;
mutFNs='unifMutation';
```

mutOps=8; % The total number of mutation

Bounds: It define the entire search space for the genetic algorithm of the solution parameter.

StartPop: This command is used to start population of the GA which is defined as 'initPop'.

Opts: It is the option of GA which consists of the precision of the string values i.e. 1e-6, the declaration of real coded values, 1, and a request for the progress of the GA to be displayed, 1, or suppressed, 0.

TermFN: This is the declaration of the termination function for the genetic algorithm once required criterion has been met. In this thesis every GA will be terminated when it reaches a certain number of generations using the 'maxGenTerm' function.

TermOps: This command defines the option, if any, for termination function. In this thesis the-termination options are set to 400 generation, which means that the GA will reproduce four hundred generations before terminating. If the GA converges quickly then the termination options can be reduced.

SelectFN: This command is used in selection process. 'NormGeomSelect' is a ranking selection function based on the normalized geometric distribution. The size of the section is proportional to the fitness of the individual. There are three selection functions in GAOT toolbox. 'normGeomSelec' is selected due to its shortest compilation time than the others [47].

SelectOps: If normGeomSelect is used in 'SelectFN' the only parameter that has to be declared in 'SelectOPs' command is the probability of selecting the fittest chromosome of each generation. The probability of selecting the fittest chromosome is set to 0.08.

XOverFN: This command is used to define crossover procedure. MATLAB genetic algorithm tool box consists of a number of crossover types. Single point crossover is too simplistic to work effectively on a chromosome with three alleles [48]. Therefore a more uniform crossover procedure throughout the chromosome is required. Heuristic crossover performs the crossover procedure a number of times and then picks the best 51th one [48]. This increases the compilation time of the program and is undesirable The Arithmetic crossover procedure is specifically used for floating point numbers [49] and is the ideal crossover option for use in this thesis.

XOverOptions: The number of crossover pint is specified by this command.

MutFNs: The **'unifMutation'** or **multi non-uniformly** distributed mutation operator, is selected as the mutation operator since it is function well with multiple variables [50].

MutOps: In this command the total number of mutation is declared since ‘mutFNS’ is selected to be unifMutation. As the result the total number of mutation selected in this thesis is 8 as the total number of population is 80 and the probability of mutation 0.1% considered. In other cases if ‘MutFNS’ is selected to be multiNonUniform function, the mutation operator takes in three options. The first one is the total number of mutations, normally set with a probability of around 0.1%. The second parameter is the maximum number of generations and the third parameter is the shape of the distribution. This last parameter is set to a value of two, three or four where the number reflects the variance of the distribution i.e. [8 400 2].

C. Performing the Genetic Algorithm

The compilation of GA is performed by using the MATLAB command explained below. The function ‘**gen.m’** is used to evaluate and iterate the genetic algorithm until it fulfils the criteria described by its termination function.

[x,endPop,bPop,traceInfo]=**gen**(bounds,evalFN,evalOps,startPop,opts,termFN,termOps,selectFN,selectOps,xOverFNs,xOverOps,mutFNs,mutOps);

Then finally when the compilation of GA is finished the above function returns the following variables:

- ✓ x = the best population found during the compilation of genetic algorithm.
- ✓ endPop = the GA’s final population.
- ✓ bestPop = the GA’s best solution tracked over generations.
- ✓ traceInfo = the best value and average value for each generation.

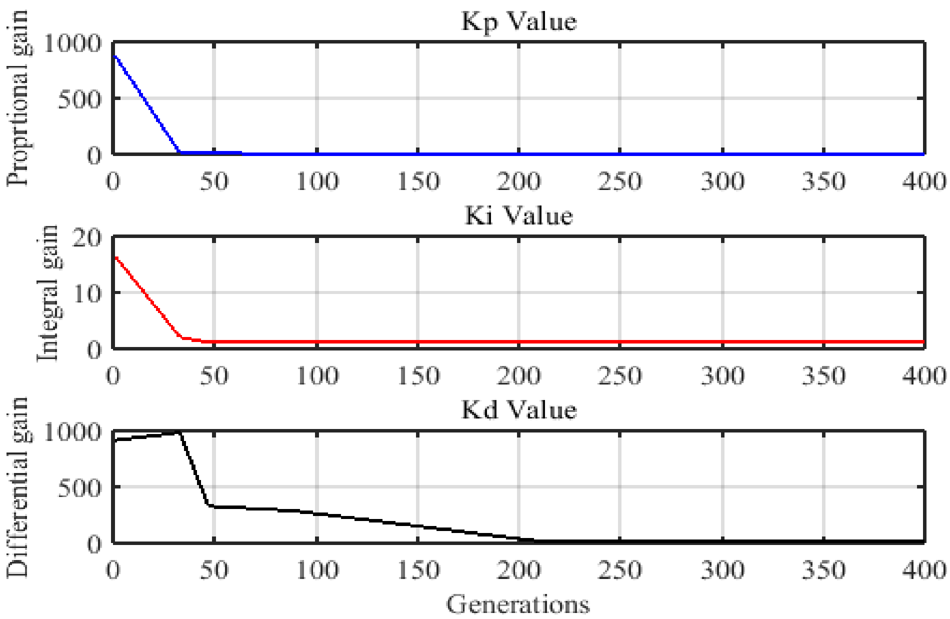

Figure 3. 33: The selected PID parameters after 400 generation

The obtained value of the Kp, Kd and Ki parameters by using GA as shown in figure (3.33) is used in the proposed BLDC motor drive system PID speed controller. Besides, the obtained value of the Kp, Kd and Ki parameters by using ZN tuning method is used in PID speed controller of the proposed BLDC motor drive system for the comparison purpose. The BLDC motor speed dynamic performance by using both PID-ZN and PID-GA based speed controller is as shown in figure (3.34).

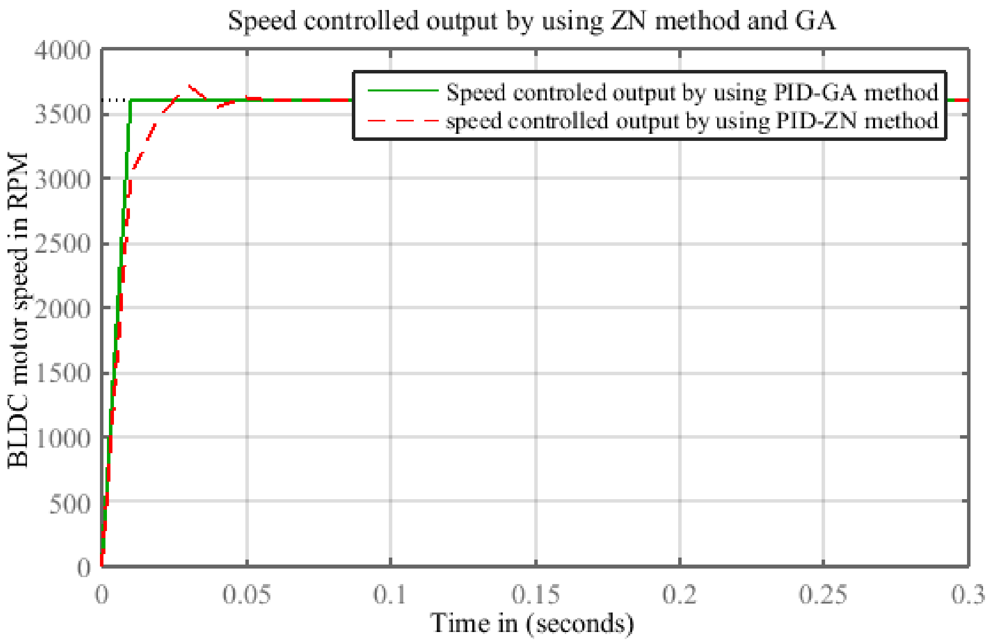

Figure 3. 34: Speed control of BLDC motor by using ZN-PID versus GA-PID

GA algorithm gives better speed dynamic response when compared with ZN based PID controller.

3.6. BLDC motor drive proposed system setup

In this section the Simulink design of BLDC motor with PWM controller is performed by using previously identified specification data's. Besides, the performance analysis of the other current controller .i.e. hysteresis current controller based inverter drive is also done. Hysteresis controller has larger torque ripple. Due to this reason PWM current controller is used for BLDC motor drive purpose. The steps to generate PWM signal for BLDC motor drive is explained. Finally the overall MATLAB code is generated.

3.6.1. Battery source

Because of its advantages mentioned in literature compared with another types of batteries Lithium-ion batteries is used. The specifications of the batteries listed in previous section is used. The Simulink block diagram of the lithium-ion battery shown in figure (3.35) is used in MATLAB simulation as the inverter DC link source voltage.

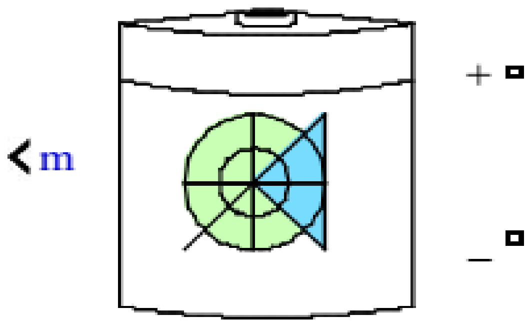

Figure 3. 35: MATLAB/Simulink model of Lithium-ion battery

The name ‘’**m**’’ shown in the left side indicates the measurement parameters values of the battery. Those are voltage, current and state of charging (SOC).

3.6.2. Speed controller

Speed controller is designed and compared for different algorithms i.e. PI controller, Ziegler Nicolas based PID optimization and genetic algorithm in the previous sections. It is shown that GA based PID optimization gives better speed dynamic performance. As the result the PID parameters obtained by using GA is used in MATLAB/Simulink and MATLAB/code for simulation purpose.

3.6.3. Hall Sensor Decoder

The hall sensors mounted on the stator of BLDC motor used to detect the position of rotor or used to determine at which time which switch have to be ON or OFF. Hall decoder is used to convert the signal from each hall sensors into a rectangular three level signals with -1, 0 and 1 which represent the normalized ideal phase currents to be injected in the motor phases.

The hall sensor decoding is performed by using the following true table.

Table 3. 7: The truth table of hall sensor decoder

No	Hall sensors			Decoded signals amplitude		
	H1	**H2**	**H3**	**emf_a**	**emf_b**	**emf_c**
0	0	0	0	0	0	0
1	0	0	1	0	-1	+1
2	0	1	0	-1	+1	0
3	0	1	1	-1	0	1
4	1	0	0	+1	0	-1
5	1	0	1	+1	-1	0
6	1	1	0	0	+1	-1
7	1	1	1	0	0	0

By using table (3.7) the Simulink modeling of hall decoder block can be performed as the shown in figure (3.36). This block is used to extract the induced EMF information from the Hall Effect signals.

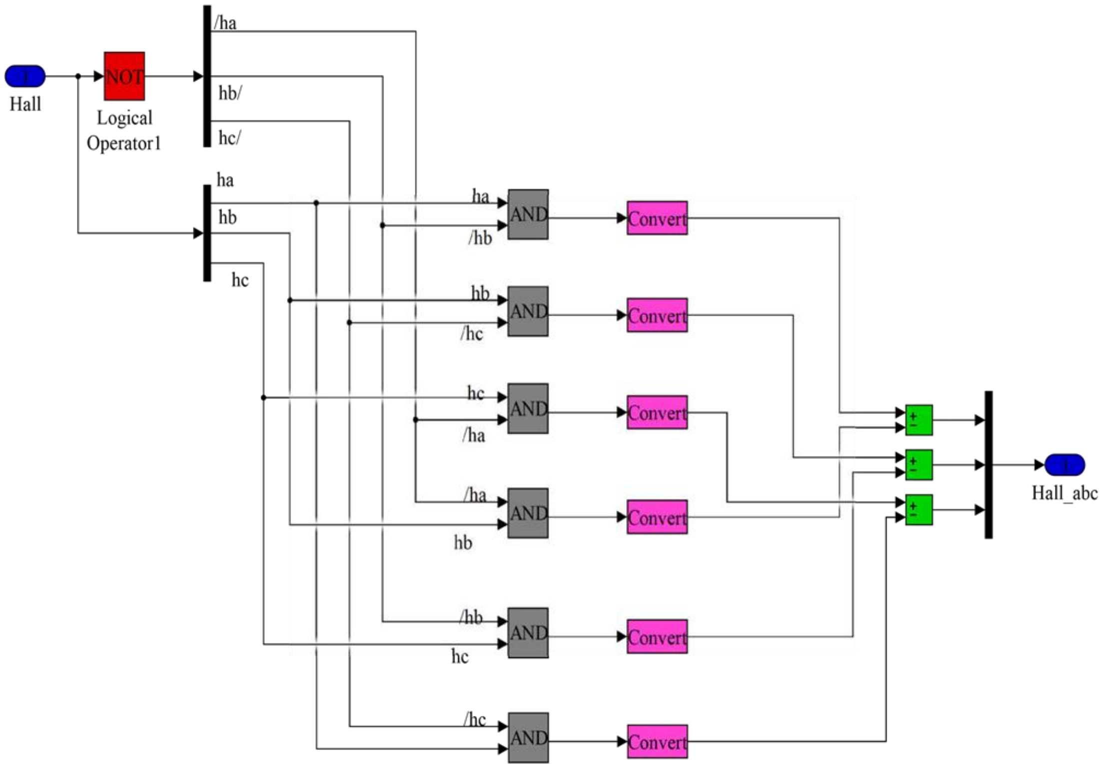

Figure 3. 36: Hall sensor decoder Simulink block diagram

The output signals of this block with the corresponding Hall Effect sensor signal is as shown in (3.37).The hall sensors are shifted from each other by 60 degree. The upper inverter switches (S1, S3 and S5) are on when the rotor reaches near by the corresponding hall sensor.

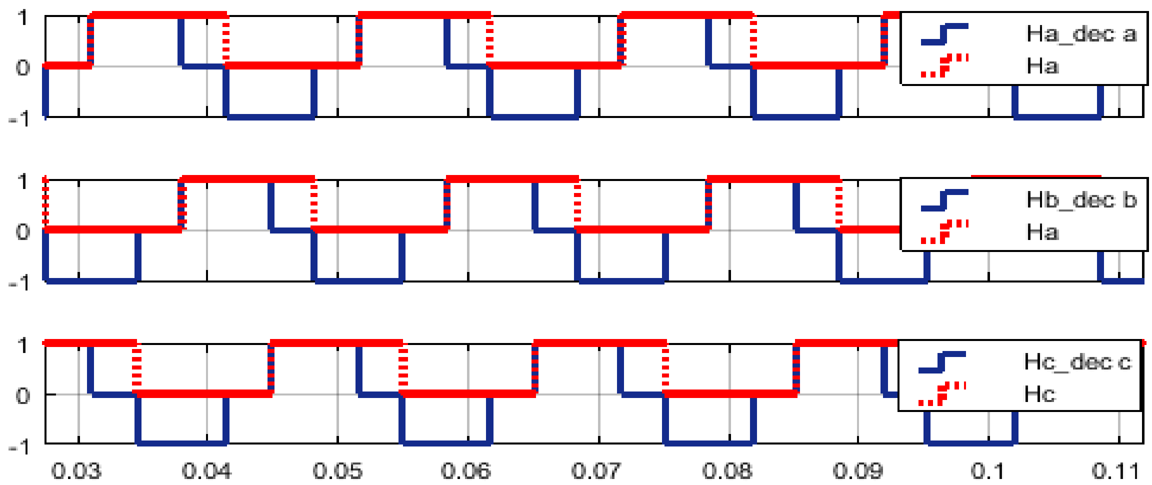

Figure 3. 37: Hall sensor with its decoded signals

The lower inverter switches ON when the corresponding hall sensor becomes zero.

3.6.4. Reference current generation

The output of the speed controller results in reference torque (T_{reff}). Division of reference torque by torque constant gives us the amplitude of reference current. Since the wave shape the of decoded signal is per unit value of its corresponding generated reference currents, the multiplication of each decoder output signal and amplitude of the corresponding reference current gives us the corresponding reference (command) currents.

$$I_{ref} = \frac{T_{ref}}{K_t} \tag{3.52}$$

The MATLAB/Simulink and the wave form of the references current with its corresponding hall decoder's output signals are as in figure (3.38 & 3.39) respectively.

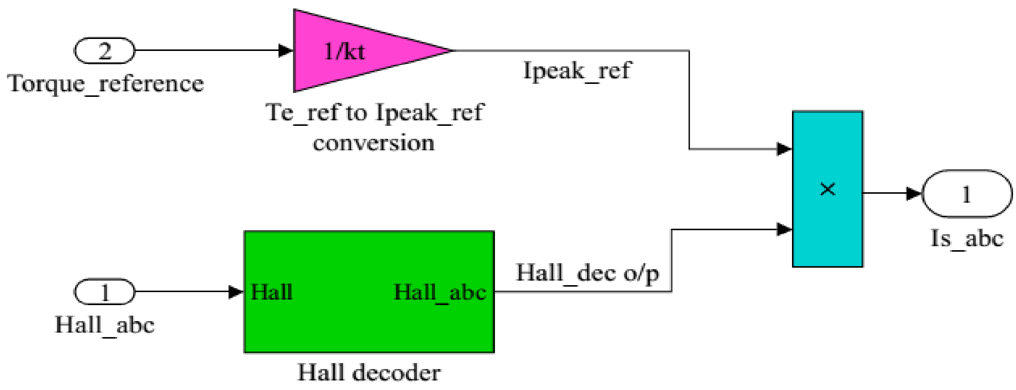

Figure 3. 38: Simulink model of reference current generation

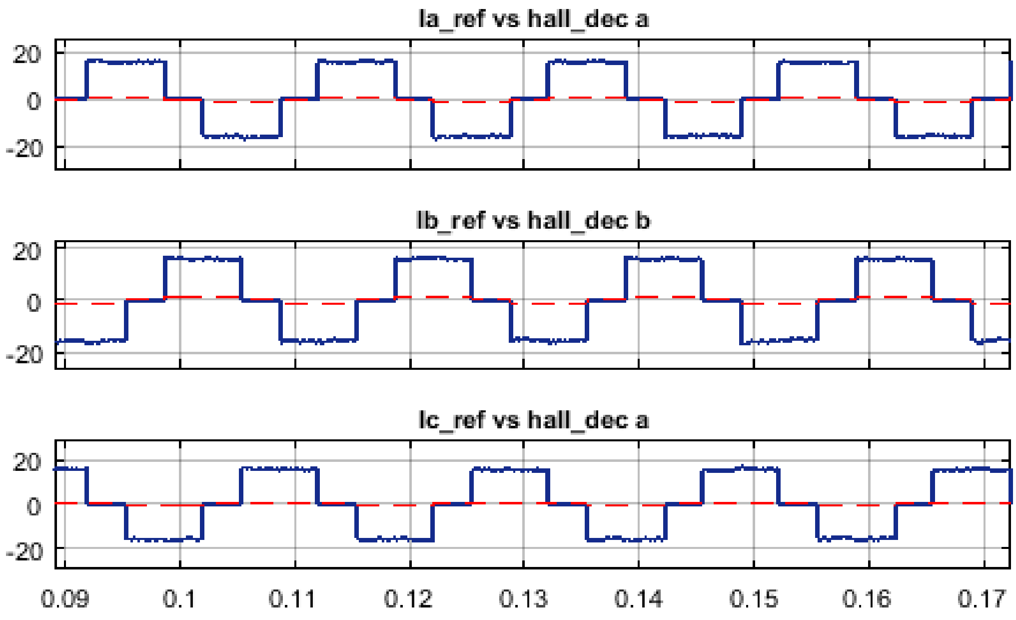

Figure 3. 39: Reference current and decoded hall sensors (dotted line)

The magnitude of current distortion depends on the smoothness of PID controller output and switching drive controller techniques used. The distortion of command current results in torque ripple that is need to be minimized. Therefore in order to reduce the current distortion and hence torque ripple the appropriate speed regulator and current controller algorithm must be used.

3.6.5. Three phase inverter drive

Three phase inverter with MOSFET switches and parallel freewheeling connected diode as shown in figure (3.40) is used. Since a signals from hall sensor changes every after 60°, six steps are necessary for a completion of electrical cycle. When field lines are perpendicular maximum torque is reached. The phase commutation sequence is AB-AC-BC-BA-CA-CB and each conducting stage is called one step. Only two phases conduct at a time and third phase is floating. To produce maximum torque, the inverter should be commutated after every 60° so that current is in phase with the back EMF. In this work two ways of switching pulse generation techniques are used. One is hysteresis current controller based and the other is PWM current controller based inverter drive. PWM current controller based and hysteresis current controller based inverter drive techniques are considered for comparison purpose.

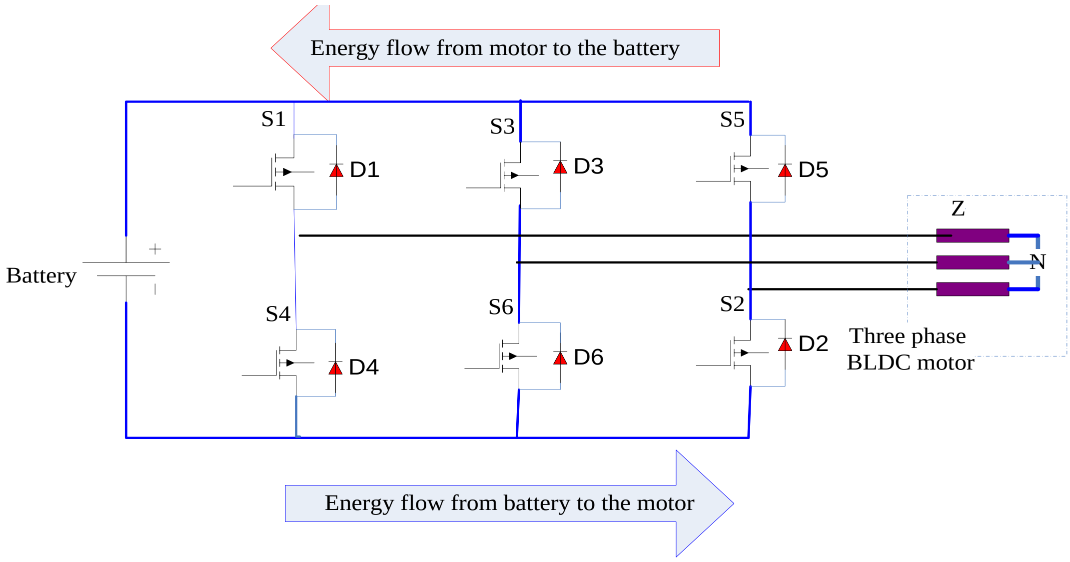

Figure 3. 40: Three phase BLDC motor inverter drive

3.6.5.1. Hysteresis current controller based inverter drive

Hysteresis current control performs in such a way that each stator phase current is compared to the corresponding command current and the error signal is feed to a two level hysteresis comparator. Each phase requires one hysteresis comparator. As the result the switching status of each leg does not depend on the other switching status of another legs. The error of each current is maintained within the hysteresis bandwidth (h). The working principle of the hysteresis controller can be explained by the following MATLAB code:

if

```
(ias_ref-ias)>=h,
S1=1 & S4=0;
   end
if (ias_ref-ias)<- h,
S1=0 & S4=1;
end
if (ibs_ref-ibs)>= h,
S3=1 & S6=0;
end
    if (ibs_ref-ibs)<- h,
    S3=0 & S6=1;
    end
If (ics_ref-ics)>= h,
S5=1 & S2=0;
end
if (ics_ref-ics) <-h,
S5=0 & S2=1;
End
```

The output of hysteresis comparator becomes one or zero which is used to drive the inverter switches. The merits of these scheme is its inherent simplicity and the good dynamic performance. But the demerit of this scheme is, when the switching frequency varies with load parameters and AC voltage, and the operation is influenced by the randomness of hysteresis controllers that are independent to each other. Due to these reasons, the current error in isolated neutral system can be twice of the hysteresis band. As the result sub harmonics can be generated. Figure (3.41) shows the Simulink diagram of hysteresis controller with its comparator and double to Boolean signal converter blocks. The output hysteresis comparator doesn't directly connected to drive the inverter rather, it is connected to the switching control logic which is used for the purpose of triggering the switches and switching process control.

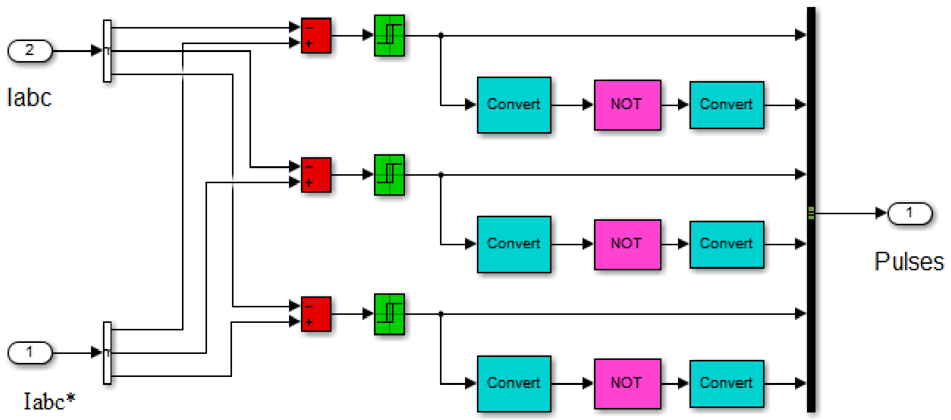

Figure 3. 41: Simulink model of current controller

The reference current vs stator current is shown in figure (3.42). This figure shows the current distortion is very high in the case of hysteresis current controller based three phase BLDC motor drive. Ideally the stator phase current of BLDC motor is rectangular. But, practically the shape of the phase current of this motor becomes trapezoidal due to the current lagging effect of the stator inductance.

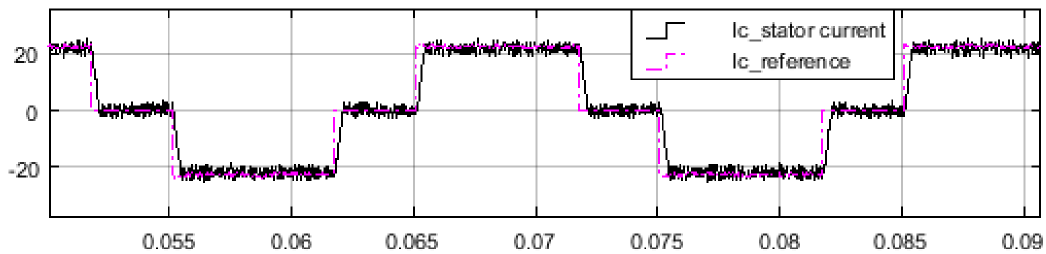

Figure 3. 42: Reference current and Stator current based hysteresis control

This current distortion need to be minimized so that the torque ripple of the motor is reduced. In order to do this PWM current controller is used for inverter circuit drive and control.

3.6.5.2. PWM current controller based inverter drive

PWM current controller based inverter drive consists of current controller, carrier signal, comparator and logical circuit. The same step is used in case of generating speed controller, hall sensor decoding and reference current generation used for the hysteresis current controller based BLDC motor drive. But, differ from hysteresis controller, PWM current controller the difference of each reference current and the corresponding stator phases current are input to the current controller. In this work V_{abc} frame is used rather than V_{dq} frame. The corresponding current controller's output of each phase is multiplied by current gain constant ($K_{pi} = 100$ in this work) and gives the corresponding phase voltage controlled modulating signal (V_{asc}, V_{bsc} and V_{csc}) as shown in appendix B, page 110 to 112.

The voltage controlled modulating signal is compared with triangular carrier signal. If voltage controlled modulating signal is greater than the amplitude of the carrier signal, the switching signal is one and the corresponding switch will be ON and if the voltage controlled modulating signal is less than the amplitude of the carrier signal the switching signal is zero and the corresponding switching state will be OFF.

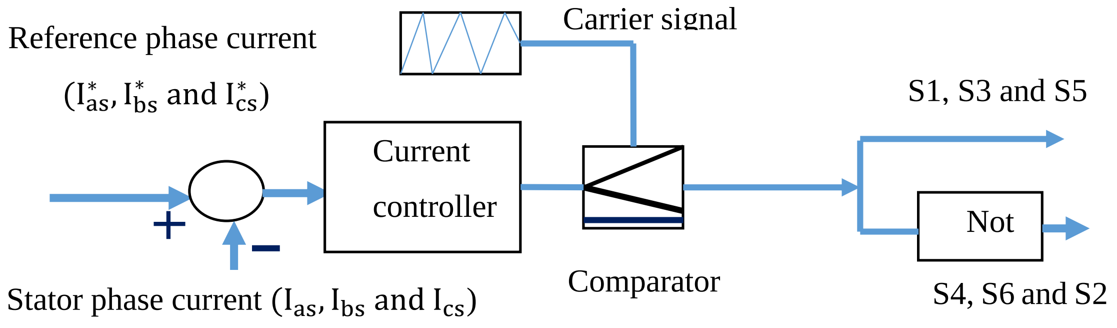

Figure 3. 43: General PWM inverter driving signal generation for each phases

3.6.5.2.1. Current controller

Three current controller is needed separately for each phases. The difference between reference current of each phase and the corresponding stator current of each phase is given to the current controller so that the smooth signal is obtained at the end of the controller. Current controller is used only in the case of PWM current controller technique. But, in the case of hysteresis controller based inverter drive two level hysteresis comparator is used implies.

3.6.5.2.2. Carrier signal generation

As per center of transportation and vehicle engineering (ASTU), the inverter frequency is given to be 8000 Hz. The carrier signal is generated by using MATLAB code as shown in Appendix B. The generated carrier signal with amplitude of 10 with frequency of 8000 Hz is shown in figure below.

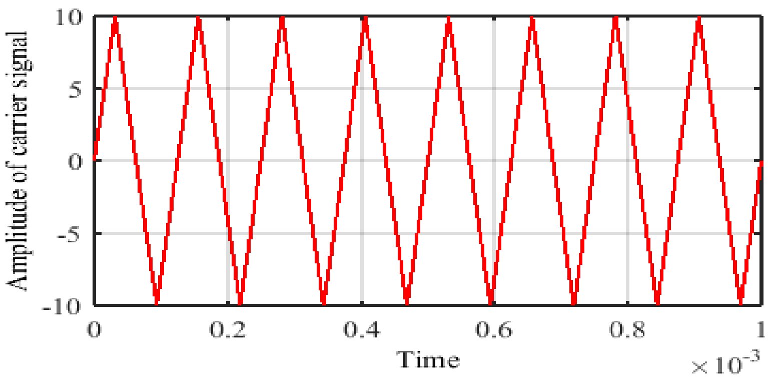

Figure 3. 44: Triangular carrier generation

3.6.5.2.3. Comparator

Comparator is the logical component which is used to compare the modulating signal and carrier signal to produce 0 and 1. In order to avoid the ON state of the switches on the same legs at the same time, the logical NOT is connected to drive lower leg switches. The output signal of the comparator is controlled by using switching logical controller. The purpose of switching logic controller is to trigger and control switching actions of the inverter.

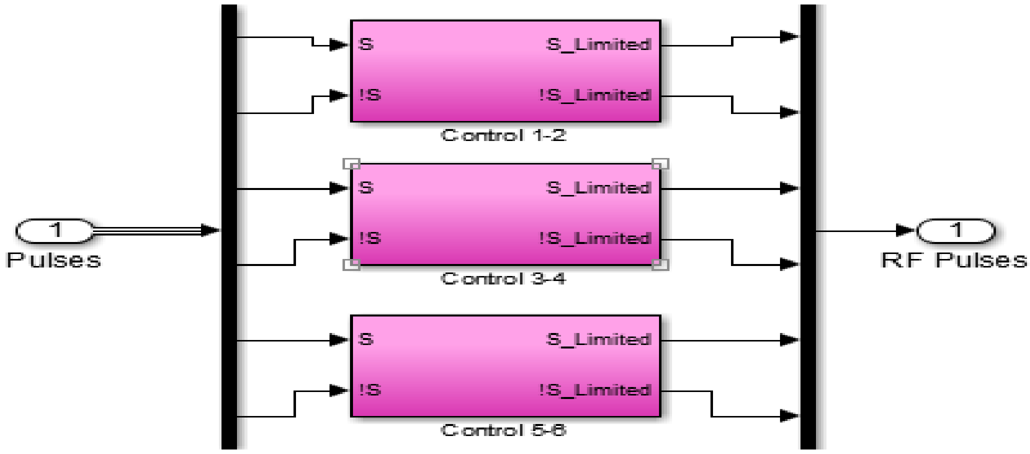

Figure 3. 45: Simulink inverter switching control logic circuit

3.7. Summary

In this chapter the collection of data analysis, proposed system modeling, speed controller design, comparison of speed controllers, proposed system setup are covered. The analyses of data shows the identified BLDC motor parameters satisfies the proposed electric vehicle by center of transportation and vehicle engineering (ASTU). The missing data's like rated torque of the motor, rated current of the motor, rated speed of the motor and other related data's are obtained by using graphical analysis. System modeling is performed for the purpose of speed controller design and system understanding. The designed speed controllers are compared and the one with better control performance is selected and used in proposed BLDC motor drive system. Finally the proposed drive system is simulated by using MATLAB software.

CHAPTER 4

4. RESULTS AND DISCUSSIONS

The simulation results explained in this chapter is performed for the same values of the system parameters under study. The system is simulated at the load torque of 10Nm and the rotor speed of 3600 RPM by using the motor parameters and speed controller parameters values previously specified in chapter three. The specification of the simulated system parameters can be found in the MATLAB sample code written in appendix B. The proposed system simulation result is compared with the closely related works mentioned in literature to fulfill the specific objectives of the research. The simulation is performed both by using actual value and per unit value for the purpose of simplicity and easy to understand.

4.1. Results

4.1.1. PWM current controller based BLDC motor driving output results

The MATLAB Simulink output result of the BLDC motor (BLDCM) speed along with its command speed and state of charging of the battery is shown in figure below:

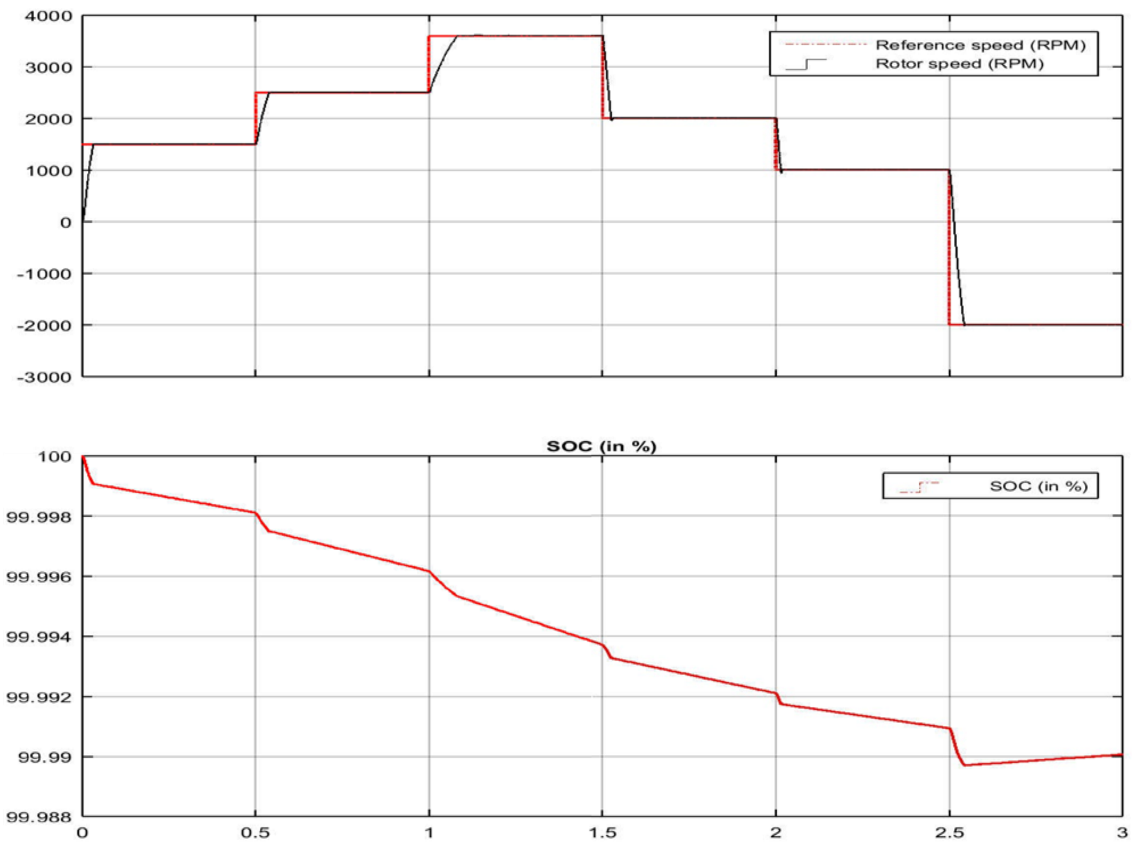

Figure 4. 1: Command speed (RPM), motor speed (RPM) and SOC %

Figure (4.1) shows the speed of the motor follows its command speed with better dynamic performance specifically, in case of rise time, settling time, percent overshoot with approximately negligible speed disturbances. In addition the state of charging in the range of the different motor speed performance is also shown in this figure. Accordingly, in the case when the speed of the motor is increasing the discharging rate of the battery also increases. In another case when the direction of the rotation of the rotor is reversed, specifically from 2.5 second to 3second, the battery is getting the charge through the freewheeling diode in the inverter. This case the motor acts as the generator. The trapezoidal EMF shown in figure (4.2) is taken at the same simulation time with that of the dynamic speed performance shown in figure (4.1). This figure shows the speed and induced EMF voltage are directly proportional to each other. The horizontal axis in this figure shows the simulation time of the system in second.

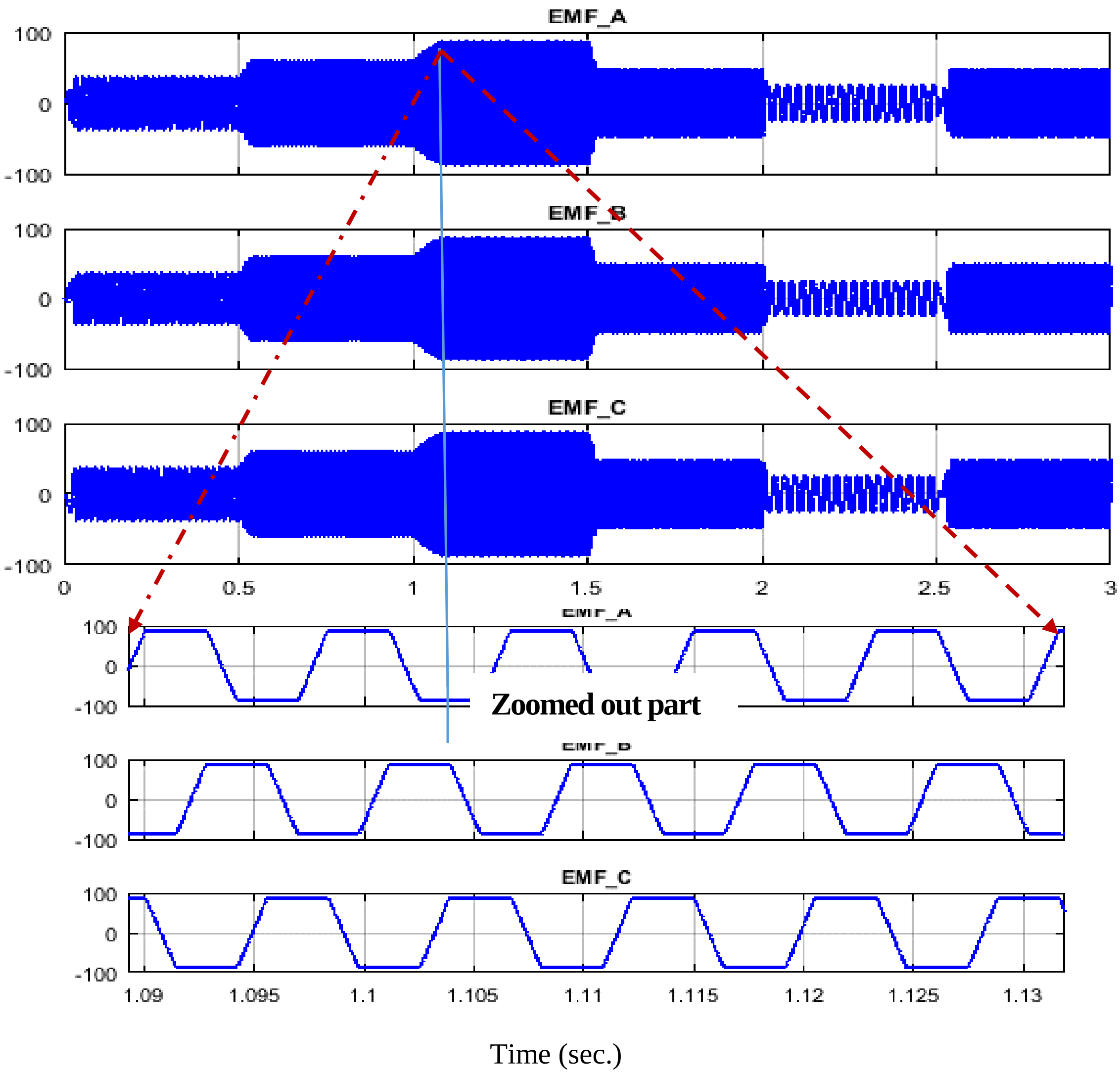

Figure 4. 2: The trapezoidal back EMF of BLDCM with its zoomed out part

The MATLAB/code output result of the reference speed versus output rotor speed, reference torque versus output torque developed by BLDC motor in per unit value as well as the rotor position in radian is shown in the figure (4.3). The base speed of 3600RPM is used. This figure is simulated in such a way that the command speed of 3600RPM is applied from time zero second to 0.3 second. Then the same command speed but opposite in direction is applied from 0.3 seconds to 0.5 second. Then finally 3600RPM command speed is applied from 0.5 second to 0.8 second again.

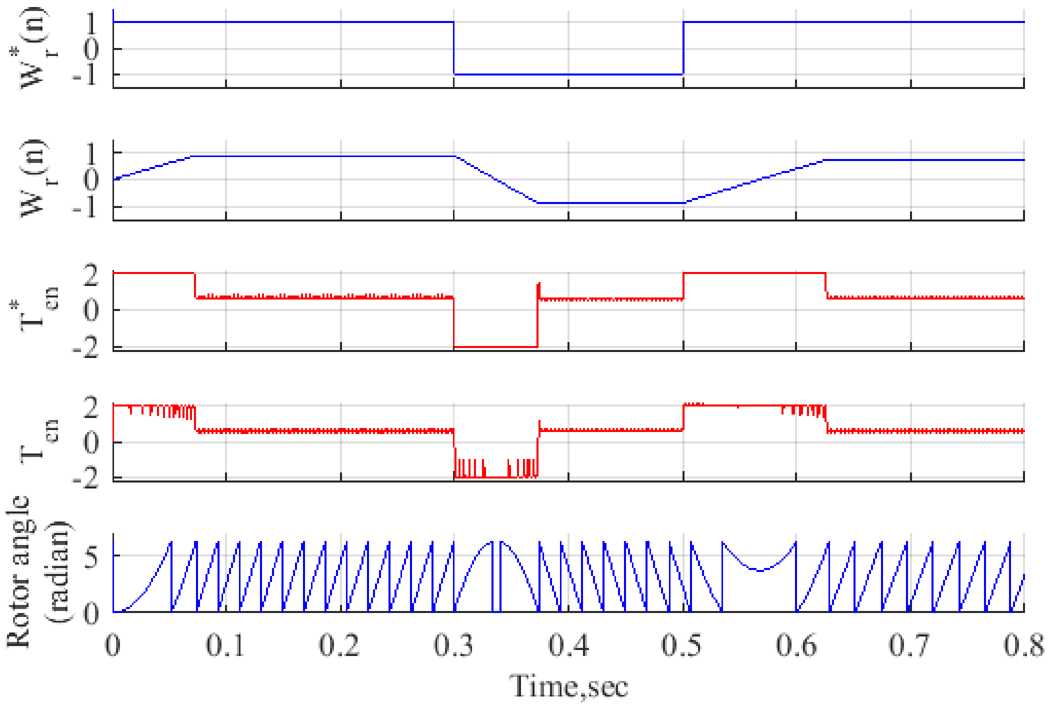

Figure 4. 3: The per unit value of the command speed (W_r^*) & motor speed (W_r), command torque (T_{en}^*) & motor output torque (T_{en}) and rotor position in radian

The result shows the rotor speed reaches one per unit speed value after 0.06second with zero percent overshot when 10Nm load is applied. But in no load case it reaches 1 per unit speed at 0.01 second. In a similar ways the reference torque versus electrical torque of the BLDC motor is also shown in per unit value for the same running time of the simulation. The result shows the electrical torque follows it is command value by having very small ripple value. Initially the torque value is larger because starting torque need to be larger in order to accelerate the rotor from zero speed to maximum speed. Once the maximum speed value is reached the torque will be reduced, because there is no acceleration force due to the inertia of the rotor and load. Negative (opposite to the previous) torque is applied to reverse the direction of the motor. Besides the rotor position is also plotted in this figure. It shows the response of the BLDC motor with the change of the direction (sign) of the command speed.

The reference current, the output stator current and output power of BLDC motor is shown in the following figure;

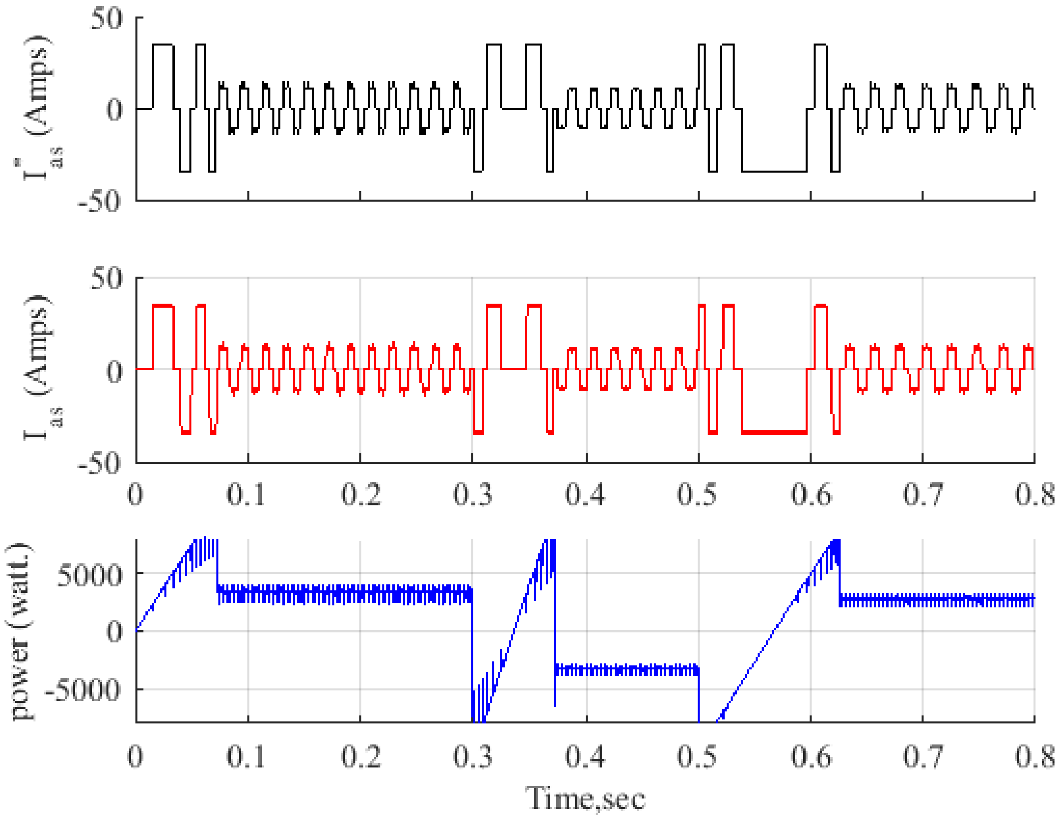

Figure 4. 4: Reference current, the output stator current and output power of BLDCM

One of the objective of this research study is to reduce the current distortion. That means to generate the stator current with lower distortion value from its reference value. As we can see from the above figure the distortion value of the stator current is very low. Figure (4.5) shows the electrical response of the EMF voltage and the rotor direction exchange for the same condition of command speed explained in figure (4.3). This figure also shows the response speed and how the proposed drive system is smooth and stable under variable speed command. The high frequency maxima and minima reaching of three phase inverter output phase voltage of BLDC motor shown in figure (4.6) is due to high inverter switching frequency. That means the inverter output voltage follows the inverter switching frequency. But, because of stator inductance the stator phase current can't follow the inverter switching frequency rather it follows the frequency of its command current.

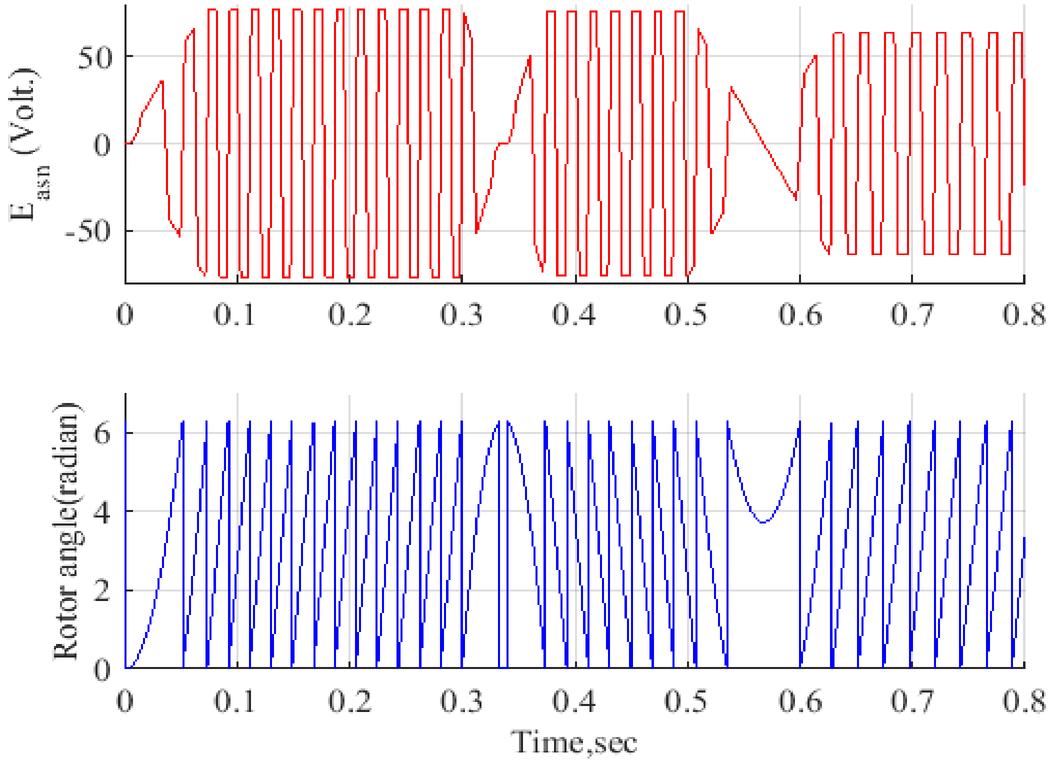

Figure 4. 5: The induced EMF and the rotor position of BLDCM

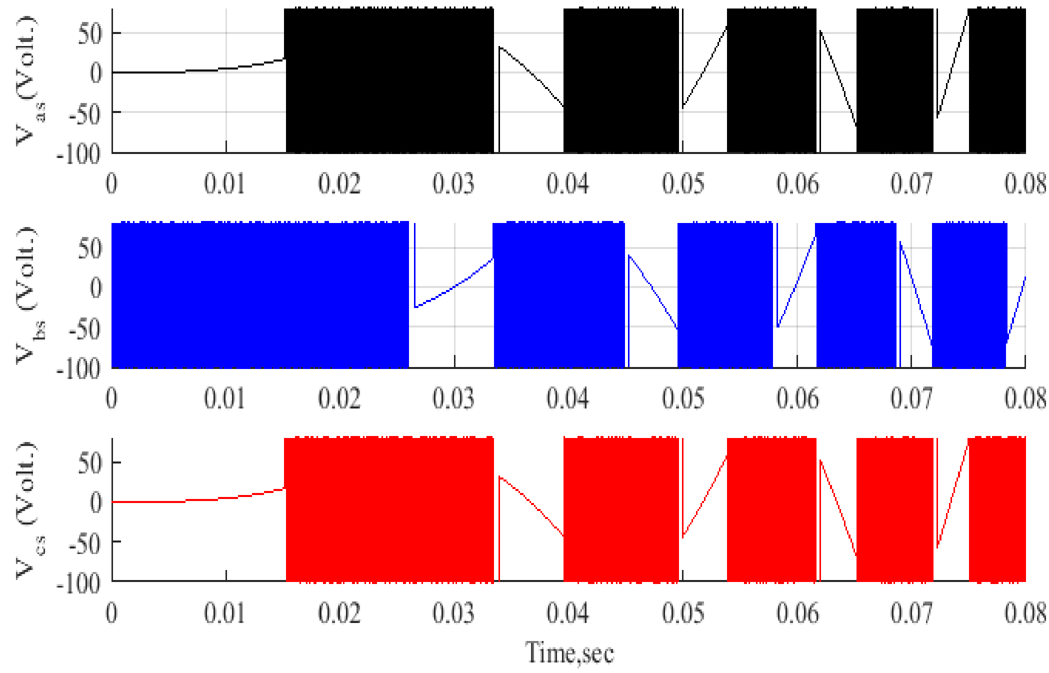

Figure 4. 6: Three phase inverter output voltage of BLDCM

4.1.2. Hysteresis current controller based BLDC motor driving output results

Reference speed versus output rotor speed, reference torque versus rotor torque of BLDC motor in per unit value are shown in the following figure.

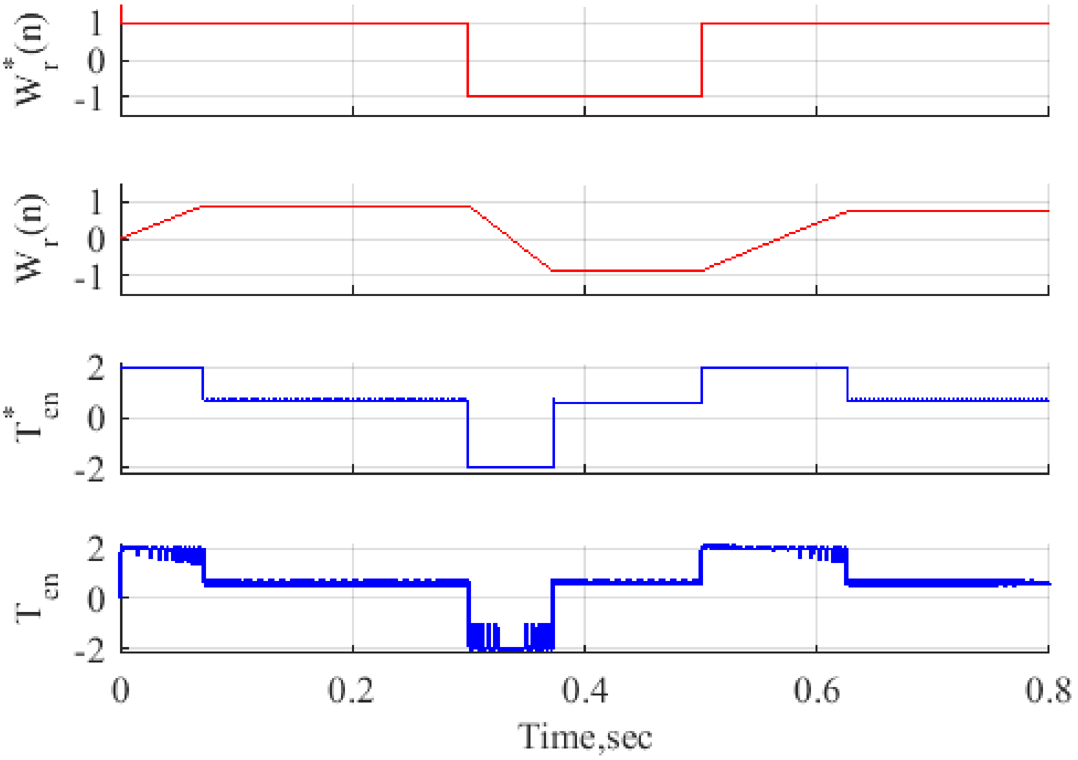

Figure 4. 7: Hysteresis controller based controlled reference speed, output rotor speed and reference torque vs output torque of BLDCM

The result shows hysteresis controller gives good speed dynamic performance but, it results in larger torque ripple. This torque ripple is due to the current distortion of hysteresis current controller modulation. As we can see from figure (4.8) the current ripple is larger in the case of hysteresis current controller modulation.

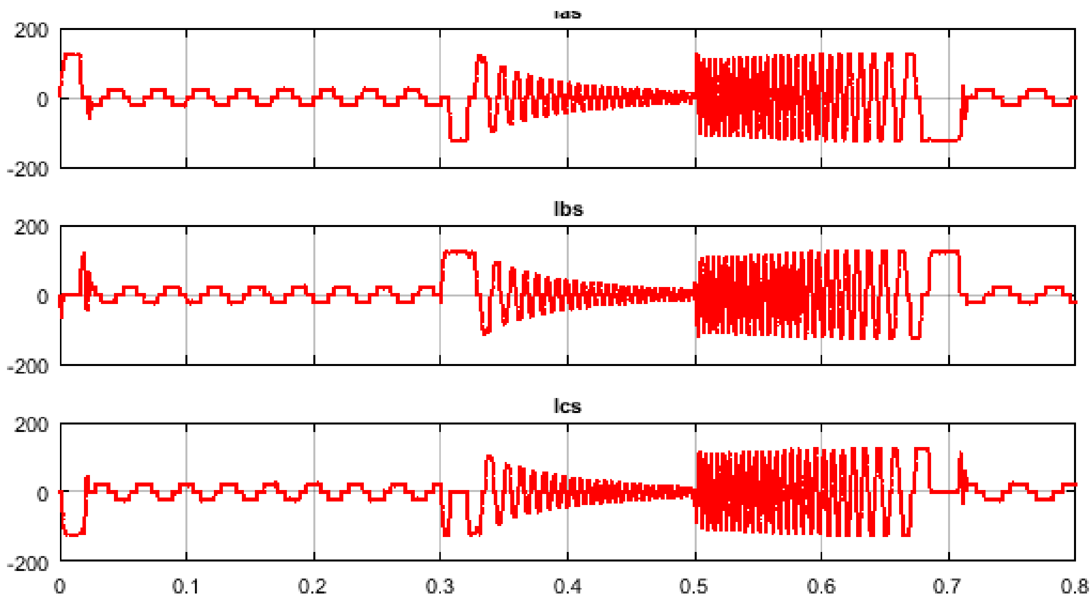

Figure 4. 8: Hysteresis current controller three phase output current of BLDCM

4.2. Discussion of the results

4.2.1. Speed dynamic performance of the BLDC motor drive

Two cases are considered for the comparison purpose of the obtained results. The first case is based on the types of speed regulators used and the second case is based on inverter driving techniques used. In the first case the performance of PWM current controller based BLDC motor drive output results by using PI, PID-ZN and PID-GA based speed controlled performance characteristics are compared and discussed. The comparison result shown in figure (4.9) is from modeling of BLDC motor drive performed in chapter three (figure 3.31 & 3.34). From control theory the system is said to have better speed dynamic performance if it has the lower rise time, lower percent overshoot, lower settling time as well as lower peak time.

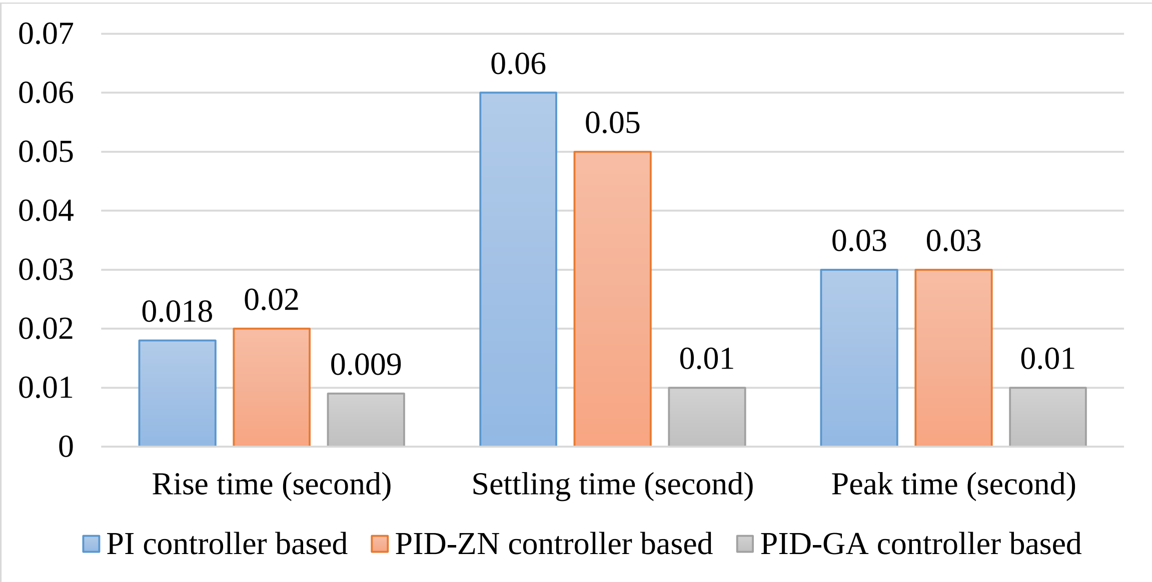

Figure 4. 9: Speed dynamic performance comparison of BLDC motor drive based on speed regulators at no load

Figure (3.31) shows that, PI controller has larger percent overshoot than PID-ZN speed controller. PID-ZN speed controller results in 2.777% overshoot. But, PID-GA fund to have zero percent overshoot (from Fig. 3.34). The genetic algorithm based speed controlled BLDC motor has better speed dynamics performance compared with PI controller based and PID tuning by using Zeigler Nicolas method based speed control. In the second case the performance of PWM current controller based BLDC motor drive output results, Hysteresis current controller based BLDC motor drive output results and Variable VS based six step inverter feed electrical torque of BLDC motor drive output results are compared and discussed by using PID-GA speed regulator. The output speed response of BLDC motor drive by using PWM current controller, hysteresis current controller and six step inverter feed variable voltage source are explained as shown in figure (4.10).

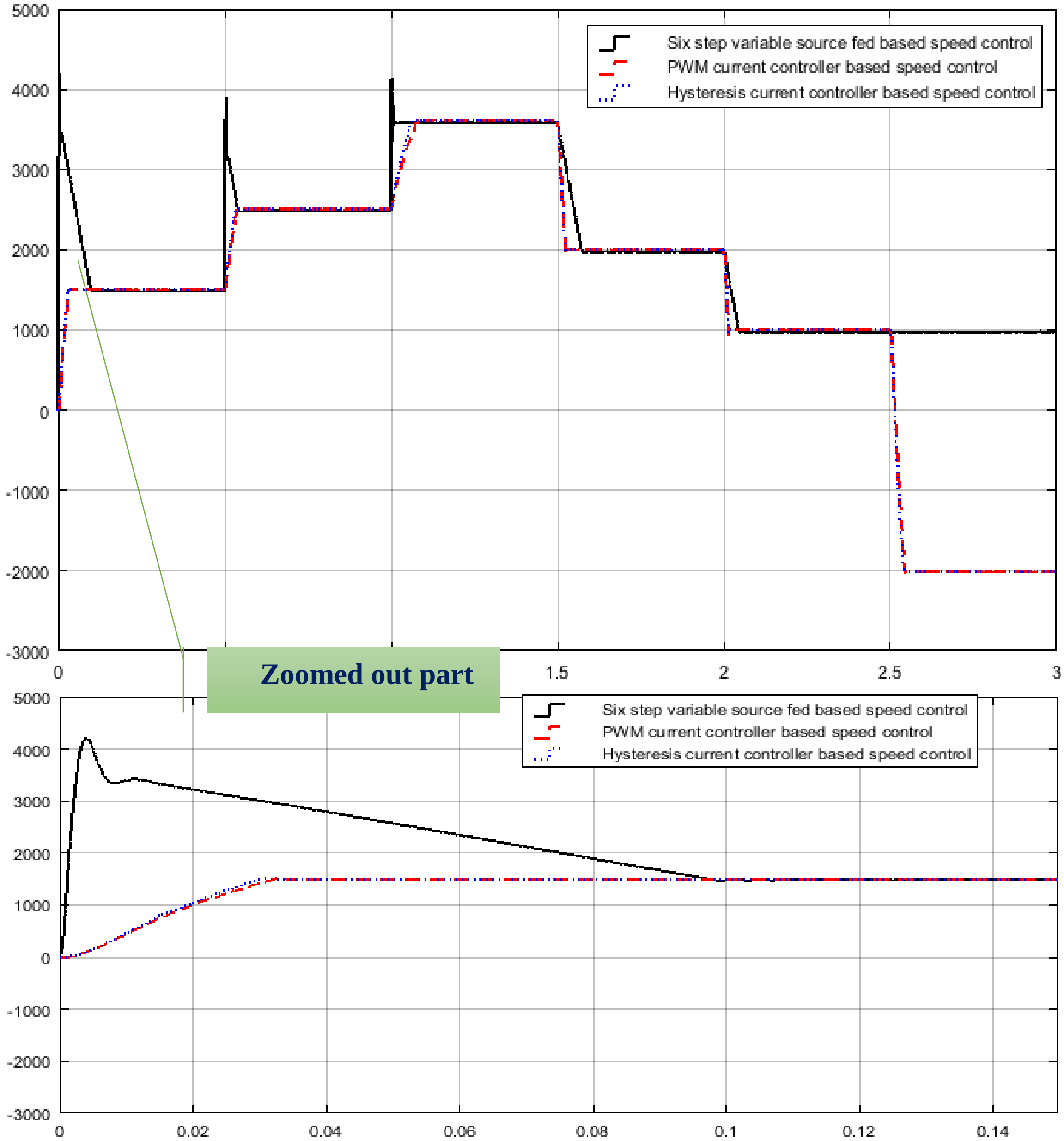

Figure 4. 10: Comparison of BLDCM speed control based on inverter commutation techniques

The speed dynamic performance of six step inverter feed variable voltage source, hysteresis current controller and PWM current controller based speed control of BLDC motor for the same speed controller and the same BLDC motor parameters is compared in terms of their rise time, settling time and peak time as shown in the following bar chart. This chart is performed by taking the simulation output data from the zoomed part of the figure (4.10).

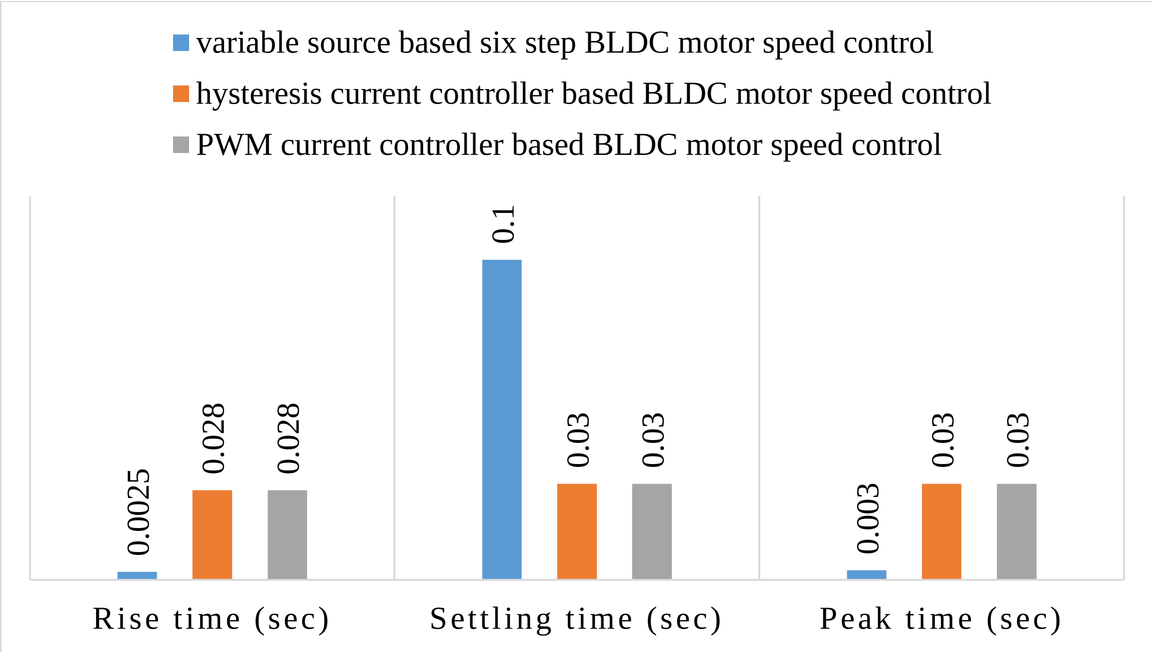

Figure 4. 11: Speed dynamic performance comparison of BLDCM drive based on inverter driving techniques

The result shows that hysteresis current controller and PWM current controller gives a good speed dynamic performance in the case if GA-PID controller is applied to both cases. However hysteresis current controller results larger current distortion and larger torque ripple when compared with PWM current controller based BLDC motor drive.

4.2.2. Current harmonic distortion

The output result of the study shows the harmonic distortion of current is minimum when the PWM current controller with GA-PID based speed controller is used.

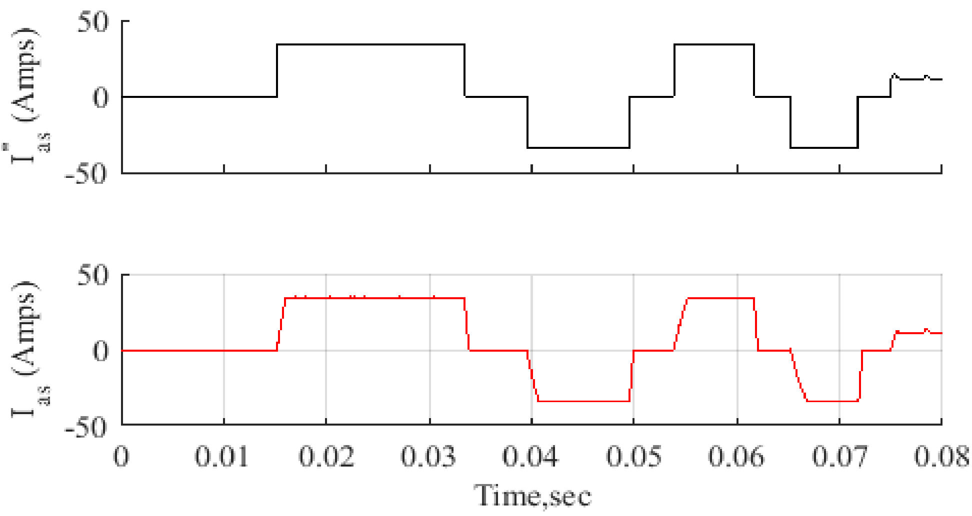

Figure 4. 12: Zoomed part of a reference current versus a phase stator current of PWM current controlled inverter

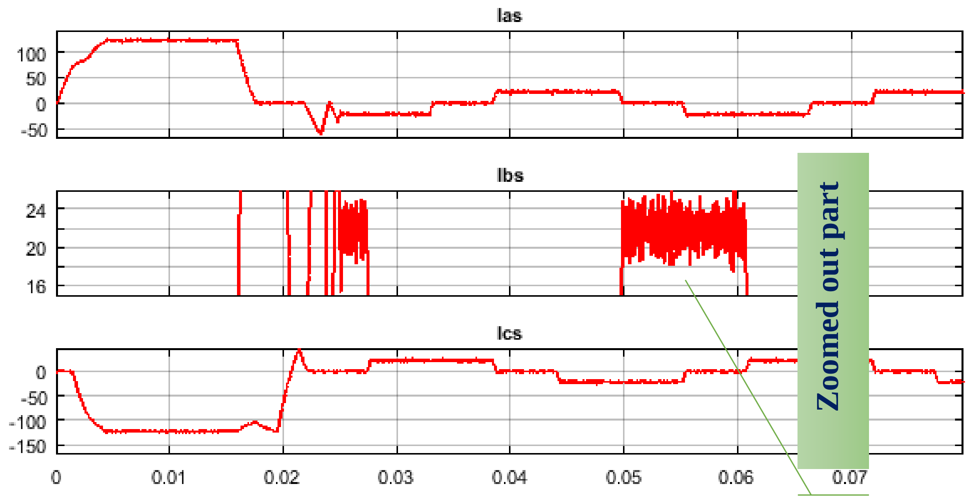

Figure 4. 13: Three phases hysteresis current controller based BLDCM speed control

From figure (4.12) we can see that, the stator current follows its corresponding reference current with very low distortion compared with the hysteresis current controller based BLDC motor drive. In the case of hysteresis current controller based BLDC motor drive (figure 4.13) the current distortion is 20% of stator peak current value. This current distortion causes larger torque ripple.

4.2.3. BLDC motor torque ripple

Figure (4.14) shows the electrical torque ripple is reduced to 8% of its reference value in the case if PWM current controller with GA-PID controller is used. Torque ripple is calculated as ripple times hundred percent divided by reference torque.

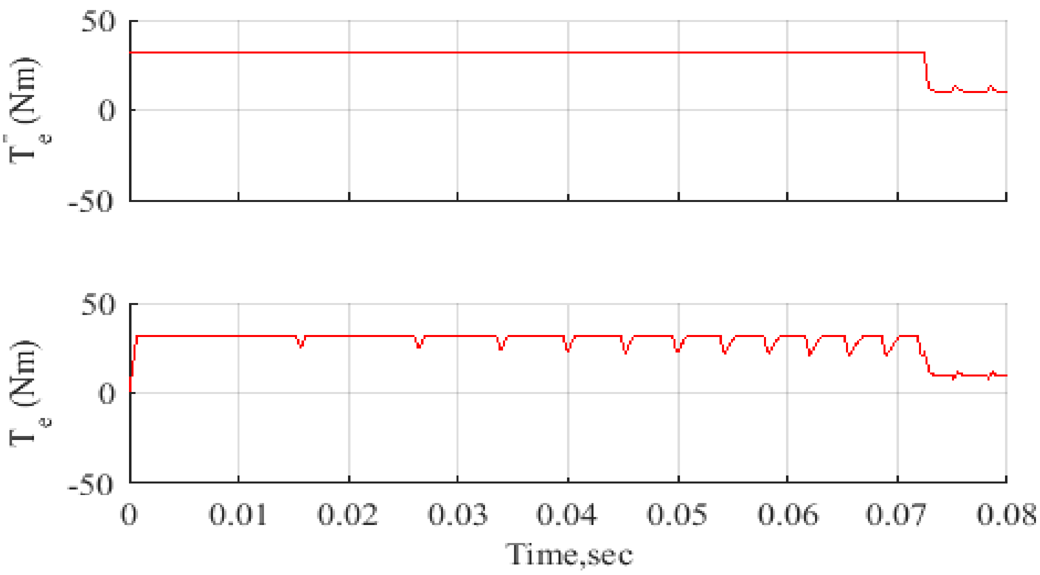

Figure 4. 14: PWM current controller based controlled electrical torque output developed by BLDCM and reference torque

Besides, if hysteresis current controller based inverter drive is used instead of PWM current controller based inverter drive the torque ripple becomes greater than 18.18%.

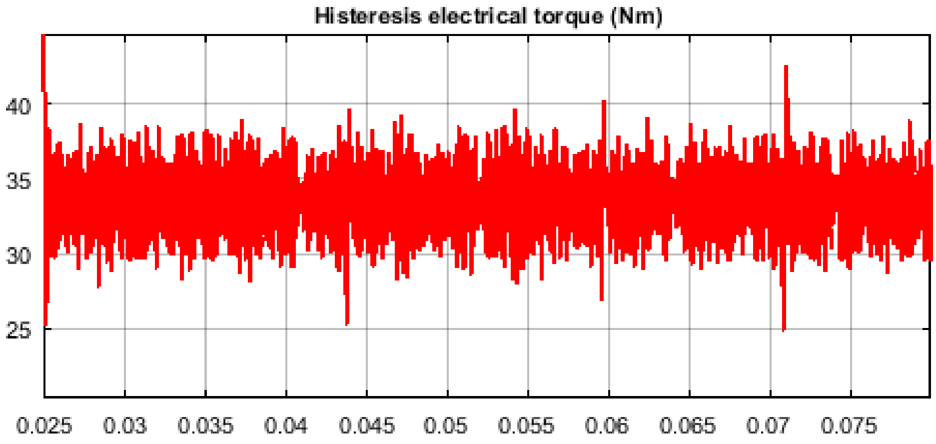

Figure 4. 15: Hysteresis current controller based controlled electrical torque output of the BLDCM

In literature it is reviewed that torque ripple of hysteresis current controller is more than 30% if PI-fuzzy logic speed controller is used (mentioned in chapter two). But here PID-GA is used instead of PI. As the result the torque ripple is found to be reduced. Besides when six step inverter feed variable voltage source controlled is used with PID-GA, then the torque ripple becomes less than 30% which is larger than if hysteresis current controller is used with PID-GA speed controller.

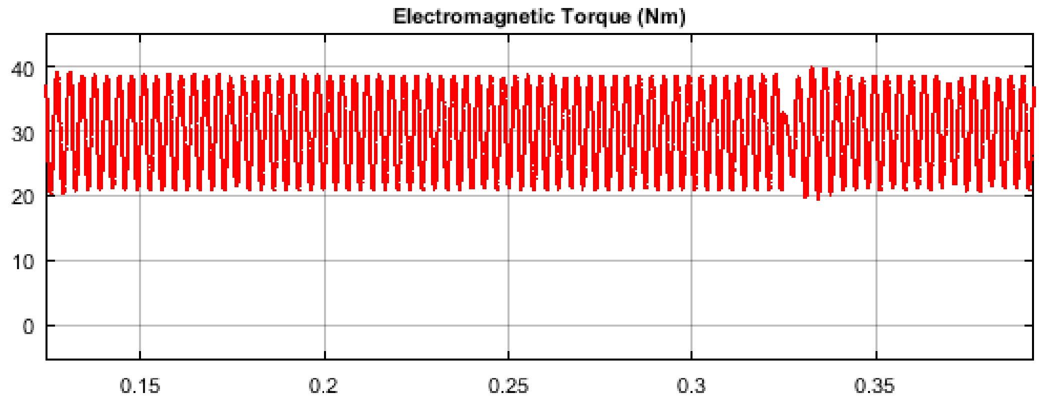

Figure 4. 16: Six step inverter feed variable VS controlled electrical torque output value of BLDCM

The torque ripple output values discussed in this subtopic is summarized as the following bar chart.

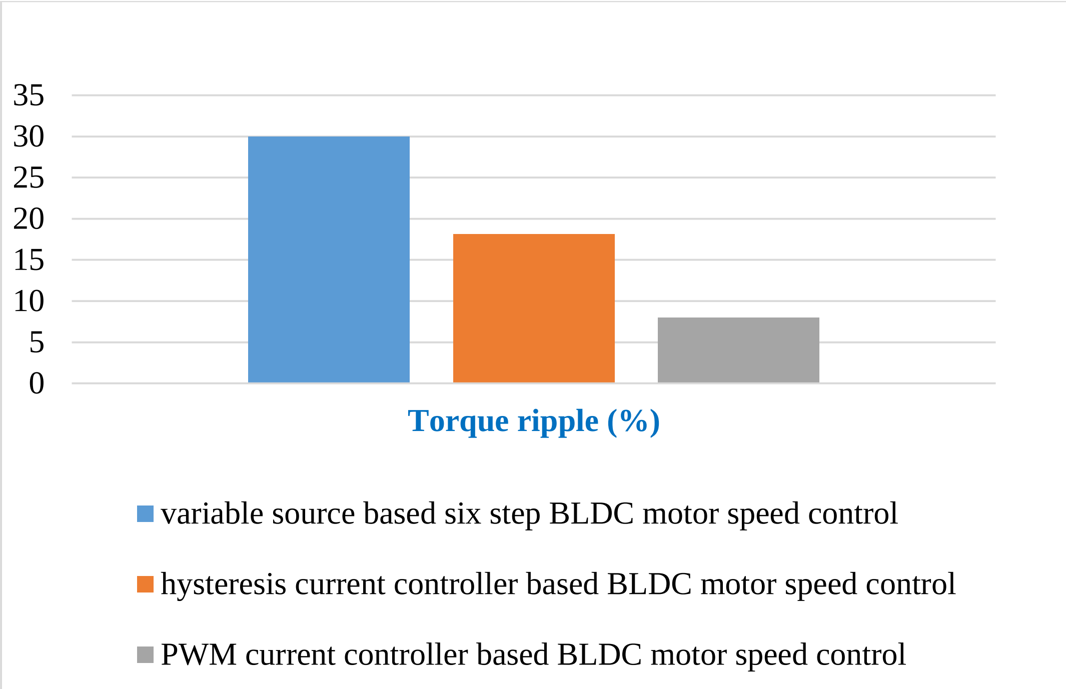

Figure 4. 17: Inverter driving techniques in terms of their torque ripple output values

This shows the torque ripple is less in the case of PWM current controller based BLDC motor drive.

CHAPTER 5

5. CONCLUSIONS AND RECOMMENDATIONS

5.1. Conclusions

Electric vehicles have been considered for the green transportation because of several reasons. The rising of the cost of the fossil fuel and the environmental pollution problems the wide world are facing today are the main reasons. In addition it is predicted that, no more fossil fuel would found in the world after a few decade. Electric motors are the main part of the electric vehicles. Even though there are many types of electric motors used for electric vehicles induction motors and BLDC motors are the most popular drive trains used today. Important technical requirements of the electric motors for an electric vehicle propulsion are: high torque output at low speed, high torque or power to size ratio, high efficiency, high dynamic response, robustness and low noise susceptibility. Since BLDC motor can fulfill these requirements it is focused as the electric vehicle traction motor. Electric vehicle traction motors need to have low torque ripple, current distortion and good speed dynamic performance. BLDC motor needs appropriate control algorithm in order to fulfill the above mentioned requirements. Many types of BLDC control mechanisms have been used by researchers.

Among them hysteresis current controller modulation, six step inverter feed variable voltage source drive along with the variety of speed regulator are discussed in literature. Speed control of BLDC motor is simulated by using PWM current controller techniques and GA-PID speed controller. Furthermore, it is also simulated by using hysteresis current controller modulation and six step inverter feed variable voltage source drive under the same condition. The result shows, the hysteresis controller gives similar speed dynamic performance characteristics compared with PWM current controller based BLDC motor drive if the same speed controller is used [Fig 4.10]. However hysteresis controller generates larger current distortion and larger torque ripple compared with if PWM current controller modulation is used implies. The result shows PWM current controller provides better speed, current and torque parameters compared with another inverter driving technique listed above. The speed dynamic performance of the BLDC motor drive by using proposed algorithm found to have the rise time of 0.028 second, settling time of 0.03 second and zero percent overshoot per 3600 RPM motor speed when 10Nm load torque is externally applied. But, at no load condition the speed dynamic performance of the motor specifically, the rise time is 0.009

second, settling time is 0.01 second with zero percent overshoot per motor speed of 3600 RPM. The trapezoidal commutation results in larger torque ripple at low speed operation, but, lower torque ripple at high speed operation. The torque ripple is reduced to be less than 8% of its command torque value by using proposed control algorithm.

After a few decades the engine based vehicle will be replaced by electric vehicle because of environmental impact, incremental of the cost of the fossil fuel and expected discontinuity of the world fossil fuel supplies in the future. Because of these reasons, BLDC motor controllers must be studied further and further for the purpose of electric vehicle propulsion.

5.2. Recommendations

The hardware implementation of speed control of BLDC motor by using PWM current controller by and DSP kit is recommended. But, it needs high caution while using this device. Besides, it is recommended that center of transportation and vehicle engineering (ASTU) members need to work strongly on DSP based BLDC motor drive in order to realize electric vehicle. In Adama Science and Technology University students are not getting DSP workshop. Therefore it is recommended to have it and teach students as DSP is the modern and smart motor drive technology. It is also recommended to implement the BLDC motor drive by using arduino micro controller.

References

[1] A. Tashakori and Etal., "Direct Torque Controlled Drive Train for Electric Vehicle," *Proceedings of the World Congress on Engineering,* vol. 2, p. 1, July 2012.

[2] Rubi batham and Rameshwar singh, "Speed Control of Brushless DC Motor Using Different Intelligence," *International Research Journal of Engineering and Technology (IRJET),* vol. 4, no. 10, p. 1, Oct. 2017.

[3] A.F.M. Sajidul Qadir, Electro-mechanical modeling of SEDM(separately excited DC motor) & performance improvement using different industrial controllers, Lulu.com, 2013, p. 2.

[4] Jian Zhao and / Yangwei Yu, "Brushless DC Motor Fundamentals Application Note," *The future of analog IC Tecnology,* vol. 109, pp. 7,9-10, July 2014.

[5] A. Tashakori and N. Hosseinzadeh, "Characteristics of suitable drive train for electric vehicle," *Proceeding of the International Conference on Instrumentation, Measurement, Circuits and Systems* , 2011.

[6] S. R. Jape, "Comparison of electric motors for electric vehicle application," *'IJRET: International Journal of Research in Engineering and Technology,* vol. 06, no. 09, p. 2, september 2017.

[7] GAGANDEEP LUTHRA, "Comparison of characteristics of various motor drives currently used in electric vehicle propulsion system," *International Journal of Mechanical And Production Engineering,* vol. 5, no. 6, 2017.

[8] Nasser Hashernnia and Behzad Asaei, "Comparative Study of Using Different Electric Motors in the Electric Vehicles," *International Conference on Electrical Machines IEEE* , p. 3, 2008.

[9] Swaraj Ravindra Jape and Archana Thosar, "Comparison of electric motors for electric vehicle application," *IJRET: International Journal of Research in Engineering and Technology* , vol. 6, no. 9, p. 3 to 5, 2017.

[10] G. LUTHRA , "Comparison of characteristics of various motor drives currently used in electric vehicle propulsion system," *International Journal of Mechanical and Production Engineering,* vol. 5, no. 6, p. 2 to 3, Jun 2017.

[11] Ektesabi and N. Hosseinzadeh, "CHARACTERISTICS OF SUITABLE DRIVE TRAIN FOR ELECTRIC VEHICLE," *International Conference on Instrumentation, Measurement, Circuits and Systems,* 2011.

[12] Jay W. Schultz and Huard(PhD) Steve, "Comparing AC Induction with Permanent Magnet motors in hybrid vehicles and the impact on the value proposition," *Parker Hannifin,* p. 15, 2013.

[13] M. T. DiRenzo, "Switched reluctance motor control basic operation and example using the tms320f240," *tech. rep., Texas Instruments,* p. 3, 2014.

[14] Fatih Korkma and Etal, "Modified direct torque control for BLDC motor drives," *International Journal of Control Theory and Computer Modeling (IJCTCM),* vol. 6, p. 2, July 2016.

[15] Adrian BĂLŢĂŢANU and Leonard Marin FLOREA, "Comparison of electric motors used for electric vehicles propulsion," *international conference of scientific paper afases brasov,* pp. 23-25, may 2013.

[16] A. Tashakori and M. Ektesabi, "Comparison of different PWM switching modes of BLDC motor as drive train of electric vehicles," vol. 6, p. 2 to 5, 2012.

[17] Marcy Lowe and Etal, "Lithium-ion Batteries for Electric Vehicles," *THE U.S. VALUE CHAIN,* 2010.

[18] Sara Hamidizadeh, "Study of Magnetic Properties and Demagnetization Models of Permanent Magnets for Electric Vehicles Application," 2016.

[19] A. Tashakori, "A Simple Fault Tolerant Control System for Hall Effect Sensors Failure of BLDC Motor," *IEEE Conference on Industrial Electronics and Applications (ICIEA 2013),* p. 1, June 2013.

[20] Amol R. Sutar and Etal, "Implementation and study of BLDC motor drive system," *International journal of engineering sciences & research technology,* pp. 3-4, May 2016.

[21] M. Zhou and Etel, "Pure Electric Vehicle Power-train Parameters Matching based on Vehicle Performance," *International Journal of Control and Automation,* vol. 8, no. 9, p. 4, 2015.

[22] M. Ravi Teja Reddy and Etal, "Investigation of Capacity of Motor and its Simulation for an Electric Vehicle," *Journal of Chemical and Pharmaceutical Sciences,* no. 5, p. 2, October 2016.

[23] Shiyoung Lee (Ph.D), "A comparison study of the commutation methods for the three-phase permanent magnet brushless dc motor," 2014.

[24] J. E. Muralidhar and A. Parveen., "Analysis of Speed Control of Brushless Dc Motor," *International Sciences Press, India,* vol. 8, pp. 9-11, Jan-June 2015.

[25] Norhazilina, Binti Bahari and Etel., "Modeling and Simulation of Torque Hysteresis Controller for Brushless DC Motor Drives," *IEEE Symposium on Industrial Electronics and Applications,* p. 4, Septe. 2012.

[26] Pinaki Mukherjee and Mainak Sengupta, "Closed loop speed control of a laboratory fabricated Brush-less DC Motor drive prototype using position sensor," *National Power Electronics Conference (NPEC),* p. 6, 2017.

[27] M. E. Blessy and M.Murugan, "Modeling and Controlling of BLDC Motor Based Fuzzy Logic," *S.A. Engineering College, Chennai, Tamil Nadu,* p. 5, 2014.

[28] Ahmed M. Ahmed, "Brushless DC Motor Speed Control using both PI Controller and Fuzzy PI Controller," vol. 109, January 2015.

[29] Ramya A and Etal, "Hybrid Self Tuned Fuzzy PID controller for speed control of Brushless DC Motor," *ATKAFF,* pp. 2-5, 2016.

[30] Akash Varshney and Bharti Dwivedi, "Performance analysis of a BLDC drive under varying load," *IEEE 1st International Conference on Power Electronics, Intelligent Control and Energy Systems (ICPEICES),* p. 4, 2016.

[31] Bambang Sujanarko, "BLDC Motor Control for Electric Vehicle Based On Digital Circuit and Proportional," *Integral Controller, International Journal of Advanced Research in Electrical, Electronics and Instrumentation Engineering,* vol. 3, no. 9, p. 7, Septeber 2014.

[32] V. V. Ram Vikas, "Speed Control of BLDC motor Drive By Using PID Controllers," *Int.Journal of Engineering Research and Applications*, vol. 4, no. 4, p. 4, April 2014.

[33] Majid and Mohammed, Matlab as a Teaching and Learning Tool for Mathematics: A Literature Review, 2013/03/03.

[34] Kadry and Seifedine, "Learning Basic Mathematics Using MATLAB," *International Journal of Information Technology and Management*, 2014.

[35] Y.-k. Kim, "Parameter determination of the BLDC motor considering the dynamic equation of vehicle," *The XIX International Conference on Electrical Machines* , 2010.

[36] C. Saurabh , "Motor Torque Calculations For Electric Vehicle," *International journal of scientific & technology research*, vol. 4, no. 08, p. 2, 2015.

[37] M. Ravi Tereja Reddy and Etel., "Investigation of Capacity of Motor and its Simulation for an Electric Vehicle," *Journal of Chemical and Pharmaceutical SciencesISSN*, no. 5, p. 2, Oct. 2016.

[38] M.V.Ramesh and J.Amarnath, "Speed Torque characteristics of Brushless DC motor in either direction on load using ARM controller," *Journal of Energy Technologies and Policy*, vol. 2, 2011.

[39] Shivraj SDudhe and Archana G Thosar, "Mathematical modelling and simulation of three phase BLDC motor using MATLAB/Simulink," *International Journal of Advances in Engineering & Technology*, vol. 7, no. 5, p. 3, Nov. 2014.

[40] M. sandeep and B. Lachulal, "Design of A Closed Loop Speed Control For BLDC Motor, International Refereed Journal of Engineering and Science," vol. 3, no. 11, p. 7, Nev. 2014.

[41] S. K. Mangal and Amit Kumar Gupta, "Optimization of Parameters for Damping in Sandwich Structures," *International Journal of Performability Engineering*, vol. 12, 2016.

[42] Poland S. Burns, "Advanced control engineering tex book".

[43] Habibur and Etal, "Power System Stability Improvement by Using SVC With TID Tuned PID Controller," India, 2012.

[44] Md Mustafa Kamal and Lini Mathew and S.Chatterji, "Speed Control of Brushless DC Motor Using Intelligent Controllers," *IEEE*, p. 2, 2014.

[45] R.G.P.V. and Bhopal India, "Speed Control of DC Motor Using Genetic Algorithm Based PID Controller," *International Journal of Advanced Research in Computer Science and Software Engineering*, vol. 3, no. 7, 2013.

[46] DUSAN PETKOVIC and MIROSLAV RADOVANOVIC, "Using enetic algorithms for optimization of turning machining process," *Journal of Engineering Studies and Research*, vol. 19, p. 2, 2013.

[47] Saneh Lata Yadav and Asha Sohal, "Comparative Study of Different Selection Techniques in Genetic Algorithm," *International Journal of Engineering, Science and Mathematics* , vol. 6, no. 3, p. 4, 2017.

[48] A. B. M. S. Siew Mooi Lim and Etal, "Crossover and Mutation Operators of Genetic Algorithms," *International Journal of Machine Learning and Computing*, vol. 7, p. 3, Feburary 2017.

[49] Huseyin Demirci and Etal, "Chaotic Crossover Operator on Genetic Algorithm," *Journal of Advances in Information Technology* , vol. 6, no. 4, p. 1, November 2015.

[50] Nitasha Soni and Dr Tapas Kumar, "Study of Various Mutation Operators in Genetic Algorithms," *Nitasha Soni et al, / (IJCSIT) International Journal of Computer Science and Information Technologies*, vol. 5, p. 3, 2014.

Reference links: L

[L1]. Reference links of Table (2.1): Traction motors used for electric vehicles available in the world market (accessed on July 12, 2018).

1. https://en.wikipedia.org/wiki/Electric_car
2. http://www.electric-cars-are-for-girls.com/electric-car-motors.html
3. www.lightningcarcompany.co.uk/Lightning/home.html
4. https://www.tesla.com/
5. www.mitsubishi-motors.com.au/vehicles/i-miev
6. www.morgan-motor.co.uk/mmc/researchanddev/pluse.html
7. http://evworld.com
8. www.buddyelectric.no
9. www.byd.com/na/auto/e6.html
10. www.theelectriccarcorporation.co.uk
11. www.smartaustralia.com.au
12. www.teslamotors.com
13. www.mahindrareva.com/Reva-Home.html
14. http://thinkev.leftbankcompanies.com
15. www.stevensvehicles.co.uk

[L2]. Link for figures (Fig 3.3) (Accessed on august 10, 2018)

1. https://www.google.com/search?q=electric+vehicle+shaft+figure&client=firefoxbab&tbm=isch&tbo=u&source=univ&sa=X&ved=2ahUKEwiz0qu6ysHdAhXxx4UKHe8DCHcQsAR6BAgCEAE&biw=1366&bih=636

[L3]. Link for figures (Fig 3.3) (Accessed on august 10, 2018)

1. https://www.google.com/search?client=firefox-b-ab&biw=1366&bih=596&tbm=isch&sa=1&ei=PWKfW4jQNq2XlwSF4LmIDA&q=3.4.3.%09Reducer+for+car+figure&oq=3.4.3.%09Reducer+for+car+figure&gs_l=img.3...19302.19302.0.20312.1.1.0.0.0.0.247.247.2-1.1.0....0...1c.1.64.img..0.0.0....0.35W_Pfyib-g

Appendixes

Appendix A: Appendixes related to Analysis of data’s and system modeling

A.1. Appendixes related to Analysis of data’s

MATLAB code for the analysis motive force versus approaching angle of the vehicle (Figure 3.7)

```
clear all; close all;
m=1500; % Mass of the car
fric=0.01; %Friction coefficient
g=9.81; %gravitational acceleration
a=0.5;   % Acceleration (m/sec)
r=0.25324; % Radius of the wheel in meter
K_friction=0.01; %Coefficient of friction by considering the asphalt road
F_tot=0;
vkph=100; % Speed of the rotor in Km/hr
Tot_effcen.M=0.95; %Efficiency
Adnsty=1.2; %Kd/m3
Af=2; % Frontal area of the car (m2)
vo=0; %Air velocity in m/s
Cw=0.3;
%Initial condition
apangle=0;
apangle1=0;
d_apangle=1e-2; %unit step increment
apangle_final=30; %final value in degree
x=1;n=1;
while(apangle<apangle_final),
   vmps=vkph*(1000/3600);
   theta=apangle*(2*pi/360);
FA=0.5*Adnsty*Cw*Af*(vmps+vo)^2;
if  apangle<=100*d_apangle;
    statfric=0.001;
else
```

```
    statfric=0;
end
Frolling=m*g*(K_friction+statfric)*cos(theta);
Fgradient=m*g*sin(theta);
F_tot=Frolling+Fgradient+FA+m*a; % Total force (Nm)
apangle=apangle+d_apangle;
apangle1=apangle1+d_apangle;
if x>16,
   F_totn(n)=F_tot;
   Fgradientn(n)=Fgradient;
   Frollingn(n)= Frolling;  %Power in KW
   FAn(n)=FA;
   apanglen(n)=apangle;
   n=n+1;
   x=1;
end
  x=x+1;
end
figure(1);
plot(apanglen, F_totn,'k',apanglen,Fgradientn,'b--',apanglen,Frollingn,'k:',apanglen,FAn,'r')
axis([0 30 0 8000]);
 grid
xlabel('Approaching angle')
ylabel('Motive forces (N)')
```

……………………………………………………………………………………….

MATLAB code for the analysis motive forces vs speed of the car in Km/hr

(Figure 3.8)

```
clear all; close all;
m=1500;
fric=0.01;
g=9.81;
a=0.5;
r=0.25324; % Radius of the wheel in meter
```

```
K_friction=0.01; %Coefficient of friction by considering the asphalt road
r=0.25324;
F_tot=0;
vkph=100; %speed of the rotor in Km/hr
Tot_effcen.M=0.95;
Adnsty=1.2; %Kd/m3
Af=2; %area in m2
vo=0; %air velocity in m/s
Cw=0.3;
%Initial condition
apangle=0;
Vkph=0;
Vkph1=0;
d_Vkph=1e-2; %unit step increment
Vkph_final=130; %final value in degree
x=1;
n=1;
while(Vkph<Vkph_final),
   vmps=Vkph*(1000/3600);
   theta=apangle*(2*pi/360);
FA=0.5*Adnsty*Cw*Af*(vmps+vo)^2;
if  Vkph<=100*d_Vkph;
    statfric=0.1;
else
    statfric=0;
end
Fac=m*a;
Frolling=m*g*(K_friction+statfric)*cos(theta);
Fgradient=m*g*sin(theta);
F_tot=Frolling+Fgradient+FA+Fac; % Total force (Nm)
Vkph=Vkph+d_Vkph;
Vkph1=Vkph1+d_Vkph;
if x>16,
   F_totn(n)=F_tot;
```

```
    Fgradientn(n)=Fgradient;
    Frollingn(n)= Frolling;  %Power in KW
    FAn(n)=FA;
    Facn(n)=Fac;
    Vkphn(n)=Vkph;
    n=n+1;
    x=1;
end
  x=x+1;
end
figure(1);
plot(Vkphn,
F_totn,'k',Vkphn,Fgradientn,'k',Vkphn,Frollingn,'k:',Vkphn,FAn,'r',Vkphn,Facn,'r--
','LineWidth',1.3)
axis([0 130 0 2500]);
grid
xlabel('Speed of the car in Kmph')
ylabel('Motive forces (N)')
set(gca, 'FontName','TimesNewRoman')
set(gca, 'FontSize',12)
```

……………………………………………………………………………………..

MATLAB code for the analysis of Repelling force, Repelling Torque and Power required to drive EV vs departure angle of the road in degree **(Figure 3.9 and others)**

```
clear all; close all;
m=1500;
fric=0.01;
g=9.81;
a=0;
r=0.25324; % Radius of the wheel in meter
c_ofriction=0.01; %Coefficient of friction by considering the asphalt road
d=0.25324;
v=14.29; %speed of the rotor in m/se=51.444km/h
Tot_effcen.M=0.95;
```

```
Adnsty=1.2; %Kd/m3
Af=2; %area in m2
vo=0; %air velocity in m/s
Cw=0.3;
%Initial condition
angleR=0;
angleR1=0;
d_angleR=1e-6; %unit step increment
angleR_final=40; %final value in degree
x=1;
n=1;
while(angleR<angleR_final),
    Fadyna=0.5*Adnsty*Cw*Af*(v+vo)^2;
    theta=angleR*2*pi/360; %Degree to radian conversion
F_tot=m*g*(sin(theta)+c_ofriction*cos(theta))+Fadyna+m*a; % Total force(Nm)
Power=F_tot*v; %W
Torque=(Power*r/v)/0.95;% Nm
angleR=angleR+d_angleR;
angleR1=angleR1+d_angleR;
if x>16,
    F_totn(n)=F_tot;
    Torquen(n)=Torque;
    Powern(n)=Power/1000;  %Power in KW
    Fadynan(n)=Fadyna;
    thetan(n)=angleR;
    n=n+1;
    x=1;
end
  x=x+1;
end
figure(1);
plot(thetan,F_totn,'b','LineWidth',2);
axis([0 40 0 8000]);
grid
```

```
xlabel('Departure angle in degree')
ylabel('F_t_o_t (N)')
figure(2);
plot(thetan,Torquen,'b','LineWidth',2);
axis([0 40 0 1600]);
grid
xlabel('Approaching angle in degree')
ylabel('Requred Torque (Nm)')
figure(3);
plot(thetan,Powern,'b','LineWidth',2);
axis([0 40 0 200]);
grid
xlabel('The approaching angle in degree')
ylabel('Power (KW)')
```

…………………………………………………………………………………….

MATLAB **code** for the analysis of aerodynamics force, Power required to drive EV vs speed in Km/hr. **(Figure 3.6, 3.10)**

```
clear all; close all;
m=1500;
fric=0.01;
g=9.81;
a=1;
r=0.25324; % Radius of the wheel in meter
K_friction=0.01; %Coefficient of friction by considering the asphalt road
F_tot=0;
v=14.29; %speed of the rotor in m/se=51.444km/h
Tot_effcen.M=0.95;
Adnsty=1.2; %Kd/m3
Af=2; %area in m2
vo=0; %air velocity in m/s
Cw=0.3;
%Initial condition
Vkph=0;
```

```
Vkph1=0;
d_Vkph=1e-2; %unit step increment
Vkph_final=140; %final value in km/hr.
x=1;
n=1;
while(Vkph<Vkph_final),
 Vmps=Vkph*(1000/3600);
Fadyna=0.5*Adnsty*Cw*Af*(Vmps+vo)^2;
if  Vkph<=100*d_Vkph;
     statfric=0.2;
else
     statfric=0;
end
F_tot=m*g*(K_friction+statfric)+Fadyna+m*a; % Total force(Nm)
Power=F_tot*Vmps/0.95; % Required input power (Watt)
Torque=(Power*r/Vmps);% Nm
Vkph=Vkph+d_Vkph;
Vkph1=Vkph1+d_Vkph;
if x>16,
    F_totn(n)=F_tot;
    Torquen(n)=Torque;
    Powern(n)=Power/1000;  %Power in KW
    Fadynan(n)=Fadyna;
    Vkphn(n)=Vkph;
    n=n+1;
    x=1;
end
  x=x+1;
end
figure(1);
plot(Vkphn,Powern,'r','LineWidth',2);
set(gca,'FontSize',12)
axis([0 130 0 110]);
grid
```

```
xlabel('Speed of the of the car(Km/hr)')
ylabel('Power (KW)')
figure(2);
plot(Vkphn,Fadynan,'r');
axis([0 110 0 300]);
grid
xlabel('Speed of the of the car(Km/hr)')
ylabel('Aerodynamic dragging force (N)')
```

……………………………………………………………………………………….

MATLAB code for motive force, torque and Power and characteristics as the speed of the motor is increasing **(Figure 3.11 and others)**

```
Ratedpower=60000; %Rated power in Watt
wrpm=0; %initial condition
wrpm1=0;
wb=187.5; %base speed in rad/sec
d_wrpm=1e-2; %unit step increment
wrpm_final=12000; %final value in RPM
x=1;
n=1;
while(wrpm<wrpm_final),
wm=wrpm*(2*pi)/60;
Torque= Ratedpower/wm;
if Torque>=320,
Torque=320;
end
if Torque<320,
Torque= Torque;
end
Power=Torque*wm;
wrpm=wrpm+d_wrpm;
wrpm1=wrpm1+d_wrpm;
if x>16,
   wrpmn(n)=wrpm;
```

```
    Torquen(n)=Torque;
    Powern(n)=Power/1000;
    n=n+1;
    x=1;
end
  x=x+1;
end
figure(1);
[AX,Torque,Power]=plotyy(wrpmn,Torquen, wrpmn,Powern);
axis([0 12000 0 350]);
set(get(AX(1),'ylabel'), 'string','Torque(Nm)')
set(get(AX(2),'ylabel'), 'string','Power(KW)')
set(Torque,'LineStyle','--')
set(Power,'LineStyle','-')
set(gca, 'FontName','TimesNewRoman')
set(gca, 'FontSize',12)
set([Torque,Power],'LineWidth',0.5)
xlabel('w_m(rpm)')
grid
legend('Torque','Power')
```

……………………………………………………………………………………………

MATLAB Codes to analyze the output power density of BLDCM Vs PMSM (Figure 3.13)

```
clear all; close all;
te_ref=320; %Torque in Nm
kb=0.925;
p=4; %poles
wr=376.9911189; %rad per sec or 3600rpm
lamda=kb*(p/2);
ip_cmd = te_ref/(2*lamda); %Rms value of BLDCM
IpeakPMSM=ip_cmd*2/sqrt(3); %peak current value of PMSM
% initial condition
tetar=0;
```

```
ias_ref=0;
ibs_ref=0;
ics_ref=0;
fas_tetar=0;
fbs_tetar=0;
fcs_tetar=0;
d_tetar=0.01;
tetar1=0;
tetar_final=(2*pi); %final thr
n=1;
x=1;
while(tetar<tetar_final)
tetar_deg = tetar*180/pi;
% adjust the range of th_deg (0<=angle in degree<=360)
if ((tetar<=0)|(tetar>2*pi));
if (tetar_final<0)
tetar = tetar+2*pi;
elseif (tetar_final>2*pi)
tetar = tetar-2*pi;
end
elseif ((tetar>=0)&(tetar<=2*pi));
% phase current command according to the rotor position
if (((tetar_deg>=0)&(tetar_deg<30))|((tetar_deg>=330)&(tetar_deg<=360)))
ias_ref = 0;
ibs_ref = -ip_cmd;
ics_ref = ip_cmd;
elseif ((tetar_deg>=30)&(tetar_deg<90))
ias_ref = ip_cmd;
ibs_ref = -ip_cmd;
ics_ref = 0;
elseif ((tetar_deg>=90)&(tetar_deg<150))
ias_ref = ip_cmd;
ibs_ref = 0;
ics_ref = -ip_cmd;
```

```
elseif ((tetar_deg>=150)&(tetar_deg<210))
ias_ref = 0;
ibs_ref = ip_cmd;
ics_ref = -ip_cmd;
elseif ((tetar_deg>=210)&(tetar_deg<270))
ias_ref = -ip_cmd;
ibs_ref = ip_cmd;
ics_ref = 0;
elseif ((tetar_deg>=270)&(tetar_deg<330))
ias_ref = -ip_cmd;
ibs_ref = 0;
ics_ref = ip_cmd;
end
% fas(thr): rotor position dependent function
if ((tetar_deg>=0)&(tetar_deg<30))
fas_tetar = tetar_deg/30;
elseif ((tetar_deg>=30)&(tetar_deg<150))
fas_tetar = 1;
elseif ((tetar_deg>=150)&(tetar_deg<210))
fas_tetar = -tetar_deg/30+6;
elseif ((tetar_deg>=210)&(tetar_deg<330))
fas_tetar = -1;
elseif ((tetar_deg>=330)&(tetar_deg<=360))
fas_tetar = tetar_deg/30-12;
end
% fbs(thr): rotor position dependent function
if ((tetar_deg>=0)&(tetar_deg<90))
fbs_tetar = -1;
elseif ((tetar_deg>=90)&(tetar_deg<150))
fbs_tetar = tetar_deg/30-4;
elseif ((tetar_deg>=150)&(tetar_deg<270))
fbs_tetar = 1;
elseif ((tetar_deg>=270)&(tetar_deg<330))
fbs_tetar = -tetar_deg/30+10;
```

```
elseif ((tetar_deg>=330)&(tetar_deg<=360))
fbs_tetar = -1;
end
% fcs(thr): rotor position dependent function
if ((tetar_deg>=0)&(tetar_deg<30))
fcs_tetar = 1;
elseif ((tetar_deg>=30)&(tetar_deg<90))
fcs_tetar = -tetar_deg/30+2;
elseif ((tetar_deg>=90)&(tetar_deg<210))
fcs_tetar = -1;
elseif (tetar_deg>=210)&(tetar_deg<270)
fcs_tetar = tetar_deg/30-8;
elseif ((tetar_deg>=270)&(tetar_deg<=360))
fcs_tetar = 1;
end
end
% compute back emf
Eas = fas_tetar*kb*wr;
Ebs = fbs_tetar*kb*wr;
Ecs = fcs_tetar*kb*wr;
Epeak=1*kb*wr;
poutBLDCM=(Eas*ias_ref+Ebs*ibs_ref+Ecs*ics_ref);
poutPMSM=3*(IpeakPMSM*Epeak)/2;
tetar=tetar+d_tetar; %Increment time
tetar1=tetar1+d_tetar;
if x>16,
Easn(n) =Eas;
Ebsn(n) =Ebs;
Ecsn(n) =Ecs;
ias_refn(n)= ias_ref;
ibs_refn(n) = ibs_ref;
ics_refn(n) =ics_ref;
poutBLDCMn(n)=poutBLDCM;
poutPMSMn(n)=poutPMSM;
```

```
PoutbldcmtoPoutpmsmn(n)=(poutBLDCM/poutPMSM)*100;
tetarn(n)=tetar;
n=n+1;
x=1;
end
x=x+1;
end
figure(4);
subplot(4,1,1)
plot(tetarn,Easn,'b--',tetarn,Ebsn,'r:', tetarn,Ecsn,'k','LineWidth',1.3); axis([0 2*pi -400
400]);
ylabel('e_a_s,e_b_s,e_c_s(Volt)'); grid off; box off;
legend('e_a_s','e_b_s','e_c_s')
subplot(4,1,2)
plot(tetarn,ias_refn,'b--',tetarn,ibs_refn,'r:', tetarn,ics_refn,'k','LineWidth',1.3); axis([0 2*pi
-200 200]);
ylabel('i_a_s,i_b_s,i_c_s (Ams)'); grid off; box off;
legend('i_a_s','i_b_s','i_c_s')
subplot(4,1,3)
plot(tetarn,poutBLDCMn,'k',tetarn,poutPMSMn,'r--','LineWidth',1.3); axis([0 2*pi 0
0.8*10^5]);
ylabel('P_o_u_tBLDC, P_o_u_t_PMSM'); grid off; box off;
legend('P_o_u_tBLDC','P_o_u_t_PMSM')
subplot(4,1,4)
plot(tetarn,PoutbldcmtoPoutpmsmn,'k','LineWidth',1.3);
axis([0 2*pi 0 120]);
ylabel('Output power ratio in(%)'); grid off; box off;
legend('P_o_u_tBLDCM/P_o_u_tPMSM')
xlabel('thr (rad.)')
set(gca, 'FontName','TimesNewRoman')
set(gca, 'FontSize',12)
```
…………………………………………………………………………………………

MATLAB code for the comparison of BLDC motor and PMSM in case of power and torque output (Figure 3.14)

```
%Initial conditions
wm=0; %initial condition
wm1=0;
wb=187.5; %base speed in rad/sec
d_wm=1e-2; %unit step increment
wm_final=1256; %final value in rad/se
x=1;
n=1;
while(wm<wm_final),
if wm<=wb,
   TeBLDCM=320; %BLDCM torque
   TePMSM=320/1.15;
elseif wm>wb,
   TeBLDCM=poutBLDCM/wm;
   TePMSM=poutPMSM/wm;% PMSM torque
end
poutBLDCM=TeBLDCM*wm; %BLDCM output power
poutPMSM=poutBLDCM/1.15;%PMSM output power
wm=wm+d_wm;
wm1=wm1+d_wm;
if x>16,
   wmn(n)=wm;
   TeBLDMn(n)=TeBLDCM;
   TePMSMn(n)=TePMSM;
   poutBLDCMn(n)=poutBLDCM;
   poutPMSMn(n)=poutPMSM;
   n=n+1;
   x=1;
end
  x=x+1;
end
```

```
figure(2);
subplot(2,1,1)
plot(wmn,TeBLDMn,'k--',wmn,TePMSMn,'r','LineWidth',1.2);
axis([0 1256 0 400]);
ylabel('Te_B_L_D_C_M,Te_P_M_S_M (Nm)')
xlabel('w_m(rad/sec)')
grid
legend('Te_B_L_D_C_M','Te_P_M_S_M')
subplot(2,1,2)
plot(wmn,poutBLDCMn,'k--',wmn,poutPMSMn,'r','LineWidth',1.2);
axis([0 1250 0 1e5]);
ylabel('P_o_u_tBLDCM, P_o_u_tPMSM (wat)')
grid
legend('P_o_u_tBLDCM','P_o_u_tPMSM (wat)')
xlabel('w_m(rad/sec')
set(gca, 'FontSize',12)
```

……………………………………………………………………………………………

MATLAB code for to calculate current rating of the motor for EV **(Figure 3.15)**

```
io=5; %No load current
v=350; %Battery voltage in volt.
i=0; %initial condition
i1=0;
d_i=1e-4; %unit step increment
i_final=320; %final value
x=1;
n=1;
while(i<=i_final),
   Rm=0.7;
piron=v*io;
pcu=(i)^2*Rm;
pin=i*v;
pout=pin-pcu-piron;
eff=pout/pin*100;
```

```
i=i+d_i;
i1=i1+d_i;
if x>16,
   effn(n)=eff;
   poutn(n)=pout;
   pcun(n)=pcu;
   pironn(n)=piron;
   pinn(n)=pin;
   in(n)=i;
    n=n+1;
    x=1;
end
  x=x+1;
end
figure(4);
 subplot(4,1,1)
plot(in,pinn,'k');
axis([0 320 -100020 100020]); set(gca,'xticklabel')
ylabel('Input power of BLDCM in (wat)')
subplot(4,1,2)
plot(in,pcun, in,pironn,'k');
axis([0 320 -100000 100000]); set(gca,'xticklabel')
ylabel('Cupper and iron loss of BLDCM in (wat)')
subplot(4,1,3)
plot(in,poutn,'k');
axis([0 320 -100000 100000]); set(gca,'xticklabel')
ylabel('Output power of BLDCM in (wat)')
subplot(4,1,4)
plot(in,effn,'k');
axis([0 320 -120 120]); set(gca,'xticklabel')
ylabel('Efficiency of BLDCM in %')
```
………………………………………………………………………………………...

MATLAB code on SOC of Battery (figure 3.17)

```
        V1=100;   %Km/hr
        Wrated=32; %KWhr
        Pm=25; %KW
S=0;
S1=0;
d_S=1e-4; %unit step increment
S_final=150; % Km final value
x=1;
n=1;
while(S<=S_final),
 W=Pm*S/V1;
 SOC=(Wrated-W)*100/Wrated;
S=S+d_S;
S1=S1+d_S;
if x>16,
   SOCn(n)=SOC;
   Sn(n)=S;
    n=n+1;
    x=1;
end
  x=x+1;
end
figure(1);
plot(Sn,SOCn,'r','LineWidth',2);
axis([0 125 0 100]); set(gca,'xticklabel')
xlabel('Distance in Km')
ylabel('SOC (%)')
grid
```

A.2. Appendixes related to system modeling

Flux for each phase is given by equation (A.1), where, $\lambda_p(\theta)$ represented as permanent magnet flux linkage of phase (A, B, C), θ is the rotor position angle, L is self-inductance and M is mutual inductance.

$$\lambda_A = L_a I_a + M_{AB} I_b + M_{AC} I_c + \lambda_p(\theta)$$
$$\lambda_B = L_b I_b + M_{BC} I_c + M_{BA} I_a + \lambda_p(\theta) \quad (A.1)$$
$$\lambda_C = L_c I_c + M_{CA} I_a + M_{CB} I_b + \lambda_p(\theta)$$

The line to line voltage of BLDCM will be as the following equation:

$$\begin{bmatrix} V_{AB} \\ V_{BC} \\ V_{CA} \end{bmatrix} = \begin{bmatrix} R & -R & 0 \\ 0 & R & -R \\ -R & 0 & R \end{bmatrix} \begin{bmatrix} i_a \\ i_b \\ i_c \end{bmatrix} + \begin{bmatrix} L-M & M-L & 0 \\ 0 & L-M & M-L \\ M-L & 0 & L-M \end{bmatrix} \frac{d}{dt} \begin{bmatrix} i_A \\ i_B \\ i_C \end{bmatrix} + \begin{bmatrix} E_{AB} \\ E_{BC} \\ E_{CA} \end{bmatrix} \quad (A.2)$$

The back EMF signals have a phase shift of 120 electrical degrees with respect to each other due to symmetrical distribution of the phase winding in the stator.

$$\begin{cases} E_a = \lambda_p \omega_r f_A(\theta_e) \\ E_b = \lambda_p \omega_r f_A\left(\theta_e + \frac{2\pi}{3}\right) \\ E_c = \lambda_p \omega_r f_A\left(\theta_e - \frac{2\pi}{3}\right) \end{cases} \quad (A.3)$$

The Simulink model of Hall Effect sensor is as shown in (Fig. A.2)

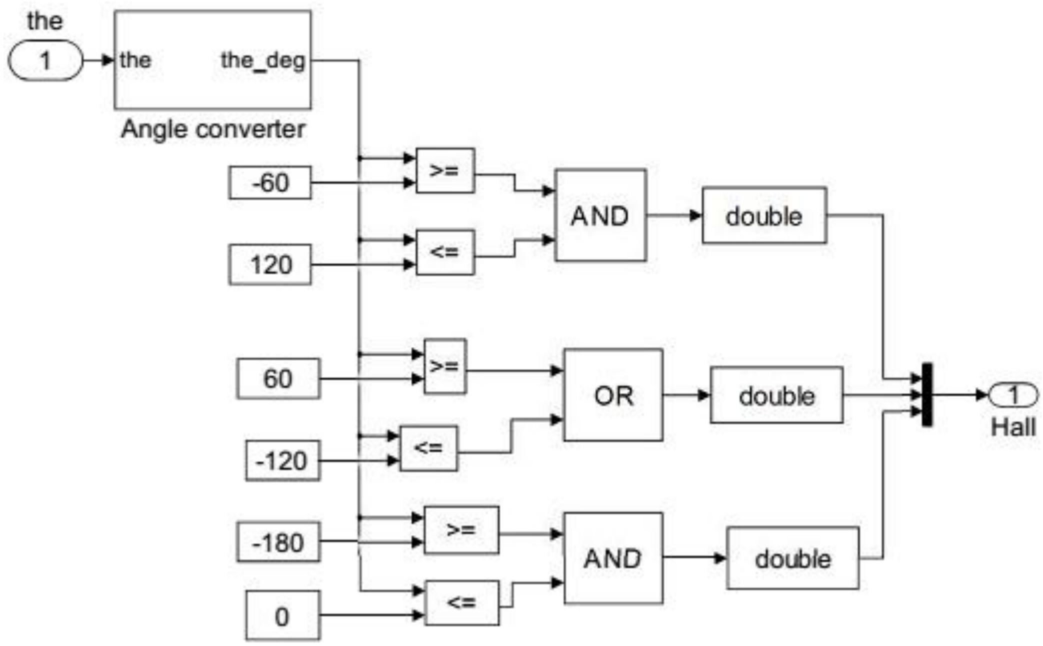

Figure A. 1: MATLAB/Simulink model of BLDC motor

The MATLAB/Simulink model of BLDC motor with its Hall Effect sensors is shown as in figure (A.2).

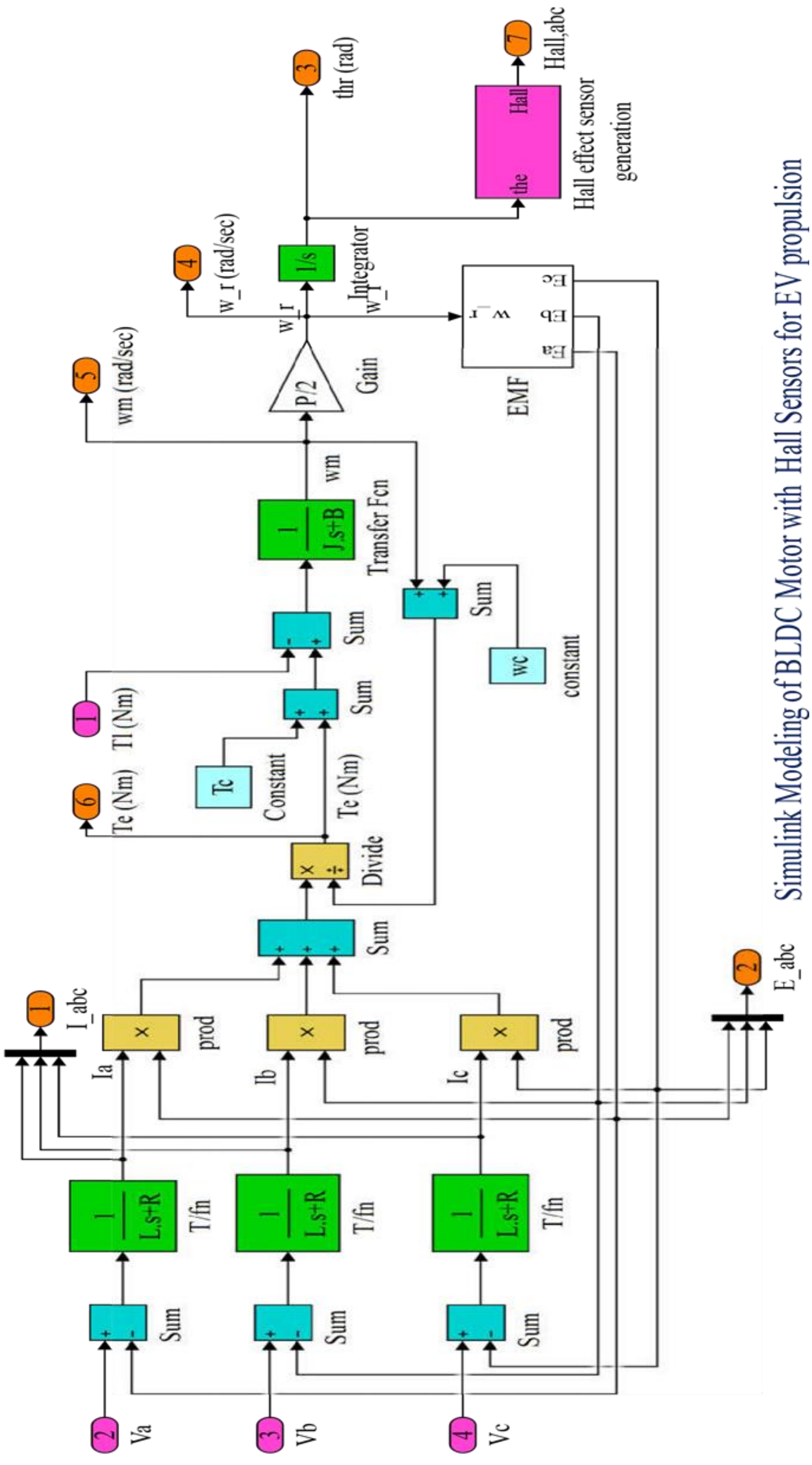

Figure A. 2: Simulink model of BLDC motor

This model can be simplified to S function as in the following figure (A.3).

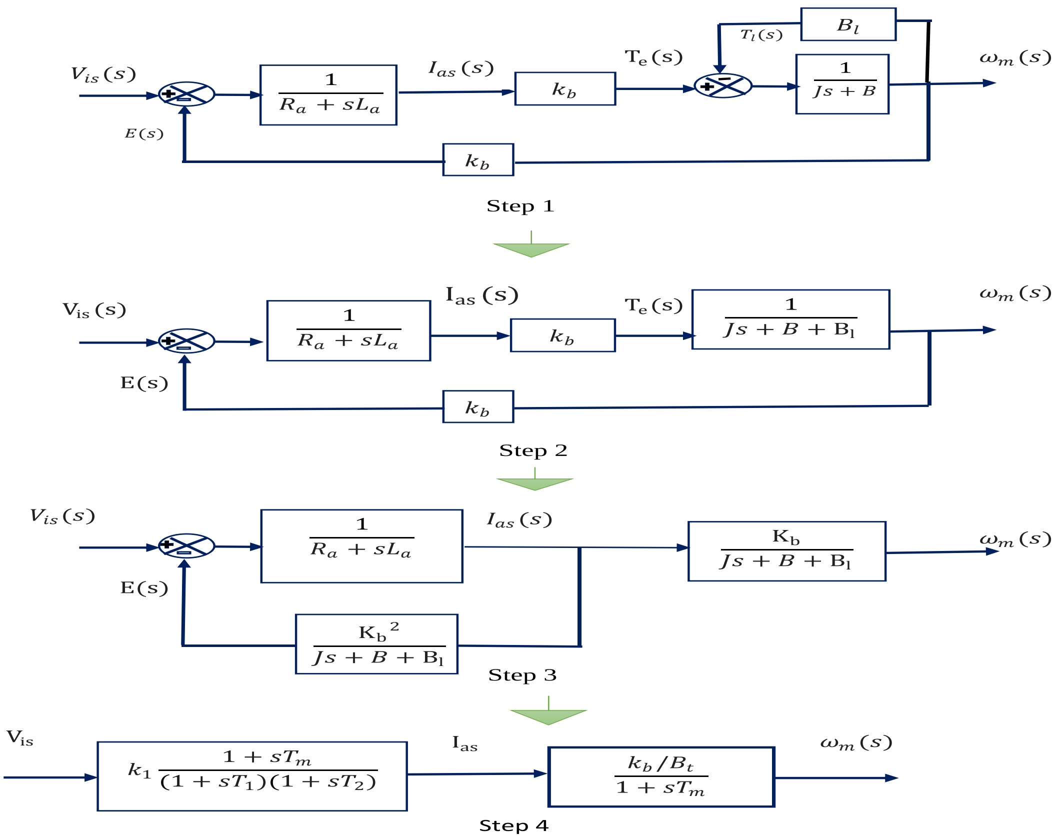

Figure A.3: Structure diagram of BLDC motor with load torque

In order to decouple the inner current loop from the machine inherent induced EMF, it is necessary to split the transfer function into two cascaded transfer functions as shown in equation (A.4) and equation (A.5).

$$\frac{\omega_m(s)}{V_{is}(s)} = \frac{\omega_m(s)}{I_{as}(s)} * \frac{I_{as}(s)}{V_{is}(s)} \tag{A.4}$$

$$\frac{\omega_m(s)}{I_{as}(s)} = \frac{K_b(s)}{B_t(1 + sT_m)} \tag{A.5}$$

Appendix B: Appendixes related to result and discussion

MATLAB sample code for speed control of BLDC motor by using PWM current controller is shown as the following;

```
clear all; close all; clc;
global phase Rs Ls_m V_as V_bs V_cs E_as E_bs E_cs
global J B_fric Pole Torque Torque_load
The motor parameters value
Rs = 1.2; Ls_m = 2.95e-3; J = 0.00895; B_fric = 0.001;
Pole = 4; Vdc = 350; K_b = 0.925/4; Lamd_p =K_b*(Pole/2);
Ipeak_rate = 172; Torque_rate = 15.9; Wr_base_rpm = 3600;
 Base values of the parameters
V_base = Vdc;
I_base = Ipeak_rate;
Te_base = Torque_rate;
Wr_base = Wr_base_rpm*(pi/30)*(Pole/2);
 Initial stator current
I_as = 0; I_bs = 0; I_cs = 0;
 Rotor speed and position
W_r=0;
Theta_r=0;
 Old initial position
Theta_r_old = Theta_r;
Wr_cmd = Wr_base; % speed command=0
Kp = 28; Ki = 3.56789; Kd=0.0000028347062; % PID-speed controller gain Parameters
Wr_intg = 0; Torqe_ref = 0; Torque_star =0;
Torque_lim_p = 2*Torque_rate; Torqe_lim_n = -2*Torque_rate;
Torque_load = 10; % load torque
Kp_i = 100; % p current controller gain
 Controller output
V_asc = 0; V_bsc = 0; V_csc = 0;
 Triangular wave frequency and peak voltage
fc = 8000; V_cm_trA = 10;  Carrier frequency
Voltage command limit
```

```
Vcom_lim_p = 9; Vcom_lim_n = -9;
Initial time, time increment, and final time
ti=0.0; %Simulation starting time
t = 0; %Initial time
t1=0;
dt = 1e-6; tf = 0.8; Time increment & Final running time
MATLAB functions for plotting purpose
Lakkaayi = 0;
Intig_no = 0;
Desim_no = fix(tf/dt/(Intig_no+1));
Plot_vabcs = zeros(Desim_no,3);
Plot_fabcs = zeros(Desim_no,3);
Plot_eabcs = zeros(Desim_no,3);
Plot_isc = zeros(Desim_no,4);
Plot_iabcs = zeros(Desim_no,3);
Plot_torq = zeros(Desim_no,5);
Plot_wrthr = zeros(Desim_no,4);
Plot_t = zeros(Desim_no,1);
Solving the dynamics of motor
iter = 0;
iter1 =0;
while (t<=tf)
Reference speed control setting
if ((t>0)&(t<=0.3))
Wr_cmd = 0.5*Wr_base;
elseif ((t>0.3)&(t<=0.5))
Wr_cmd = -0.5*Wr_base;
elseif(t>0.5)
   Wr_cmd=0.5*Wr_base;
end
Speed controller and torque command generation by using PID.
Wr_err = Wr_cmd-W_r;
Wr_dif=Kd*Wr_err;
Wr_intg = Wr_intg+Ki*(Wr_err+Torqe_ref-Torque_star)*dt;
```

```
Torque_star=Wr_intg+Kp*Wr_err+Wr_dif;
if (Torque_star>=Torque_lim_p)
Torqe_ref = Torque_lim_p;
elseif (Torque_star<=Torqe_lim_n)
Torqe_ref = Torqe_lim_n;
else
Torqe_ref = Torque_star;
end
 Conversion of the unit (rad to degree)
Ipeak_cmd = Torqe_ref/(2*Lamd_p);
 Adjustment of the range of degree between (0<=360)
Thetar_deg = Theta_r*180/pi;
while ((Thetar_deg<0)|(Thetar_deg>360))
if (Thetar_deg<0)
Thetar_deg = Thetar_deg+360;
elseif (Thetar_deg>360)
Thetar_deg = Thetar_deg-360;
end
end
Phase current command depending on the rotor position
if (((Thetar_deg>=0)&(Thetar_deg<30))|((Thetar_deg>=330)&(Thetar_deg<=360)))
mode = 1;
Ias_ref = 0;
Ibs_ref = -Ipeak_cmd;
Ics_ref = Ipeak_cmd;
elseif ((Thetar_deg>=30)&(Thetar_deg<90))
mode = 2;
Ias_ref = Ipeak_cmd;
Ibs_ref = -Ipeak_cmd;
Ics_ref = 0;
elseif ((Thetar_deg>=90)&(Thetar_deg<150))
mode = 3;
Ias_ref = Ipeak_cmd;
Ibs_ref = 0;
```

```
Ics_ref = -Ipeak_cmd;
elseif ((Thetar_deg>=150)&(Thetar_deg<210))
mode = 4;
Ias_ref = 0;
Ibs_ref = Ipeak_cmd;
Ics_ref = -Ipeak_cmd;
elseif ((Thetar_deg>=210)&(Thetar_deg<270))
mode = 5;
Ias_ref = -Ipeak_cmd;
Ibs_ref = Ipeak_cmd;
Ics_ref = 0;
elseif ((Thetar_deg>=270)&(Thetar_deg<330))
mode = 6;
Ias_ref = -Ipeak_cmd;
Ibs_ref = 0;
Ics_ref = Ipeak_cmd;
end
```

Induced EMF reference generation for phase 'A'

```
if ((Thetar_deg>=0)&(Thetar_deg<30))
fas_thr = Thetar_deg/30;
elseif ((Thetar_deg>=30)&(Thetar_deg<150) )
fas_thr = 1;
elseif ((Thetar_deg>=150)&(Thetar_deg<210) )
fas_thr = -Thetar_deg/30+6;
elseif ((Thetar_deg>=210)&(Thetar_deg<330))
fas_thr = -1;
elseif ((Thetar_deg>=330)&(Thetar_deg<=360))
fas_thr = Thetar_deg/30-12;
end
```

Induced EMF reference generation for phase 'B'.

```
if ((Thetar_deg>=0)&(Thetar_deg<90))
fbs_thr = -1;
elseif ((Thetar_deg>=90)&(Thetar_deg<150))
fbs_thr = Thetar_deg/30-4;
```

```
elseif ((Thetar_deg>=150)&(Thetar_deg<270))
fbs_thr = 1;
elseif ((Thetar_deg>=270)&(Thetar_deg<330))
fbs_thr = -Thetar_deg/30+10;
elseif ((Thetar_deg>=330)&(Thetar_deg<=360))
fbs_thr = -1;
end
```

Induced EMF reference generation for phase 'C'.

```
if ((Thetar_deg>=0)&(Thetar_deg<30))
fcs_thr = 1;
elseif ((Thetar_deg>=30)&(Thetar_deg<90))
fcs_thr = -Thetar_deg/30+2;
elseif ((Thetar_deg>=90)&(Thetar_deg<210))
fcs_thr = -1;
elseif ((Thetar_deg>=210)&(Thetar_deg<270))
fcs_thr = Thetar_deg/30-8;
elseif ((Thetar_deg>=270)&(Thetar_deg<=360))
fcs_thr = 1;
end
```

Computation of induced back EMF

```
E_as = fas_thr*K_b*W_r;
E_bs = fbs_thr*K_b*W_r;
E_cs = fcs_thr*K_b*W_r;
```

Triangular carrier wave generation

```
V_tr = rem(4*fc*V_cm_trA*t,4*V_cm_trA);
if (V_tr<V_cm_trA)
V_tr = V_tr;
elseif (V_tr<(3*V_cm_trA))
V_tr = 2*V_cm_trA-V_tr;
else
V_tr = V_tr-4*V_cm_trA;
End
```

Position difference of the rotor to know the direction of the rotor

```
Change_Theta = Theta_r-Theta_r_old;
```

```
Theta_r_old = Theta_r;
 Voltage control of phase ‘A’ computation and control of freewheeling diode
if ((mode~=1)&(mode~=4))
Ias_det = 1;
V_asc = Kp_i*(Ias_ref-I_as);
if (V_asc>Vcom_lim_p)
V_asc = Vcom_lim_p;
elseif (V_asc<Vcom_lim_n)
V_asc = Vcom_lim_n;
end
if (V_asc>=V_tr)
V_as = Vdc/2;
else
V_as = -Vdc/2;
end
elseif (((Change_Theta<0)&(mode==1))|((Change_Theta>=0)&(mode==4)))
if (I_as<=0)
Ias_det = 0;
I_as = 0;
V_as = E_as;
else
Ias_det = 1;
V_as = -Vdc/2;
end
elseif (((Change_Theta>=0)&(mode==1))|((Change_Theta<0)&(mode==4)))
if (I_as>=0)
Ias_det = 0;
I_as = 0;
V_as = E_as;
else
Ias_det = 1;
V_as = Vdc/2;
end
end
```

Voltage control of phase B computation and control of freewheeling diode

```
if ((mode~=3)&(mode~=6))
Ibs_det = 1;
V_bsc = Kp_i*(Ibs_ref-I_bs);
if (V_bsc>Vcom_lim_p)
V_bsc = Vcom_lim_p;
elseif (V_bsc<Vcom_lim_n)
V_bsc = Vcom_lim_n;
end
if (V_bsc>=V_tr)
V_bs = Vdc/2;
else
V_bs = -Vdc/2;
end
elseif (((Change_Theta<0)&(mode==3))|((Change_Theta>=0)&(mode==6)))
if (I_bs<=0)
Ibs_det = 0; I_bs = 0; V_bs = E_bs;
else
Ibs_det = 1;
V_bs = -Vdc/2;
end
elseif (((Change_Theta>=0)&(mode==3))|((Change_Theta<0)&(mode==6)))
if (I_bs>=0)
Ibs_det = 0; I_bs = 0; V_bs = E_bs;
else
Ibs_det = 1;
V_bs = Vdc/2;
end
end
```

Voltage control of phase C computation and control of freewheeling diode

```
if ((mode~=5)&(mode~=2))
I_cs_det = 1;
V_csc = Kp_i*(Ics_ref-I_cs);
if (V_csc>Vcom_lim_p)
```

```
V_csc = Vcom_lim_p;
elseif (V_csc<Vcom_lim_n)
V_csc = Vcom_lim_n;
end
if (V_csc>=V_tr)
V_cs = Vdc/2;
else
V_cs = -Vdc/2;
end
elseif (((Change_Theta<0)&(mode==5) )|( (Change_Theta>=0)&(mode==2) ) )
if (I_cs<=0)
I_cs_det = 0;
I_cs = 0;
V_cs = E_cs;
else
I_cs_det = 1;
V_cs = -Vdc/2;
end
elseif (((Change_Theta>=0)&(mode==5))|((Change_Theta<0)&(mode==2)))
if (I_cs>=0)
I_cs_det = 0;
I_cs = 0;
V_cs = E_cs;
else
I_cs_det = 1;
V_cs = Vdc/2;
end
end
Phase A current computation by using rk4 order method
if (Ias_det==1)
phase = 1;
k1=(V_as-E_as-I_as*Rs)/Ls_m;
k2=(V_as-E_as-(I_as*Rs+dt*k1/2)*Rs)/Ls_m;
k3=(V_as-E_as-(I_as*Rs+dt*k2/2)*Rs)/Ls_m;
```

k4=(V_as-E_as-(I_as*Rs+dt*k3)*Rs)/Ls_m;

I_as = I_as+(k1+2*k2+2*k3+k4)*dt/6;

end

Phase B current computation by using rk4 order method

if (Ibs_det==1)

phase = 2;

k1=(V_bs-E_bs-I_bs*Rs)/Ls_m;

k2=(V_bs-E_bs-(I_bs+dt*k1/2)*Rs)/Ls_m;

k3=(V_bs-E_bs-(I_bs+dt*k2/2)*Rs)/Ls_m;

k4=(V_bs-E_bs-(I_bs+dt*k3)*Rs)/Ls_m;

I_bs = I_bs+(k1+2*k2+2*k3+k4)*dt/6;

end

Phase C current computation by using rk4 order method

if (I_cs_det==1)

phase = 1;

k1=(V_cs-E_cs-I_cs*Rs)/Ls_m;

k2=(V_cs-E_cs-(I_cs+dt*k1/2)*Rs)/Ls_m;

k3=(V_cs-E_cs-(I_cs+dt*k2/2)*Rs)/Ls_m;

k4=(V_cs-E_cs-(I_cs+dt*k3)*Rs)/Ls_m;

I_cs = I_cs+(k1+2*k2+2*k3+k4)*dt/6;

end

Torques due to each phases

Torque_as = (Pole/2)*K_b*fas_thr*I_as;

Torque_bs = (Pole/2)*K_b*fbs_thr*I_bs;

Torque_cs = (Pole/2)*K_b*fcs_thr*I_cs;

Torque = (Torque_as+Torque_bs+Torque_cs);

Phase Rotor electrical speed computation by using rk4 order method

L1=((Torque-Torque_load)*(Pole/2)-B_fric*(W_r))/J;

L2=((Torque-Torque_load)*(Pole/2)-B_fric*(W_r+dt*L1/2))/J;

L3=((Torque-Torque_load)*(Pole/2)-B_fric*(W_r+dt*L2/2))/J;

L4=((Torque-Torque_load)*(Pole/2)-B_fric*(W_r+dt*L3))/J;

W_r = W_r+(L1+2*L2+2*L3+L4)*dt/6;

Phase Rotor electrical angle computation by using rk4 order method

M1=(W_r);

```
M2=(W_r+dt*M1/2);
M3=(W_r+dt*M2/2);
M4=(W_r+dt*M3);
Theta_r = Theta_r+(M1+2*M3+2*M3+M4)*dt/6;
 Save some variables for plotting
if (iter==Intig_no)
iter = iter;
Lakkaayi = Lakkaayi+1;
Plot_vabcs(Lakkaayi,:) = [V_as V_bs V_cs];
Plot_fabcs(Lakkaayi,:) = [fas_thr fbs_thr fcs_thr];
Plot_eabcs(Lakkaayi,:) = [E_as E_bs E_cs];
Plot_isc(Lakkaayi,:) = [Ias_ref Ibs_ref Ics_ref Ipeak_cmd];
Plot_iabcs(Lakkaayi,:) = [I_as I_bs I_cs];
Plot_torq(Lakkaayi,:) = [Torqe_ref Torque Torque_as Torque_bs Torque_cs];
Plot_wrthr(Lakkaayi,:) = [W_r Theta_r Thetar_deg Wr_cmd];
Plot_t(Lakkaayi,:) = t;
else
iter = iter+1;
end
if (iter1==1000)
iter1 = 0;
else
iter1 = iter1+1;
end
Time is increment by dt
t = t+dt;
end
 Plotting function
figure(1)
subplot(5,1,1); plot(Plot_t,Plot_wrthr(:,4)/(Wr_base*0.5),'b');
axis([ti tf -1.5 1.5])
set(gca,'xticklabel',[])
ylabel('W_r^*(n)'); box off;
grid
```

```
subplot(5,1,2); plot(Plot_t,Plot_wrthr(:,1)/(Wr_base*0.5),'b');
box off; axis([ti tf -1.5 1.5])
set(gca,'xticklabel',[])
ylabel('W_r(n)');
grid
subplot(5,1,3); plot(Plot_t,Plot_torq(:,1)/Te_base,'r');
set(gca,'xticklabel',[])
ylabel('T_e_n^*'); box off; axis([ti tf -2.2 2.2])
grid
subplot(5,1,4); plot(Plot_t,Plot_torq(:,2)/Te_base,'r');
set(gca,'xticklabel',[])
ylabel('T_e_n'); box off; axis([ti tf -2.2 2.2])
grid
subplot(5,1,5); plot(Plot_t,Plot_wrthr(:,3)*pi/180,'b');
%set(gca,'xticklabel',[])
ylabel('Rotor angle'); box off;
axis([ti tf 0 7])
grid
xlabel('Time,sec')
figure(2)
subplot(3,1,1); plot(Plot_t,Plot_isc(:,1),'r');
axis([ti tf -50 50])
set(gca,'xticklabel',[])
ylabel('I_a_s^*'); box off;
grid
subplot(3,1,2); plot(Plot_t,Plot_iabcs(:,1),'r');
axis([ti tf -50 50])
set(gca,'xticklabel',[])
ylabel('I_a_s_n^*'); box off;
grid
subplot(3,1,3); plot(Plot_t,Plot_eabcs(:,1),'b');
ylabel('E_a_s_n'); box off;
grid on
axis([ti tf -80 80])
```

```
grid
xlabel('Time,sec')
figure(3)
subplot(4,1,1); plot(Plot_t,Plot_wrthr(:,4)/(Wr_base*0.5),'r');
ylabel('R_e_f. Speedn'); grid on; box off;
axis([ti tf -1.5 1.5])
set(gca,'xticklabel',[])
grid
subplot(4,1,2); plot(Plot_t,Plot_wrthr(:,1)/(Wr_base*0.5),'r');
ylabel('Actual speedn'); grid on; box off; axis([ti tf -1.5 1.5])
set(gca,'xticklabel',[])
grid
xlabel('Time,sec')
subplot(4,1,3); plot(Plot_t,Plot_torq(:,1)/Te_base,'b','LineWidth',0.1);
ylabel('R_e_f. Ten'); grid on; box off; axis([ti tf -2.2 2.2])
set(gca,'xticklabel',[])
grid
subplot(4,1,4); plot(Plot_t,Plot_torq(:,2)/Te_base,'b','LineWidth',0.1);ylabel('Actual Ten');
grid on; box off; axis([ti tf -2.2 2.2])
grid
xlabel('Time,sec')
figure(4)
subplot(2,1,1); plot(Plot_t,Plot_isc(:,1),'k');
axis([ti tf -50 50])
set(gca,'xticklabel',[])
ylabel('I_a_s^* (Amps)'); box off;
subplot(2,1,2); plot(Plot_t,Plot_iabcs(:,1),'r');
axis([ti tf -50 50])
ylabel('I_a_s (Amps)'); box off;
grid
xlabel('Time,sec')
figure(5)
subplot(2,1,1); plot(Plot_t,Plot_eabcs(:,1),'r');
ylabel('E_a_s_n (Volt.)'); box off;
```

```
axis([ti tf -80 80])
grid
subplot(2,1,2); plot(Plot_t,Plot_wrthr(:,3)*pi/180,'b');
ylabel('Rotor angle(radian)'); box off;
axis([ti tf 0 7])
xlabel('Time,sec')
grid
figure(6)
subplot(3,1,1); plot(Plot_t,Plot_vabcs(:,1),'k');
ylabel('V_a_s(Volt.)'); box off;
axis([ti tf -100 80])
grid
subplot(3,1,2); plot(Plot_t,Plot_vabcs(:,2),'b');
ylabel('V_b_s (Volt.)'); box off;
axis([ti tf -100 80])
grid
subplot(3,1,3); plot(Plot_t,Plot_vabcs(:,1),'r');
ylabel('V_c_s (Volt.)'); box off;
axis([ti tf -100 80])
xlabel('Time,sec')
grid
figure(7)
subplot(2,1,1); plot(Plot_t,Plot_torq(:,1),'r');
set(gca,'xticklabel',[])
ylabel('T_e^* (Nm)'); box off; axis([ti tf -50 50])
grid
subplot(2,1,2); plot(Plot_t,Plot_torq(:,2),'r');
ylabel('T_e (Nm)'); box off; axis([ti tf -50 50])
xlabel('Time,sec')
grid
```

MATLAB/Simulink model for speed control of BLDC motor by using PWM current controller is shown as the following:

MATLAB/Simulink model of three phase BLDC motor drive circuit

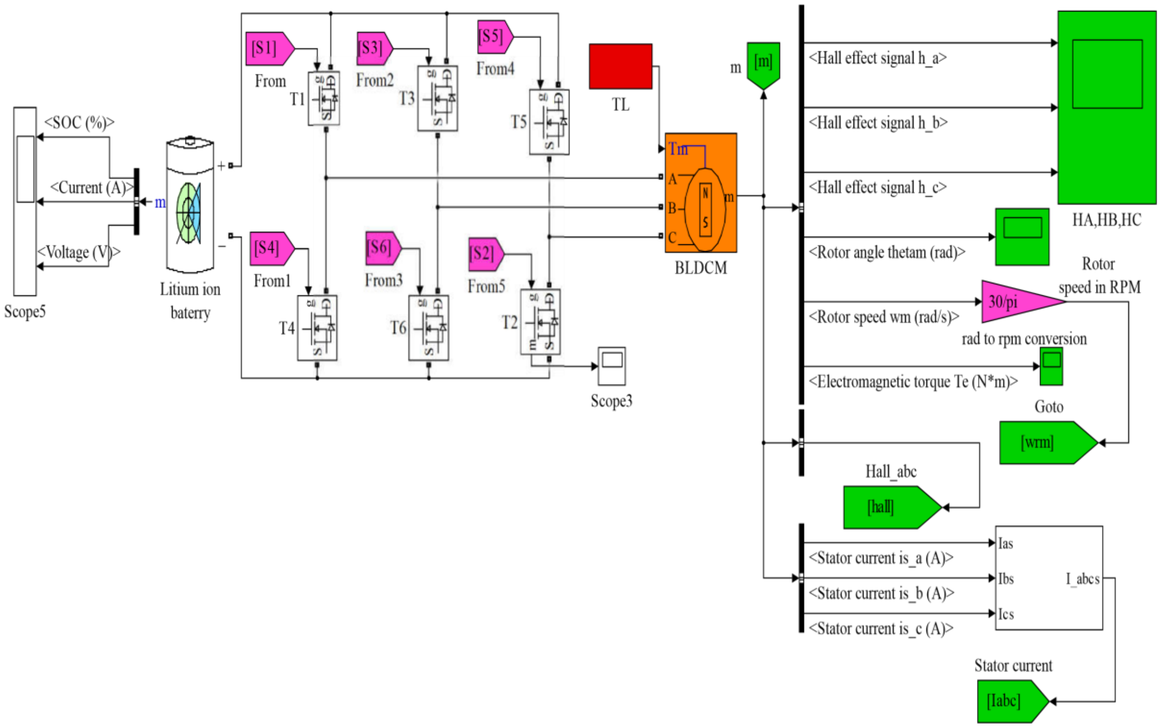

MATLAB/Simulink model of three phase BLDC motor controller circuit part

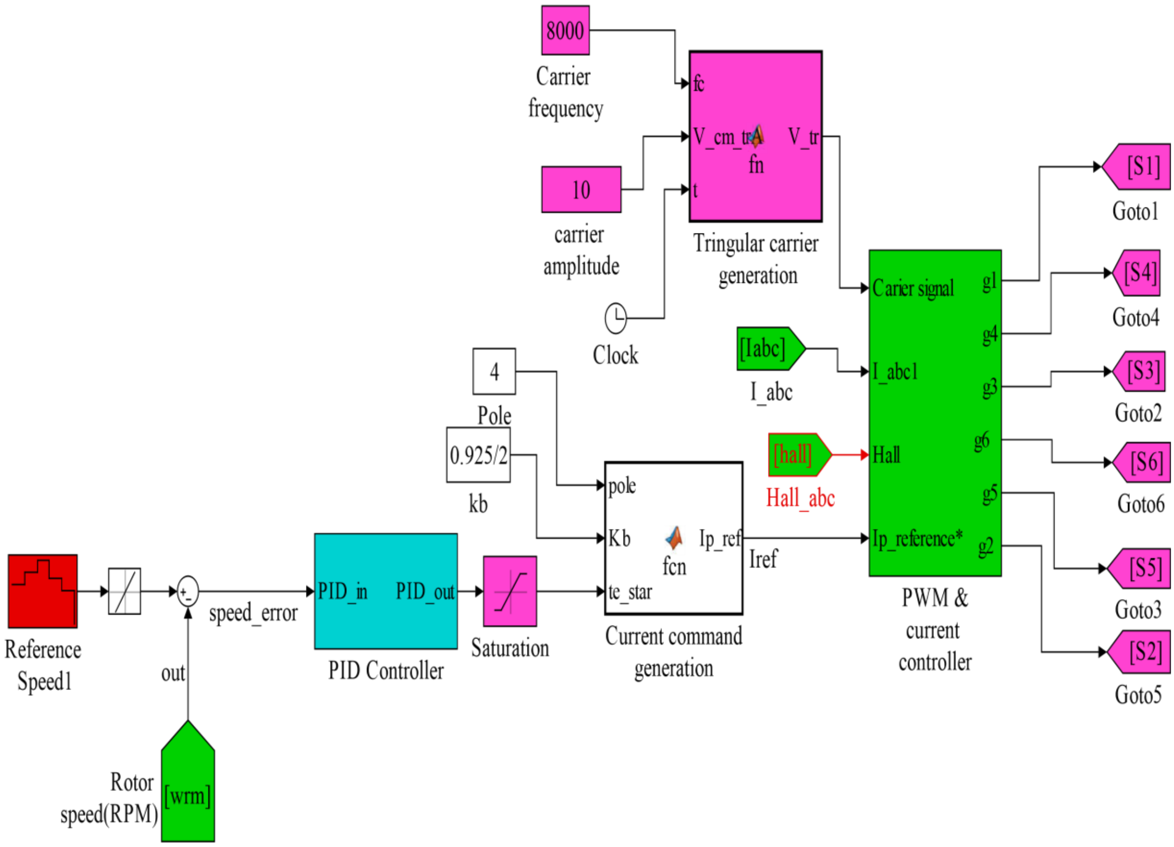

Appendix C: Appendixes related to data collection

C.1. Data's from Center of transportation and Vehicle engineering 'ASTU'

I. Traction motor performance and dimension

No	**Performance**	**Value**
1	Power (peak)	100KW
2	Power (rated)	60KW
3	Torque (max)	320Nm
4	Speed (max)	1200rpm
5	Current (max)	320Ams
6	Efficiency (max)	97% (@3600(rpm)
	Dimension	**Value**
7	Length Power (peak)	374mm
8	Height Power (rated)	340mm
9	Stator diameter	340mm
10	Speed (max)	311mm
11	Weight	62.5kg

II. Traction inverter and dimension

No	**Parameters**	**Value**
1	Output current (max)	320Ams
2	Efficiency (max)	98%
3	Switching frequency	8KHz
4	Communication	CAN2.0
Dimension		
	Parameters	Value
5	Length	324mm
6	Height	320mm
7	Weight	14kg

III. Reducer 320Nm & drive shaft

No	Parameters	Value
1	Torque (max)	320Nm
2	Speed (max)	12000rpm
3	Gear Ratio	9.96
4	Torque (max)	320Nm
Dimension		
	Parameters	Value
5	Length	521mm
6	Height	388.6mm
7	Stator diameter	253.24mm
8	Weight	28kg

C.2. Data’s from BISHOFTU Bus Factory of similar but engine based vehicle (received on July 20, 2018) from the industry ‘’Bishoftu’’

Figure A. 3: Bishoftu Buss Industrial factory

I. HUANGHAI AUTO PRICE LIST

Vehicle Model	DOUBLE CABIN PICKUP	CODE	DD1022TA *4X4*
Standard Items		Option Item	

SG Plutus Double Cabin Pickup 2008

- ◆ 4JB1TI turbo diesel engine 2.771L
- ◆ Mechanical A/C
- ◆ SABS
- ◆ Remote control door lock system
- ◆ Power window glass
- ◆ Power steering
- ◆ Adjustable steering wheel
- ◆ Radio with MP3+SD card slot
- ◆ Anti-glazing interior mirror
- ◆ Power rear view mirror
- ◆ Crystal diamond headlights
- ◆ High position brake lamp
- ◆ Leather seat
- ◆ Rear cargo bed liner
- ◆ 17'Alum-alloy wheel
- ◆ 235 tire

- ● Displacement (L) 2.771 L
- ● Rated power (hp/rpm) 84/3600
- ● Curb weight (kg) 1730
- ● Outlined dimensions (mm) 5350*1725*1690
- ● Cargo Box Dimension(mm): 1715×1455×476
- ● Wheelbase (mm) 3380
- ● Max. speed （km/h） 120
- ● Max. Torque (Nm) 210 (2000r/min)
- ● Approaching angle/departure angle (°) 26/24
- ● Seating capacity (persons) 5
- ● Average fuel consumption under limited conditions (L/100km) 7 L/100km
- ● Drive type: 4x4

II. HUANGHAI AUTO PRICE LIST

<table>
<tr><td>Vehicle Model</td><td>Landscape CUV</td><td>CODE</td><td>DD6470CA 4X4</td></tr>
<tr><td colspan="2">Standard Items</td><td colspan="2">Option Item</td></tr>
<tr><td colspan="2">SG Landscape SUV
◆ VM R425 diesel engine 2.499L
◆ Safety airbag
◆ Mechanical A/C
◆ ABS+EBD
◆ Remote control door lock system
◆ Motor-operated window glass
◆ Power steering
◆ Safety energy-absorbing steering column
◆ Adjustable steering
◆ DVD with back view monitor
◆ Back door window wiper
◆ Anti-glazing interior mirror
◆ Power rear view mirror
◆ Adjustable rear seat
◆ Crystal diamond headlights
◆ High position brake lamp
◆ Green heat insulation glass
◆ Leather seats;
◆ Aluminum alloy rim 17’’
◆ 235/65 tire</td><td colspan="2" rowspan="2">• Displacement (L) 2.499 L
• Rated power (hp/rpm) 142/4000
• Curb weight (kg) 1860
• Outlined dimensions (mm) 4620×1860 ×1830
• Wheelbase (mm) 2730
• Max. speed （km/h） 130
• Max. Torque (Nm) 210 (2100r/min)
• Approaching angle/departure angle (°) 26/28
• Seating capacity (persons) 5
• Fuel type Diesel
• Average fuel consumption under limited conditions (L/100km) 7.8 L/100km
• Drive type 4*4

</td></tr>
<tr><td></td><td></td></tr>
</table>

C.3. Data's from INTERNET: Data's of similar size of motor used for EV (accessed on august 30, 2018)

I. https://xindaenergy.en.made-in-china.com/product/MSYJFfyXEAke/China-35kw 60kw-3500rpm-Brushless-Permanent-Magnet-Motor-for-Vehicle.html

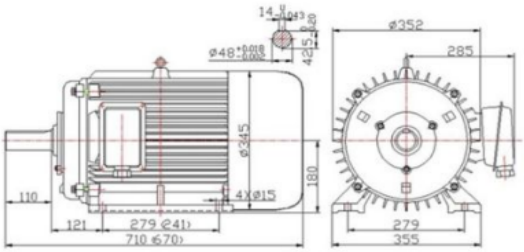

35kw-60kw 3500rpm Brushless Permanent Magnet Motor for Vehicle

Get Latest Price >

Purchase Qty. / Reference FOB Price	
1-9,999 Pieces	US $500
10,000+ Pieces	US $50,000

Production Capacity:	10000PCS/Year
Transport Package:	Polywood Case
Payment Terms:	L/C, T/T, Paypal, Western Union
Motor:	Brushless
Brake:	Front V-brake / Rear Drum Brake
Certification:	CE
Voltage:	Customized
Shaft:	Customized
Protect:	IP54

Power	The battery voltage	Speed	Rated torque	Peak torque	Peak power	current	Peak current	Efficiency	Weight
35 kw	228V	3500rpm	95.5Nm	210Nm	75KW	181.5A	350A	94.5%	162kg
37 kw	228V	3500rpm	101Nm	220Nm	80KW	188.1A	360A	94.6%	175kg
40kw	228V	3500rpm	109Nm	230Nm	86KW	203.5A	380A	94.7%	183kg
45 kw	228V	4500rpm	95.5Nm	220Nm	100KW	224.4A	420A	94.8%	175kg
50 kw	288V	4500rpm	106Nm	250Nm	110KW	190.3A	360A	94.9%	182kg
60 kw	288V	6000rpm	95.5Nm	220Nm	130KW	228.8A	420A	95.0%	190kg

II. https://xindaenergy.en.made-in-china.com/product/oKRQwlCPAGVM/China-50kw-100kw-High-Speed-Brushless-Sychronous-Permanent-Magnet-Motor.html

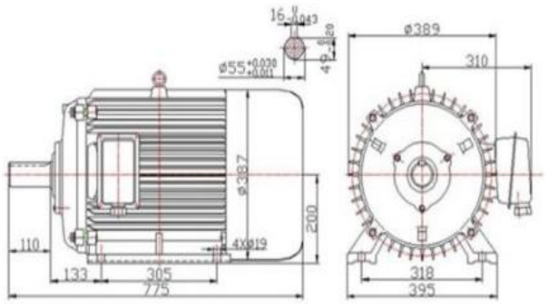

50kw-100kw High Speed Brushless Sychronous Permanent Magnet Motor

Get Latest Price >

Purchase Qty. / Reference FOB Price	
1-9,999 Pieces	US $500
10,000+ Pieces	US $50,000

Production Capacity:	10000PCS/Year
Transport Package:	Polywood Case
Payment Terms:	L/C, T/T, D/P, Paypal, Western Union
Motor:	Brushless
Certification:	CE
Voltage:	Customized
Protect:	IP54
Bearing:	SKF
Specification:	CE

Power	The battery voltage	Speed	Rated torque	Peak torque	Peak power	current	Peak current	Efficiency	Weight
50 kw	360V~540V	3500rpm	136Nm	300Nm	110KW	140A	320A	95.4%	250kg
60 kw	360V~540V	3500rpm	164Nm	350Nm	130KW	172A	380A	95.6%	260kg
75kw	360V~540V	3500rpm	205Nm	260Nm	160KW	212A	430A	95.7%	270kg
100kw	380V~540V	5000rpm	191Nm	400Nm	220KW	289.3A	590A	96.0%	270kg